UNIVERSITY OF SIENA
Doctorate in Medical Biotechnology
Department of Pathological Anatomy
Coordinator: Professor Lorenzo Leoncini

THE UTILITY OF INTERPHASE FLUORESCENCE IN SITU HYBRIDIZATION IN THE DIAGNOSIS OF LYMPHOMAS

Supervisor :

Professor: Lorenzo Leoncini

Candidate:

Raffaella Guazzo

Raffaella Guazzo

Academic Year: 2018/2021

ABBREVIATIONS

DLBCL	DIFFUSE LARGE B CELL LYMPHOMA
B-NHL	B-CELL NON-HODGKIN LYMPHOMA
WHO	WORLD HEALTH ORGANIZATION
NOS	NOT OTHERWISE SPECIFIED
NHL	NON-HODGKIN LYMPHOMA
FL	FOLLICULAR LYMPHOMA
BK	BURKITT LYMPHOMA
FISH	FLUORESCENCE IN SITU HYBRIDIZATION
HL	HODGKIN LYMPHOMAS
LBCL	LARGE B CELL LYMPHOMA
ABC	ACTIVATED B CELL-LIKE
GBC	GERMINAL CENTER B CELL-LIKE
VDJ	VARIABLE, DIVERSITY, JOINING
Ig	IMMUNOGLOBULIN
CSR	CLASS SWITCH RECOMBINATION
SHM	SOMATIC HYPERMUTATION
AID	CYTIDINE DEAMINASE
FDC	FOLLICULAR DENDRITIC CELL
DC	DENDRITIC CELL
T REG	REGULATORY T
ETPS	EARLY THYMIC PROGENITORS
DN	DOUBLE NEGATIVE
SP	SINGLE POSITIVE
ALCL	ANAPLASTIC LARGE CELL LYMPHOMA
HGBL	HIGH GRADE B CELL LYMPHOMA
TME	TUMOR MICROENVIRONMENT
BCLU	LARGE B-CELL LYMPHOMA AND BURKITT LYMPHOMA

INDEX

ABSTRACT

Lymphomas are characterized by heterogeneous biology, pathologic features, and clinical outcome. They are classified based on the normal counterpart, or cell of origin, from which they arise. Because lymphocytes have physiologic immune functions that vary both by lineage and by stage of differentiation; the classification of lymphomas coming from these normal lymphoid populations is complex. Genomic instability is a feature of lymphomas due to aberrant alterations at genetic, epigenetic, transcriptional, protein, and dysregulated oncogenic signaling pathways. Detection of specific chromosomal abnormalities is essential in diagnosing of several lymphoproliferative disorders. Interphase FISH investigates cytogenetic alterations, the gold standard technique localizes fluorescent signals to specific interphase non-dividing cells.

Translocations and rearrangements are the common chromosomal alterations of lymphomas involving proto-oncogenes and tumor suppressors.

The common abnormalities include: t (11;14) (q13; q32) in mantle cell lymphoma and in some cases of plasma cell myeloma; t(14;18)(q32;q21) in follicular lymphoma; t(8;14)(q21;q32) in Burkitt lymphoma; t(11;18)(q21;q21) in MALT lymphoma; BCL6 rearrangement in Large B-cell Diffuse Lymphoma (LBCL); IRF4/DUSP22 rearrangement in LBCL; t(2;5)(p23;q35) NPM-ALK in T-cell lymphomas. Less commonly are deletions, trisomy 12 or partial trisomy 12q13 in Chronic Lymphocytic Leukaemia (CLL).

The WHO has recently introduced a particular type of lymphoma morphologically similar to Burkitt Lymphoma but without t (8;14) (q24; q32): instead, the following entity is cytogenetically characterized by a peculiar pattern of an 11q aberration consisting of a gain in 11q23.2-23.3 followed by a telomeric loss in 11q24.1-qter.

This study aims to standardize Interphase FISH for diagnosing lymphoma associated with immunophenotypic features, focusing our attention on particular cases showing interested genic abnormalities, such as 11q alterations and t (11;14) in Precursor T-Lymphoblastic Transformation of Mantle Cell Lymphoma**.**

During this study, we have also performed ImmunoFISH, a method combining immunolabelling with fluorescent in situ hybridization (FISH) to simultaneously detect the nucleo-cytoplasmic distribution of proteins and specific nucleotide sequences within the chromosomes.

INTRODUCTION

B-cell differentiation and function

B cells develop from hematopoietic stem cells in the fetal liver during gestation and bone marrow after birth. Each newly generated B lymphocyte carries a transmembrane Ig receptor that is composed of two identical Ig heavy chain (H) molecules and two identical Immunoglobulin (Ig) light chain (L) molecules, which can be either Igk or Igʎ (1). The IgH and IgL chain molecules include an antigen-binding variable region encoded by recombined $V_HD_HJ_H$ and V_LJ_L genes, respectively. The V, D, J segments of these genes are organized in multiple families within the IgH and IgL loci. Normal B-cell differentiation begins with B lymphoblasts, which undergo IG VDJ gene rearrangement and differentiate into mature surface immunoglobulin (slg)-positive (IgM+IgD+) naive B cells via pre-B cells with cytoplasmic mu heavy chains and immature IgM+ B cells. Naive B cells, often CD5 positive, are small lymphocytes that circulate in the peripheral blood and occupy primary lymphoid follicles and follicle mantle zones (called recirculating B cells). When an antigen fits its Ig receptors, naive B cells transform, proliferate, and develop into antibody-secreting plasma cells and memory B cells. Transformed cells derived from naive B cells that have encountered antigen may mature directly into plasma cells that produce the early IgM antibody response to antigen. Other antigen-exposed B cells migrate into the centre of a primary follicle and proliferate forming a germinal centre (2-3). In the germinal centre, somatic hypermutation can result in a non-functional gene or a gene that produces antibody with a lower or higher affinity for antigen. Also in the germinal centre, some cells switch from IgM production to IgG or IgA production. The germinal centre reaction gives rise to the higher-affinity IgG or IgA antibodies of the late primary or secondary immune response. Post-germinal centre memory B cells circulate in the peripheral blood and account for at least some cells in the follicular marginal zones of lymph nodes, spleen, and mucosa-associated lymphoid tissue (MALT). Marginal-zone B cells express pan -B-cell antigens and surface IgM, lacking CD5 and CD10. Plasma cells produced in the germinal centre enter the peripheral blood and home to bone marrow. They contain IgG or IgA. Both memory B cells and long-lived plasma cells have mutated IGV genes, but do not undergo mutation. Post-germinal centre B cells retain the homing ability to tissues where they have experienced antigen stimulation, probably through surface integrin expression.

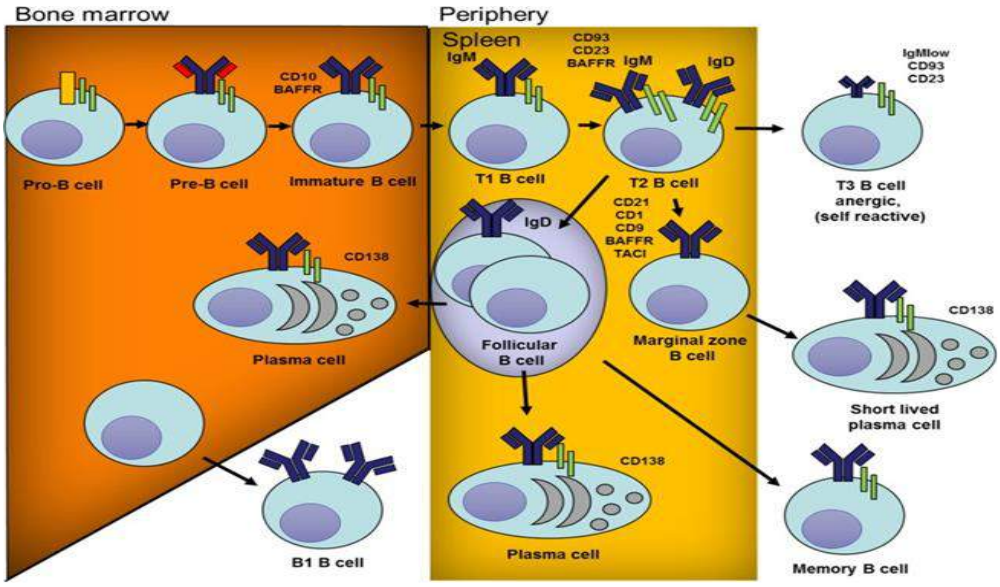

Fig.1 Pathway of B cell development and differentiation (Clinical Reviews in Allergy & Immunology)

B cells are generated from hematopoietic progenitor cells in the bone marrow. This process involves the expression of B lineage cell-specific proteins and the rearrangement of V(D)J genes to generate the BCR repertoire. Pre-B cells express the pre-B cell antigen receptor (BCR) on the cell surface with the fully arranged heavy chain associated with the surrogate light chain. At later stages, light chain V and J mini genes are rearranged and a complete BCR is expressed in association with the Ig-α and Ig-β subunits of the BCR complex. Immature B cells undergo tolerance mechanisms with B cells recognizing self-protein undergoing light chain editing, apoptosis or functional inactivation (anergy). Surviving immature B cells then exit the bone marrow and migrate to secondary lymphoid organs, developing into transitional (T) B cells. Transitional B cells can be subdivided into several developmental subsets. These include T1 B cells and T2 B cells. These B cells undergo a range of tolerance checkpoints, and cells that recognize self-antigens with high affinity are deleted. Transitional B cells develop into either marginal zone (MZ) B cells or follicular B cells. MZ B cells sample antigens and those that recognize antigens expand independently of T cell help. For their expansion, MZ B cells require TLR signaling into short-lived plasma cells that produce antibodies with limited avidity for their target antigens. Follicular B cells are activated when they encounter their target antigens in the presence of T cell help. Activated follicular B cells migrate to B cell follicles and initiate somatic maturation in germinal centres. During this process, the cells proliferate, acquire somatic mutations, produce antibodies with higher avidity and class switch to IgG. Antigen-specific mature B cells then leave germinal centres and differentiate into either plasma cells or memory B cells. Plasma cells can either remain secondary lymphoid organs or travel to the bone marrow to

produce antibodies. B1 cells comprise a distinct subset of B cells that develop in the bone marrow and migrate to the periphery. B1 cells produce polyreactive IgM antibodies and partake in providing the first line of immunity against pathogens. (4)

V(D)J Recombination

In 1976, the revolutionary discovery was made that the DNA in lymphoid cells encoding the antigen receptors is altered from other somatic tissues and germ-line cells (5). This DNA rearrangement allows B and T cells to generate a highly diverse array of antigen receptor molecules, allowing a virtually unlimited set of antigen molecules to be recognized with a high degree of specificity. A series of site-specific recombination events collectively termed V(D)J recombination assembles antigen receptor genes from arrays of gene segments (6-7). VDJ means V (variable), D (diversity), or J (joining) genes.

Pro-B cells initially recombine D and J segments in the IgH locus and form a DJ segment that recombines with a V segment to assemble a complete $V_HD_HJ_H$ gene. These events randomly target individual members of multiple V, D, and J gene families and require the induction of double-stranded DNA breaks in specific recombination signal sequences by heterodimeric recombination activating gene (RAG) complex including RAG1 and RAG2 proteins (8-9). $V_HD_HJ_H$ stops the expression of RAG proteins, leading to the transcription of RAG proteins, leading to the transcription of the V_HDJ_H gene together with the constant (C) heavy chain gene μ(Cμ) gene to form a complete IgH chain. (10). Subsequent assembly of the IgH chain with surrogate variant IgL proteins is followed by transient surface expression of a pre-B-cell receptor (pre-BCR) complex that includes Igα and Igβ subunits with signaling function. Signals emanating from pre-BCR are critical checkpoint for B-cells and their differentiation into immature B cells (11). Immature B cells re-express RAG proteins to initiate the rearrangement of V and J segments from the IgL locus and form a complete Ig molecule. Assembly of the IgL chain with the IgH chain is followed by the expression of a fully competent IgM receptor which functions as a surface BCR (12).

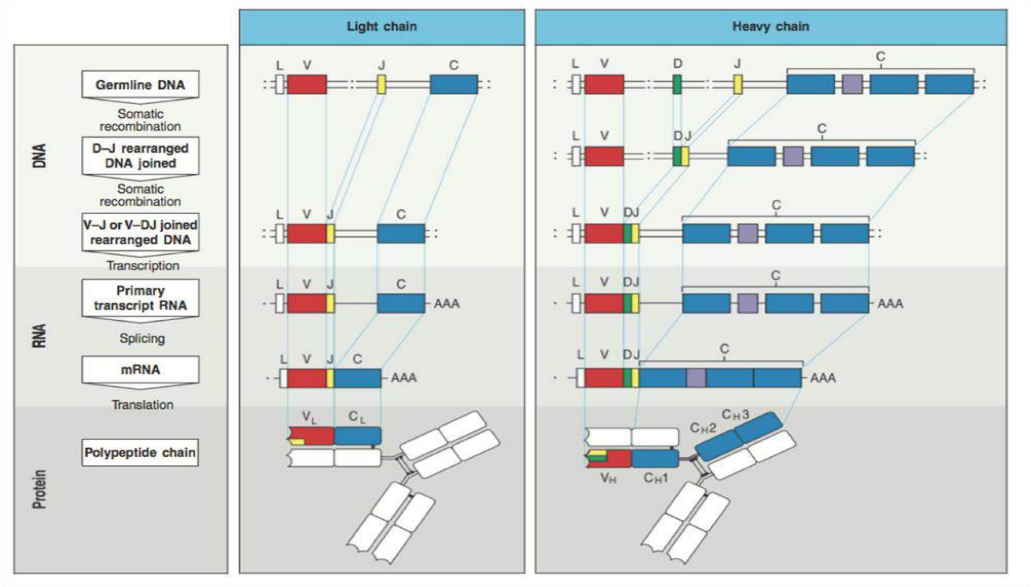

Fig.2 V(D)J recombination (Immunology)

CLASS SWITCH RECOMBINATION

After going through V(D)J recombination, B cells subsequently undergo two genetic modifications, Somatic Hypermutation (SHM) and Class Switch Recombination (CSR)**.**

CSR is the gene rearrangement process by which B lymphocytes change Ig heavy chain constant region to permit a switch of Ig isotype from IgM to IgG, IgA, or IgE.

CSR occurs between switch (S) regions located upstream of each of the C_H regions except Cδ and results in a change from IgM and IgD expression by naive B cells to the expression of one of the downstream isotypes. IgD expression occurs by alternative transcription termination/splicing of the Cμ-Cδ genes. Cytokine signals are essential to target specific C_H genes. Germline transcription yields a primary transcript encompassing the S region and its downstream CH gene. Later spliced into a non-coding germline, the primary transcript plays a central role in CSR. The RNA associated with the template DNA strand of the targeted S region forms a stable DNA-RNA hybrid that becomes the substrate of cytidine deaminase (AID), a DNA-editing enzyme induced by CSR-inducing signals. AID deaminates cytosine residues on both DNA strands of the transcribed S region to generate multiple DNA lesions processed by a complex DNA repair machinery to form double-stranded DNA breaks. Fusion of double-stranded DNA breaks via the nonhomologous end-joining pathway induces looping-out deletion of the intervening DNA with subsequent replacement of Cμ with downstream

C_H gene. The resulting juxtaposition of the recombined VDJ gene with Cy, Cα or Cε gene permits B cells to acquire an Ig with novel effector functions but identical specificity for antigen.

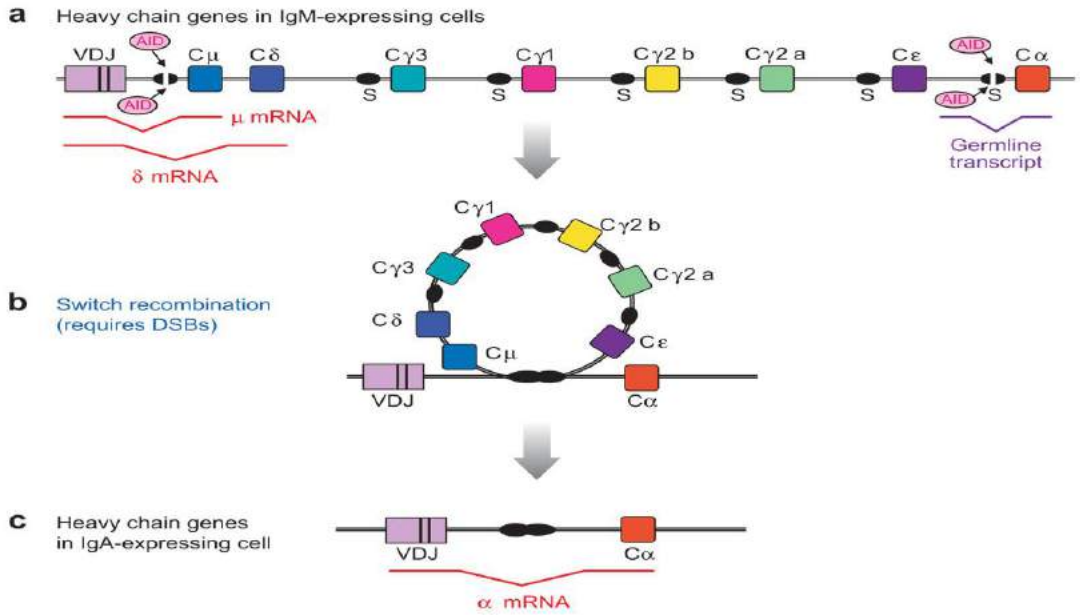

Fig.3 Diagram of Ig CSR (Annu Rev Immuno 2008)

SOMATIC HYPERMUTATION

Somatic Hypermutation (SH) is a process that introduces the point of mutations in the V(D)J exons encoding the antigen-binding V region of an antibody. In the germinal centre of secondary lymphoid follicles, these point mutations provide the structural correlate for selecting of high-affinity B cells by antigen exposed on Follicular dendritic cells (FDCs). During affinity maturation, the point mutations induced by AID generate amino acid replacements in CDRs, which play a crucial role in forming of the antigen-binding pocket formed by V regions of IgH and IgL chains. SHM includes an initial phase that requires the mutagenic activity of AID, followed by a second phase that involves the error-prone repair of AID-induced mutations. DNA polymerases perform error-prone DNA repair. Amino acid replacements brought about by SHM increase the affinity and fine specificity of an antibody but do not modify the framework regions (FRs) that regulate Ig molecules' structural organization. SHM does not induce amino acid replacements in the promoter and intronic enhancer, which regulate the Ig locus's transcriptional activity.

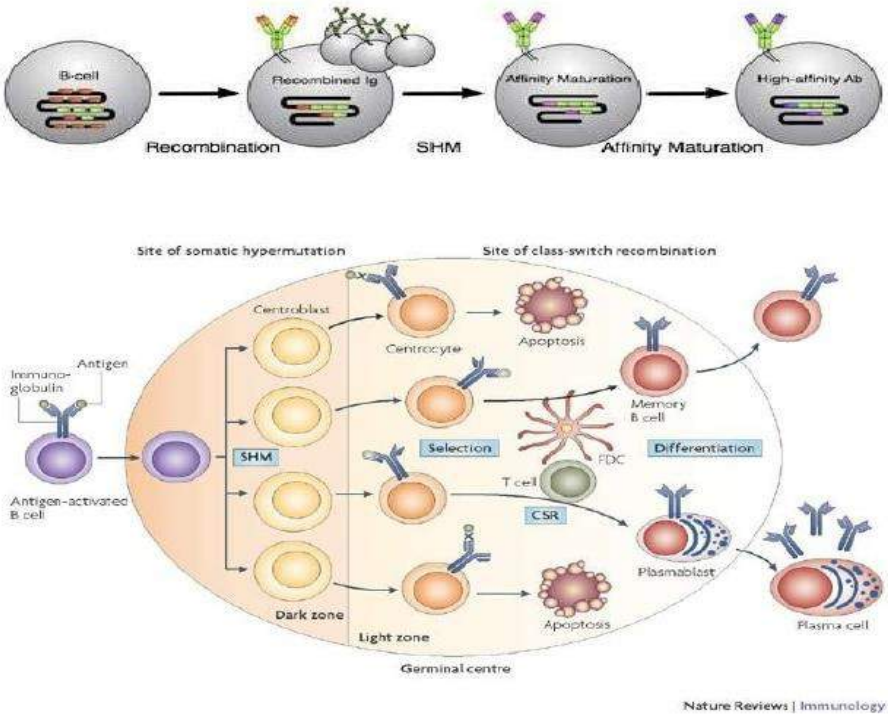

Fig.4 Somatic Hypermutation (Nature Review-Immunologye)

T-CELL DEVELOPMENT

T lymphocytes originate from bone marrow progenitors that migrate to the thymus for maturation, selection, and subsequent export to the periphery. Peripheral T cells comprise different subsets, including naïve T cells, which can respond to new antigens, memory T cells, and regulatory T (Treg) cells that keep immune responses in control.

The thymus is the primary site of T cell development, where progenitor cells, called thymic progenitor (ETPs), differentiate into double-negative (DN) thymocytes that are committed to the T-cell lineage. The Notch receptor and IL-7 regulate the initial phase of thymocyte development. DN thymocytes express neither the TCR nor the CD4 or CD8 molecules and differentiate in the thymic cortex through DN1, DN2, DN3, and DN4. DN1 expresses CD117 and CD44 and progresses to the DN2 stage by up-regulating CD25 expression in response to thymic environmental signals. At this stage, RAG1 and RAG2 complex induces the rearrangement of TCR ɤ, TCRβ, and TCRδ gene loci through V(D)J recombination. The down-regulation of CD117 and CD44 characterizes the DN3 stage. In the DN3 stage, the newly rearranged TCRβ chain is associated with pre-TCRα, and CD3 forms a pre-TCR complex. Signals from the pre-TCR complex induce cessation of TCRβ chain gene rearrangement, down-regulation of CD25 and entry into the DN4 stage. Thymocytes acquire double expression of CD4 and CD8 and become Double positive (DP). They are tested for recognition of self-MHC molecules. DP cells selected by TCR interaction with MHC-I develop into CD4-and CD8 single-positive (SP) thymocytes, whereas DP cells selected by TCR interaction with MHC-II molecules differentiate into CD4+CD8-SP thymocytes.

Following these selections, SP thymocytes migrate to the thymic medulla, where they undergo negative selection where self-reactive T cells are eliminated or clonal deletion. Following negative selection, mature naïve T cells migrate toward post-capillary venules located at the corticomedullary junction and enter the general circulation to colonize secondary lymphoid organs (13).

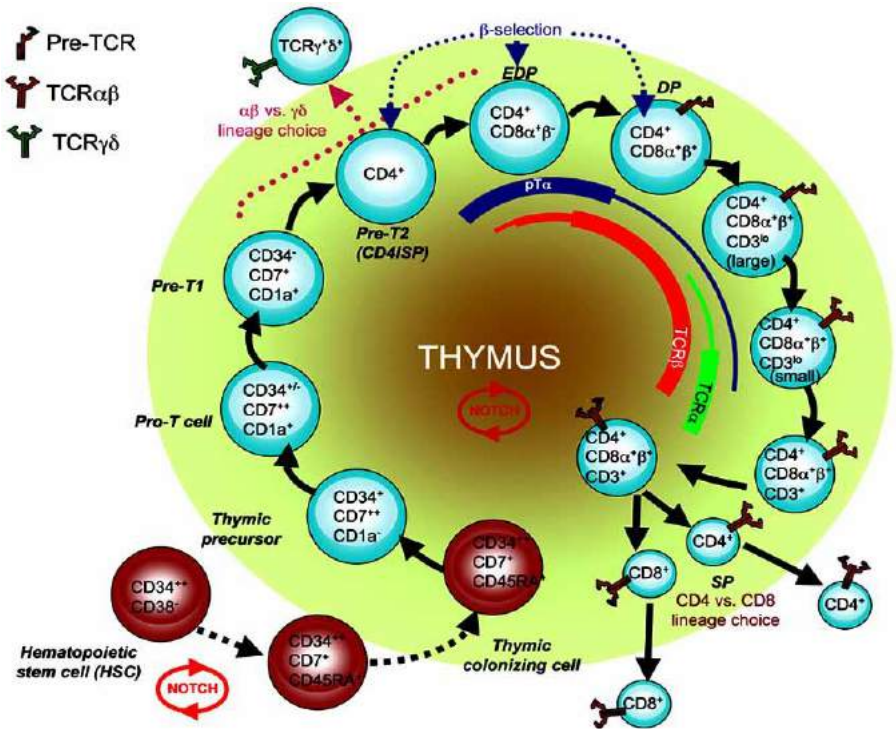

Fig.5 T-cell development (Current Immunology Reviews 2007)

PART II

THE IMPLICATION OF GENETIC ALTERATIONS FOR THE DEVELOPMENT OF LYMPHOMAS

Genetic alterations are one of the critical drivers of the pathogenesis of lymphomas. In lymphoid neoplasm, during lymphocytes development, the lymphoid cells undergo several cytogenetic alterations that occur in their genome and may cause neoplastic transformation. A variety of primary and secondary non-random clonal cytogenetic abnormalities are found in lymphoid neoplasm: deletions, inversions, chromosomal translocations, and reinsertion of DNA segments (excised during normal V(D)J recombination). These events can activate oncogenes, inactivate tumor suppressor genes and cause inappropriate expression. Alterations in the expression of genes located at the breakpoints of the chromosomal alterations or in the proprieties of the encoded proteins play an important role in the process of malignant transformation. The transforming genes involved in chromosomal translocations are transcriptional factors, tyrosine proteins kinases, cell surface receptors, growth factors, and regulators of apoptosis. There are two general subtypes of chromosomal translocations that result in altered gene function. The first results in inappropriate expression of an oncogene with no alteration in protein structure. The second mechanism is the expression of a novel fusion protein, resulting from the juxtaposition of coding sequences from two genes usually located on different chromosomes.

As reported in figure 6, hematopoietic stem cells first colonize the bone marrow during normal B-cell development and give rise to typical lymphoid progenitor cells, some of which will differentiate to B-cell lineage. In the bone marrow, V(D)J recombination machinery rearranges germline immunoglobulin (Ig) gene loci that lead to the formation of chromosomal translocations. Mature naïve B-cells that express the B-cell receptor exit the bone marrow to lymph nodes and extra-lymphatic follicles. There, B-cells become activated, undergoing a proliferative burst, generating germinal centres (GCs). In GCs, proliferating B-cells are subjected to somatic hypermutation directed at Ig genes. (14)

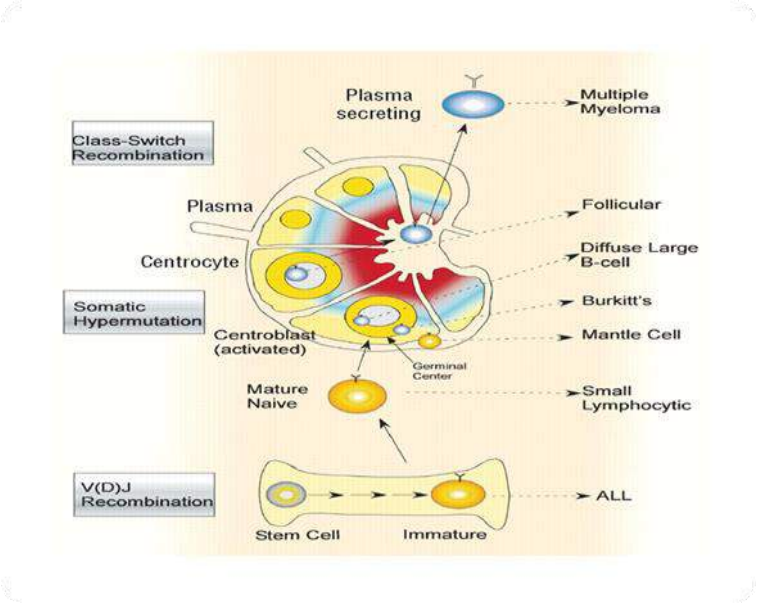

Fig.6 The normal life cycle of B-lymphocytes and the derivation of lymphoma subtype (Haematologica 2007)

The malignant lymphomas, including both Hodgkin lymphoma (HL) and non-Hodgkin lymphoma (NHL), represent a diverse group of diseases that arise from a clonal proliferation of lymphocytes. Lymphomas are classified according to a system established by the World Health Organization (WHO) with the most recent edition published in 2017 (15). The WHO classification distinguishes lymphoid neoplasms derived from precursor lymphoid cells from mature lymphoid cells and further separates each group into neoplasms of B-cell or T-cell origin. For the most part, mature lymphoid neoplasms comprise the NHLs; HLs are considered separately (16). NHL is the most common hematologic malignancy globally (17): it comprises about 60 distinct subtypes that are heterogeneous in their clinical and biologic features. In the 2017 classification, more than 80 mature lymphoma entities are recognized, grouped into B-cell neoplasms, T-cell and NK- cell neoplasms, and HLs (16). Molecular genetic abnormalities in NHL pathogenesis, representing the pontential therapeutic targets (18). The prognosis depends on the histologic type, clinical factors and molecular characteristics.

B-cell neoplasms have characteristic genetic abnormalities that are important for their biological features and useful in the differential diagnosis. These genetic abnormalities include: t(11;14)(q13;q32) in mantle cell lymphoma and in some cases of plasma cell myeloma, t(14;18)(q32;q21) in follicular lymphoma, t(8;14)(q21;q32) in Burkitt lymphoma and t(11;18)(q21;q21) in MALT lymphoma.

Regarding T-cell lymphomas, genetic alterations regard the ALK gene, which is positive in anaplastic large cell lymphoma that is the first T-cell lymphoma to be linked to a specific aberration.
Chromosomal rearrangements and translocations are the common cytogenetic alterations in lymphomas, but other cytogenetic abnormalities are found in lymphoid neoplasms, comprising inversions: inv (14) (q11.2; q32.2) in T-cell tumors, insertions, duplications, amplifications, deletions, and aneusomy (e.g. monosomy and trisomy) (19). In CLL deletion in 13q14.3, trisomy 12 or partial trisomy 12q13 are frequent, while deletion in 11q22-23 or 6q21 is less common. Cytogenetic alterations, including amplification and deletion, are typical in 1ymphoma with an 11q pattern, characterized by proximal gains and telomeric losses, observed in a subset of lymphomas that resemble BL morphologically but lack *MYC* rearrangements. For the first time, this entity has been designated as Burkitt-like lymphoma with 11q aberration (20), subsequently modified in Large B-cell lymphoma with 11q aberration in WHO 2022 classification of lymphomas.
Cytogenetic aberration may be detected by Cytogenetic analysis of metaphase cells, reverse transcription-polymerase chain reaction (RT-PCR) and Fluorescence in situ hybridization (FISH).
Cytogenetic analysis by FISH has historically proved invaluable for detecting chromosomal abnormalities in tumor samples. It is still considered to be the "gold standard" technique in tumor cytogenetics because it is the only technique providing a complete overview of all chromosomal changes within a tumor cell.

INTERPHASE FISH FOR THE DETECTION OF CYTOGENETIC ALTERATIONS IN LYMPHOMAS

FISH is a molecular cytogenetic technique that involves the hybridization of DNA- specific probes onto interphase chromosomal DNA.
In situ hybridization techniques initially developed by Joseph Gall and Mary Lou Pardue in the 1960s (21) were used for determining the chromosomal location of hybridized nucleic acid. The basic principle involved is the hybridization of nuclear DNA of either interphase cells or metaphase chromosomes affixed to a microscopic slide with a nucleic acid probe. The probes are either labeled directly through the incorporation of a fluorophore. After denaturation, the labeled probe and the target DNA are mixed, which allows the annealing of complementary DNA sequences. The most frequently used reporter molecules for direct detection are fluorescein (fluorescein isothiocyanate, FITC), rhodamine, Texas Red, et al. Using differentially labeled probes, chromosome aberrations on particular chromosomes or chromosomal regions can be easily defined (22). The standard FISH protocol includes five steps: sample pretreatment, denaturation of probe and sample, hybridization of

the probe to target cells, post-hybridization washing, and detection using a simple epifluorescence microscope with appropriate filter sets. When a FISH test is initially implemented, the assay performance characteristics assessed should include sensitivity, accuracy, precision, and specificity (23). There are different types of FISH probes used in clinical genetics laboratories: whole-chromosome painting (WCP) probes for deciphering cytogenetic aberrations (24); repetitive sequence probes for chromosome enumeration (25), and locus-specific identifier (LSI) probes for gene fusions (26), gene deletions or duplications. An advantage of FISH is the ability to localize fluorescent signals to specific interphase nuclei in non-dividing cells. Two categories of probes: break-apart and fusion, are used to detect chromosomal translocations and aid the lymphoma diagnosis.

With the break-apart strategy, probes are labeled with two fluorochromes (fluorescent chromophores), often orange and green, which hybridize to sequences that flank a known chromosomal breakpoint region. When these two probes hybridize with a normal gene/locus, they are close and appear as a combined or single signal (signal of fusion usually yellow). When a rearrangement occurs in the gene, the signals from two probes are split, and separate orange and green signals are detected while the not arranged locus/chromosome is yellow. Break apart probes cannot identify the translocation pattern. On the other hand, two probes labeled with two distinct fluorochromes (usually green and orange) target two loci located on a different chromosome in the fusion pattern. In a normal intact cell, two separate red and two separate green individual signals will be visible, whereas a reciprocal translocation will generate two fused red/green signals (often appearing as single yellow signals), accompanied by one red and one green signal (representing the normal loci). Of note, this is the "classical" abnormal pattern: variant and complex patterns may also be seen (e.g. because of gains, amplifications, or deletions) (27).

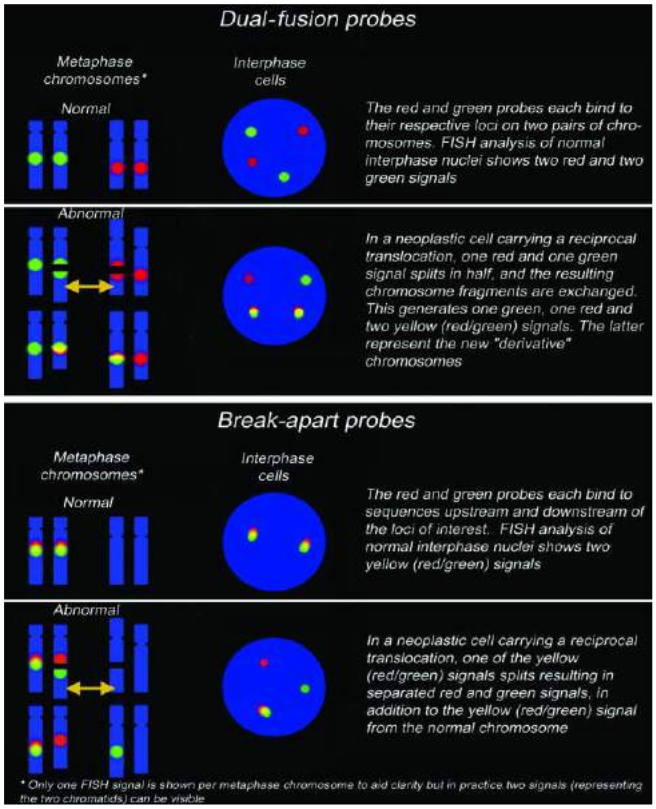

Fig. 7: Schematic representation of the characteristics of dual-fusion and break-apart probes (Journal of molecular diagnostic 2006)

Non-Classical FISH rearrangement, studied for MYC gene, called complex distribution of MYC rearrangement MYC genetic heteroclonality, is characterized by one of these pattern: 1G2For 1R2F. This heteroclonality results from MYC rearrangement coupled with additional alterations (extra copies of the normal allele, extra copies of derivatives, extra copies of both, or deletion of one of the derivatives) (28)**.** Chromosomal translocations and rearrangements are the common cytogenetic alterations in lymphomas, but, in the last 5 years, WHO has introduced another type of lymphoma which shows aberration in chromosome 11 (29). This genetic aberration characterizes a subset of MYC-negative high-grade B-cell lymphomas resembling Burkitt lymphoma. For the qualitative detection of 11q alterations, is used a tri- color probe which targets sequences mapping in the minimal gained region (MGR) of chromosome 11, sequences mapping in the minimal loss region (MLR) of the same chromosome, and polynucleotides which target sequences mapping the alpha satellite region on centromeric region of chromosome 11.

TYPES OF CYTOGENETIC ALTERATIONS IN LYMPHOMAS

BCL2 Translocation: t(14;18)(q32;q21)

BCL2 is encoded by the BCL2 gene located on chromosome 18q21.3

BCL2 came from the BCL family proteins. BCL2 represses apoptotic cell death, and protects the cell from cytotoxic insults: cytokine deprivation and ultraviolet irradiation. Deregulation of BCL2 leads to over-expression of BCL2, making the cell resist cell death (30). In contrast, BCL2 inhibition eliminate cell survival advantage and allow apoptosis to occur. Similar to C-MYC translocation characteristic in DLBCL, a chromosomal rearrangement that mix the BCL2 gene situated on chromosome 18 involving the IgH gene deregulates the BCL2 expression.

In t (14;18), the BCL2 gene on 18q21 is juxtaposed with the IGH gene on 14q32, resulting in overexpression of structurally intact and functional BCL2 protein.

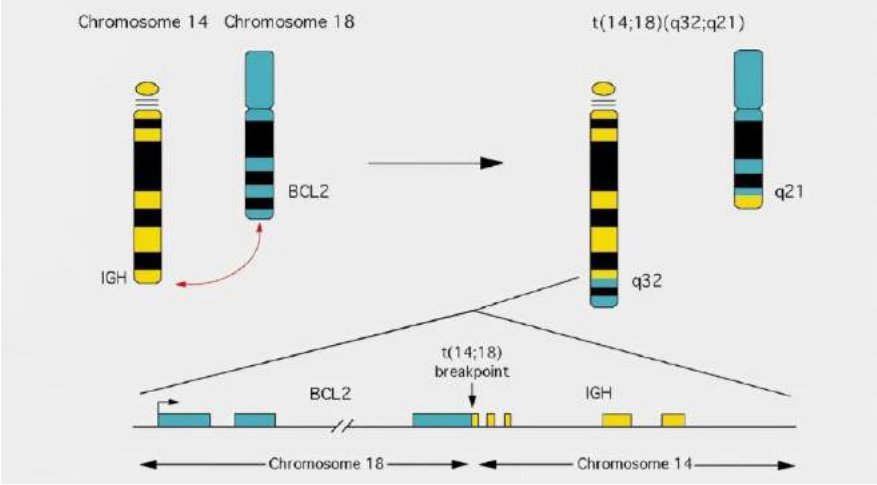

Fig.8 BCL2 Translocation: t (14;18) (q32; q21)

BCL2 translocation, t (14;18) (q32; q21), is observed in about 15-20% of Diffuse Large B-cell lymphoma (DLBCL) cases and approximately in 80-90% of Follicular Lymphoma (FL) (31).

BCL2 gene aberrations, other than t (14;18) (q32; q21), such as 18q21 amplification or activation of the nuclear factor-kB pathway, has been suggested to be the main responsible act for dysregulation of BCL2 protein expression in the DLBCL non-GCB subtype (32).

BCL6 Translocations: t (3; var) (q27;var)

BCL6 is a proto-oncogene that acts as a transcriptional repressor in cell cycle control, proliferation and differentiation, apoptosis, and DNA damage response. Loss of normal control mechanisms regulating BCL6 expression causes lymphoproliferative disease, resembling DLBCL. BCL6 translocation, t(3q27), is responsible for up to 35% of DLBCL cases, the largest compared to other DLBCL gene translocations (33).

The BCL6 gene can be juxtaposed with several pattern chromosome loci (more than 20) in addition to IGH, including 4p13, 6p21.3, 9p22, 14q11, and IG loci: 14q32 (IGH), 2p12 (IgK) and 22q11 (IGλ). IGH is the most common pattern loci. (34). Deregulation of BCL6 located on chromosome 3 contributes to malignant transformation in germinal center–derived B cells (GCB). Detection of point mutations of the regulatory region of the BCL6 gene has been frequently found in GCB and post–GCB lymphomas, including FL, DLBCL, and BL (35). *MYC* and *BCL6* rearrangements occurred primarily in *IGH* switch regions upstream of constant gene segments, indicating their likely origin during AID-mediated class switch recombination in the germinal center reaction.

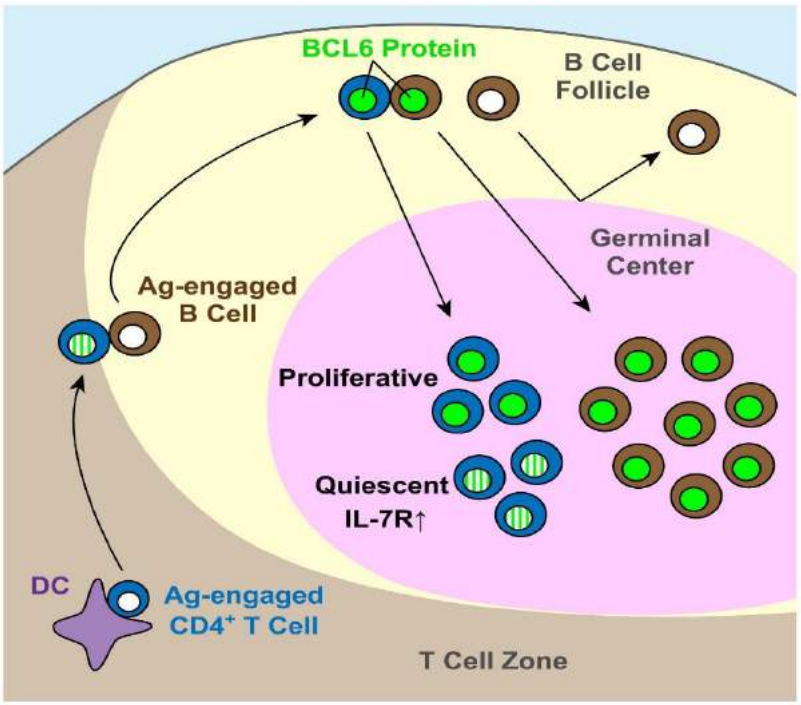

Fig.9 BCL6 and GC formation (Immunity 2011)

MYC Translocations: t (8;14) (q24; q32)

The proto-oncogene MYC encodes the Myc protein, a typical pleiotropic transcription factor involved in almost every cell biology and oncology process, by regulating thousands of target genes involved in oncogenesis, malignant transformation, and aggressive clinical features.

The transcriptional program regulated by MYC includes 10% to 15% of all human genes. The primary cell functions and pathways under control of MYC are cell proliferation and growth, DNA replication, protein biosynthesis, and metabolism and energy regulation. MYC promotes the transition from the G0/1 phase to the S phase, activating directly and indirectly the expression of CCND2 and CDKs and down-regulating cell cycle inhibitors (36). A paradoxical role of MYC is the induction of apoptosis because MYC activation in cancer cells can result from constitutive activation of a pathway such as WNT in tumors with loss of APC or through direct alterations of the MYC gene such as amplification or chromosomal translocation, resulting in DNA damage that in turn triggers a TP53-mediated response, leading to apoptosis.

Chromosomal translocations (8;14) affecting the *MYC* oncogene are the biological hallmark of Burkitt lymphomas but also occur in other B-cell lymphomas including FL, DLBCL, and "B-cell lymphoma, unclassifiable, with features intermediate between diffuse large B-cell lymphoma and Burkitt lymphoma" (BCLU) (37).

In BL, the *MYC* translocation always involves one of the immunoglobulin loci (most commonly *IGH*, alternatively *IGL* or *IGK*) and is considered a disease-initiating event. Rearrangement of the C-MYC gene situated on chromosome 8 next to the IgH gene, or lambda (λ) and kappa (κ) light chain genes subsequently caused upregulation of gene expression commonly observed in BL. In addition to MYC translocations, BL also harbors MYC and TP53 mutations.

In contrast, *MYC* translocations in other mature B-cell lymphomas frequently involve non-*IG* partners and are mostly found in complex karyotypes, often in addition to aberrations, including the *IGH-BCL2* translocation (38) that can occur during disease progression rather than disease initiation. Indeed, in 20–80% of cases of DLBCL and BCLU with a *MYC* breakpoint, there is an associated *BCL2* and/or *BCL6* breakpoint.

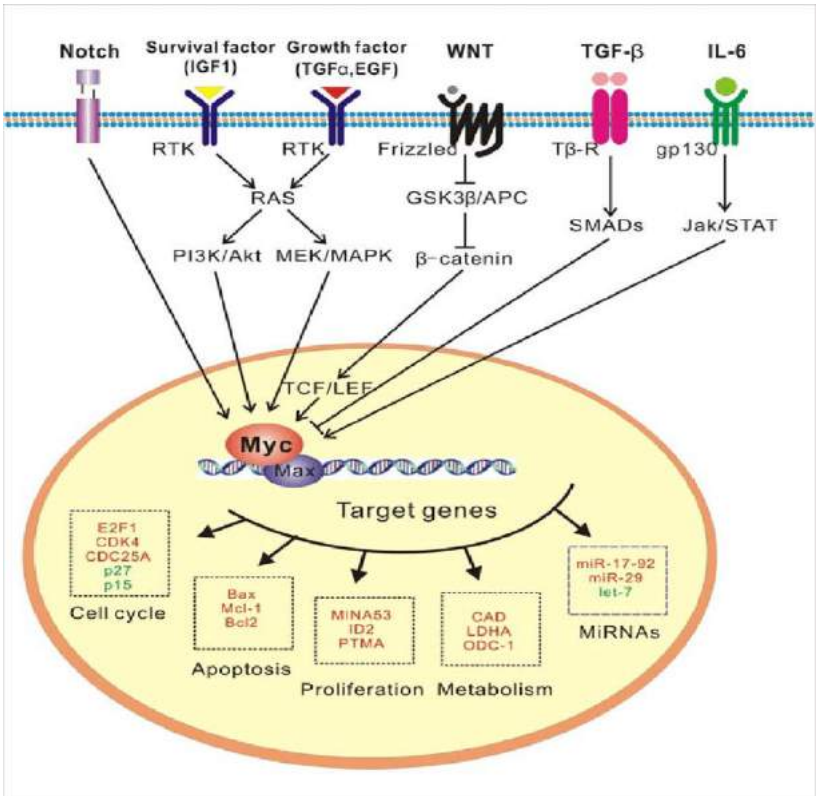

Fig.10 MYC pathway in cancer

(source: Attacking c-Myc: Targeted and Combined Therapies for Cancer)

REARRANGEMENT IRF4/DUSP22 (6p25.3)

IRF4 is a gene located at the 6p25.3 locus and encodes for the IRF4 protein belonging to the interferon regulatory factor (IRF) family of transcription factors controlling the B-cell proliferation and differentiation and the proliferation of mitogen-activated T cells. IRF4 rearrangement is a common cytogenetic anomaly reported in some B-cell neoplastic lymphoproliferative disorders, including myeloma, follicular lymphoma, and diffuse large B-cell lymphoma (LBL), and also in some T-cell neoplastic lymphoproliferative disorders including primary cutaneous anaplastic large cell lymphoma, lymphomatoid population, and peripheral T-cell lymphoma not otherwise specified.

Large B-cell lymphoma with IRF4 rearrangement is neoplasm characterized by 6p25/IRF4 rearrangement, detected by using Interphase FISH (39). The histological pattern of these neoplasms can be follicular, follicular and diffuse, or entirely diffuse. Comparative genomic hybridization showed complex changes with gains of 7q32.1-qter, 11q22.3-qter, and Xq28 and losses of 6q13–16.1, 15q14–22.3, and 17p (40). The gene expression profile supports germinal centre B-cell cell-of-origin and some distinctive features. (41).

CCND1 Translocation: t(11;14) (q13; q32)

Cyclin D1 protein plays a critical role in cell cycle control. Cyclin D1 interacts with CD4/6 Kinases to promote inactivation of the retinoblastoma 1 protein (RB1) by phosphorylation. The formation of Prb1 leads to the E2 transcription factor dissociation, promoting the progression from the G1 to the S phase. Additional abnormalities may enhance this pathway in MCL, such as the loss of the CDKN2A locus on chromosome 9p.

T (11;14) (q13; q32), the hallmark of mantle cell lymphoma, places the CCND1gene under the control of the IGH locus. This translocation is identified in >95% of cases (42). The t (11;14) juxtaposes the immunoglobulin heavy-chain joining region in chromosome 14 to a region on 11q designated BCL1(B-cell lymphoma/leukemia1). A translocation involving CCND1 causes cell cycle deregulation, alteration in DNA damage response pathways, deregulation of survival, and apoptosis.

CCND1/IGH Dual Color Dual Fusion is designed to detect translocation t (11;14) (q13.3; q32.3). Fusion Probe is a mixture of an orange fluorochrome direct labeled CCND1 probe spanning the major translocation cluster (MTC) region upstream of CCND1 and a green fluorochrome direct labeled IGH probe spanning the breakpoint cluster region of IGH.

Mantle cell lymphoma (MCL) is defined in the WHO classification as a B-cell neoplasm composed of monomorphic small to medium-sized lymphoid cells with irregular nuclei that morphologically resemble centrocytes but often have less irregular nuclear contours. This neoplasm is characterized by 11q13 translocations and rearrangement of the BCL1 region, leading to an overexpression of Cyclin D1. MCL represents 2.5% to 10% of all NHL and occurs in older men with a median of 60 years. Extranodal involvement is frequent in MCL.

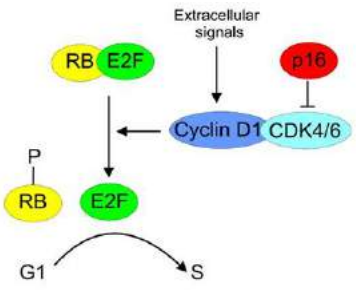

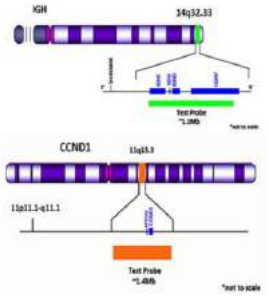

Fig.12 Cyclind1 pathway (breast cancer 2013) ***Fig.13 t (11;14)(q13;q32)***

MALT TRANSLOCATION: t (11;18)

MALT lymphoma is characterized by various genetic abnormalities, including trisomies of 3,12 and 18 and the specific chromosomal translocations t (11;18) (q21; q21), t (1;14) (p22; q32) and t (14;18) (q32; q21).

The translocation (11;18) involves the API2 and MALT1 genes and generate a functional API2-MQLT1 fusion product. The other translocations juxtapose the BCL10 and MALT1 genes, respectively, to the Immunoglobulin gene locus in 14q32, leading to deregulated expression of the oncogene. These translocations cause the activation of the Nf-kB pathway**.** The t (11;18) can be detected by the FISH assay.

MALT lymphoma is a disease characterized by small B cells and small lymphocytes infiltration. The onset of MALT lymphoma is often preceded by chronic inflammation due to infection of Helicobacter pylori in a high portion of cases. MALT lymphoma accounts for 7% to 8% of all B-cell lymphomas and at least 50%of primary gastric lymphomas. It occurs in adults with a median age of 61 years and a slight female predominance that is most marked in salivary gland and thyroid MALT lymphomas.

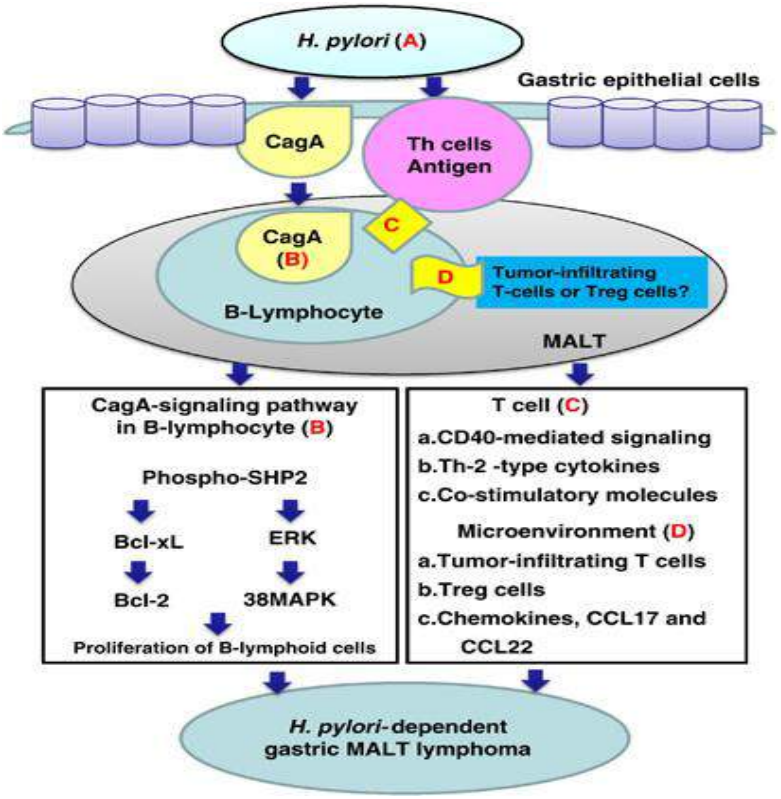

Fig.14 pathway in MALT lymphoma (Blood Cancer Journal 2013)

NPM- ALK : t(2;5)(p23;q35)

The t (2;5) (p23; q35) is the most common translocation in anaplastic lymphoma kinase ALK-positive, a neoplasm common in younger patients. The t (2;5) uses the nucleophosmin NPM on 5q35 with ALK gene at 2p23, forming a fusion pattern that determines the localization of the fusion protein in the cell. ALK is an orphan receptor protein-tyrosine kinase that was more fully characterized in 1997(43). ALK participates in embryonic nervous system development, but its expression decreases after birth. ALK is a member of the insulin receptor superfamily and is most closely related to leukocyte tyrosine kinase (Ltk), a receptor protein-tyrosine kinase. Twenty different ALK-fusion proteins have been described that result from various chromosomal rearrangements, and they have been implicated in the pathogenesis of several diseases, including anaplastic large-cell lymphoma (ALCL), diffuse large B-cell lymphoma, and inflammatory myofibroblastic tumors.

ALK rearrangement can be evaluated by Interphase FISH, using a break-apart probe that detects centromeric and telomeric regions of the ALK gene on chromosome 2.

About 70–90% of ALCL cases (ALK+ and ALK-) show clonal rearrangement of the TCR genes irrespective of the T-cell antigen status (44). TCR clonality supports a diagnosis of ALK-ALCL in cases showing the appropriate morphology, the expression of CD30, and a “null” phenotype (44-45). ALCL is a subtype of CD30+ large T-cell lymphoma (TCL) that comprises ~2% of all adult NHLs. Based on the presence/absence of the rearrangement and expression of anaplastic lymphoma kinase (ALK), ALCL is divided into ALK+ and ALK-, and both differ clinically and prognostically.

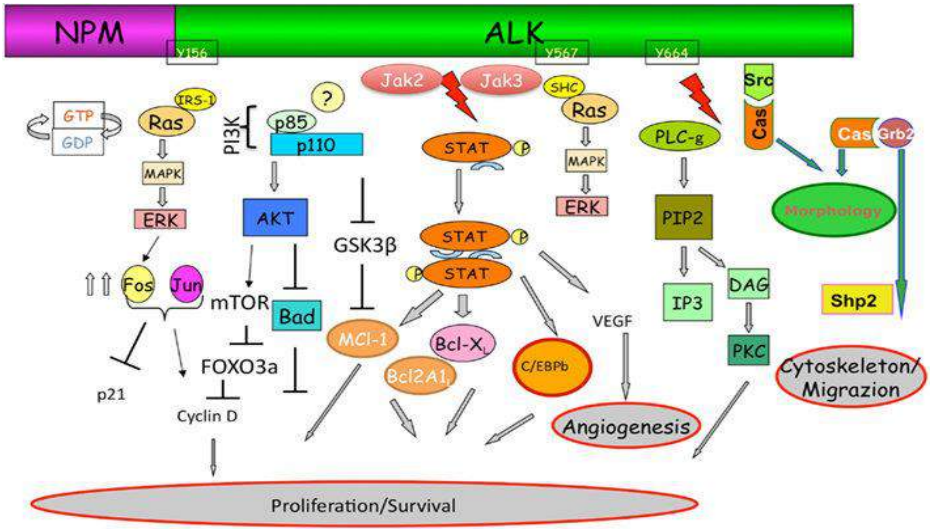

Fig.15 NPM/ALK translocation in ALCL (Frontiers of oncology 2014)

11q ABERRATION

Burkitt lymphoma (BL) is a well-defined aggressive B-cell lymphoma with rearrangements characteristically involving MYC and the immunoglobulin (IG) heavy t (8;14) or, more rarely, light chain loci t(2;8) and t(8;22). The term Burkitt like lymphoma with 11q (BLL-11q) aberration has emerged as a new provisional diagnostic entity in the Revised 4th Edition of the WHO Classification of Tumors of Haematopoietic and Lymphoid Tissues to describe cases morphologically resembling BL that have unique clinical, cytogenetic, and molecular features (46).

BLL,11q subsequently classified as Large B-cell lymphoma with 11q aberration (LBCL-11q) *is a* subset of high-grade B-cell lymphomas morphologically and phenotypically similar to BL but without its peculiar t (8;14). Lymphomas with the typical 11q-gain/loss pattern seem to have more frequent nodal presentation than BL from patients younger than 40 years (47). It is cytogenetically characterized by a peculiar pattern consisting of a gain in 11q23.2-23.3 and a telomeric loss in 11q24.1-qter. The study of Ferreiro et al. detected overexpression of USP2, CBL, and PAFAH1B2 oncogenes located in the gained 11q23.3 region and simultaneous down-regulation of TBRG1, EI24, and ETS1 tumor suppressor genes mapped in the lost 11q24q25 region (48-49). As the identification of patients with 11q gain/loss aberration is clinically important but cytogenetically changing, Interphase FISH assay, using a probe to target the minimal region of gain and loss defined at 11q23.3 and at 11q24.1-q25, respectively, is a valuable diagnostic tool to evaluate both post-transplant and immunocompetent Burkitt and Burkitt-like lymphoma patients. The 11q-gain/loss pattern in high-grade B-cell lymphoma is significantly more frequent in lymphoma occurring in the setting of transplantation and immunosuppression than in immunocompetent patients: therefore, suggesting that immunosuppression may favour its formation.

Havelange et al. published cases of MYC-positive high-grade B-cell lymphomas, not otherwise specified (HGBL, NOS) categories with 11q aberrations, including one case with 11q-gain/loss, suggesting that 11q aberration might not be specific for this new entity of mature B-cell lymphoma (50).

Additionally, gains/amplifications of 11q22-11q24 can be seen in 8–15% of DLBCL and GC-derived *IRF4*-translocation-positive lymphomas **(**47**).** Therefore, assessment of morphology and immunophenotype remains paramount for recognizing this rare entity.

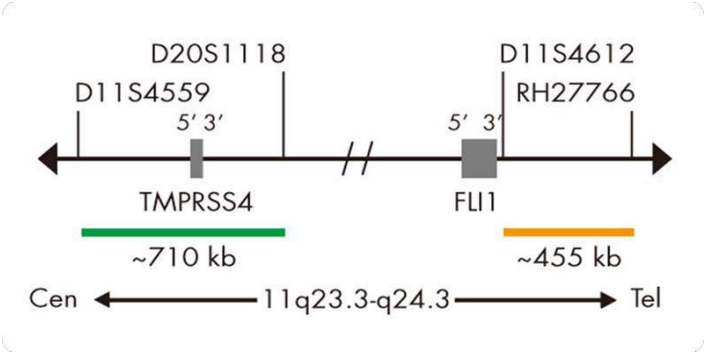

Fig.11 map of chromosome 11, FISH probe SPEC 11q gain/loss

AIM OF THIS STUDY

This study aims to standardize the Interphase FISH technique for diagnosing lymphoma in association with immunophenotypic features. We examined MYC protein expression scoring and its impact on the prognosis of aggressive B-cell lymphoma patients, investigating the relation between MYC-IHC and MYC gene alterations. Our group showed that immunohistochemistry (IHC) for MYC is highly reproducible when cut-off values of >70% are used. FISH currently represents the gold standard for identifying rearrangements, but it cannot detect genetic deregulation affecting gene expression at transcriptional and post-transcriptional levels that might result in protein overexpression and neoplastic transformation. Our results support the role of MYC protein as the active trigger of the MYC-mediated oncogenic effects since protein expression levels likely represent a more direct measure of the activity of a particular gene, and MYC-IHC should be undertaken in all cases.

We studied some Burkitt lymphoma (BL) cases lacking MYC protein expression despite the MYC gene's translocation. Based on this peculiarity, we identified two sub-groups of MYC protein negative BL: one lacking detectable MYC protein expression but presenting MYCN mRNA and protein expression; the second characterized by the lack of both MYC and MYCN proteins but showing MYC mRNA. These sub-groups presented a different pattern of SNVs affecting MYC gene family members that may induce the switch from MYC to MYCN. It is conceivable that MYCN determined molecular effects in transcriptional regulation, similar to those exerted by MYC in BL cells thanks to a cross-talk between the two genes involving a significant number of targets shared by MYC and MYCN.

Our group diagnosed particular lymphoma cases phenotypically similar to BL but without t (8;14), classified as LBCL-11q. Among these cases, we report a 25-year-old patient developing Burkitt like lymphoma with 11q aberration after kidney transplant in childhood and presenting with simultaneous papillary renal cell carcinoma. We performed FISH to evaluate gain in 11q23.3q24.1 and loss in 11q24.1q25 both on lymph node and renal cell carcinoma. Interphase FISH detected the peculiar 11q pattern only in the lymph node. Array-based copy number analyses, in line with FISH, revealed the amplification of 11q23.3q24.1 and loss localized in the 11q24.1q25 region. In renal cell carcinoma, both FISH both Array-copy number reported only the gain on whole chromosome 11.

Finally, we have standardized ImmunoFISH, a technique which combines conventional double immunofluorescence with standard FISH technique. Recently we observed a case of a 79-year-old man with multiple lymphadenopathies. Lymph node biopsy showed two lymphoid cell populations: the major component was CD3+, CD5+, CD10+ and Tdt+ with 80% of ki67; while, the minor lymphoid cell population was CD20+, PAX5+, CD5+, SOX-11+ and CYCLIN-D1+ with 30% of ki-67.

The combination of immunolabeling for CD3 and Interphase FISH with IGH/CCND1 Dual Fusion probe, allowed us to identify t (11;14) in both lymphoid populations: mantle cell B lymphoma phenotype and lymphoblastic T cell phenotype. This case may represent a T-lymphoblastic transformation of Mantle Cell lymphoma, probably due to methylation of PAX-5, and is the first case reported in the literature showing this phenotype and cytogenetic alterations.

We applied double Immunofluorescence in HL, a type of lymphoma characterized by a small number of putative malignant cells, the mononuclear Hodgkin, and multinucleated Reed Sternberg cells. These cells usually comprise less than 2% of the tumor mass, among a background of lymphocytes, plasma cells, histiocytes, neutrophils, eosinophils, and stromal cells. One of the major characteristics of these cells is the occurrence of complex and hyperdiploid chromosomal aberrations that reflect chromosomal instability and aberrant spindle mitotic fuse. To identify morphological alterations of mitotic fuse, we used alpha-tubulin acetylated and gamma-tubulin antibodies, which target respectively microtubules and centrosome, to determine the presence of atypical mitotic spindles.

PAPER I: MYC protein expression scoring and its impact on the prognosis of aggressive B-cell lymphoma patients

PAPER II: Molecular switch from MYC to MYCN expression in MYC protein negative Burkitt lymphoma cases

PAPER III (work in progress): Molecular features of simultaneous Large B-cell lymphoma with 11q aberration and papillary renal carcinoma occurring after pediatric kidney transplant

PAPER IV (work in progress): Precursor T-Lymphoblastic Transformation of Mantle Cell Lymphoma

PAPER V (work in progress) : Chromosomal instability in Hodgkin Lymphoma

DISCUSSION

Lymphomas are a group of hematologic malignancies originating from lymphoid cells and may have heterogeneous outcomes and variable responses to the standard of care regimens, and the prognosis depends on the histologic type, clinical factors and cytogenetic characteristics. Genomic alterations, including deletions, inversions, chromosomal translocations, and reinsertion of DNA segments (excised during normal V(D)J recombination) may occur during lymphocyte development due to heavily DNA rearrangement. These events can activate oncogenes, inactivate tumor suppressor genes, and trigger pathways implicated in cell-cycle and DNA damage repair.

In this study, we focused on the standardization of Interphase FISH, the gold standard technique for identifying rearrangements in Lymphomas.

During the FISH analysis, we remember several factors: be aware of the architecture of the tissue, time of fixation, the presence of truncated nuclei, and the complex nature of genetic arrangements seen in some lymphoid neoplasm. The complete hybridized area should be screened for the presence of subclonal changes that might be of diagnostic and prognostic importance. FISH signals should be assessed, looking for areas with bright, distinct signals and low backgrounds that distinguish individual nuclei. When we use break-apart probes, a nucleus with one fused (normal-table 1) and one single-color signal suggests the presence of gene rearrangement (table 2). Similarly, using a dual-fusion probe, a nucleus with two single-color (normal-table3) signals accompanied by only one fused signal would also suggest the presence of a translocation (table 4) in a cell that has lost one fused sequence by tissue sectioning (this may also occur because of a chance co-localization of red and green signals in a normal cell). When evaluating samples, it is also important to consider the possibility that signals are lost due to a chromosomal loss rather than a cell truncation.

MYC has a relevant role in the development of lymphomas. MYC genetic alteration is typical in BL, and it is described in approximately 5 to 15% of DLBCL cases, correlates with worse prognosis and poor response to R-CHOP treatment (28). Accurate detection of MYC gene rearrangement, and its protein expression, has become increasingly important for its diagnostic and consequent therapeutic implications in DLBCL. For this, we have investigated the possible MYC protein expression cut off with the predictability of gene translocation. Our group showed that immunohistochemistry (IHC) for MYC is highly reproducible when cut-off values of >70% is used (51).

When using the threshold of MYC-IHC ≥80% in BL and ≥70% in non-BL, around 99% BL and 88% non-BL cases with MYC rearrangements can be predicted. Therefore, considering the high correlation between MYC gene rearrangement and MYC protein expression in BL, the FISH analysis could

theoretically be limited to cases with atypical morphology and/or immunophenotype and MYC-IHC <80%. In non-BL, a cut-off of MYC-IHC ≥70% would identify cases at a higher probability of MYC rearrangement. However, it should be noted that roughly 10% of HGDH have a lower expression of MYC; in these cases, FISH should be recommended. FISH currently represents the gold standard for identifying rearrangements, but it cannot detect genetic deregulation affecting gene expression at transcriptional and post-transcriptional levels that might result in protein overexpression and neoplastic transformation. Considering the high correlation between MYC gene rearrangement and MYC protein expression in BL, the FISH analysis could theoretically be limited to cases with atypical morphology and/or immunophenotype and MYC-IHC <80% (51).

In correlation to the complexity of the MYC gene, we described two sub-groups of MYC protein negative BL: one lacking detectable MYC protein expression but presenting MYCN mRNA and protein expression; the second characterized by the lack of both MYC and MYCN proteins but showing MYC mRNA. The two sub-groups presented a different pattern of SNVs affecting MYC gene family members that may induce the switch from MYC to MYCN. It is conceivable that MYCN determined molecular effects in transcriptional regulation, similar to those exerted by MYC in BL cells thanks to a cross-talk between the two genes involving a significant number of targets shared by MYC and MYCN (52). Our results identified two sub-groups of MYC protein negative BL: one lacking detectable MYC protein expression but presenting MYCN mRNA and protein expression; the second characterized by the lack of both MYC and MYCN proteins but showing MYC mRNA.

A particular lymphoma that is phenotypically similar to BL but without t (8;14), is Large B-cell lymphoma with 11q aberration. This entity is frequent in young people, in particular in post-transplants patients. Among cases with 11q aberration analyzed, we report the case of a 25- year- old patient developing Burkitt-like lymphoma with 11q aberration after kidney transplant in childhood and presenting with simultaneous papillary renal cell carcinoma of the kidney. We performed FISH to evaluate gain in 11q23.3q24.1 and loss in 11q24.1q25 both on lymph node and renal cell carcinoma (table 5); array-copy based analysis was performed in another center. MYC rearrangement was negative in both samples. In lymph-node, FISH in line with Array-based copy number analyses showed amplifications in 11q23.3q24.1 and loss in 11q24.1q25, whereas a gain of whole chromosome 11 was shown in the papillary Renal cell carcinoma. These results confirm that similar to classical Burkitt lymphoma, a subgroup of immundeficiency-related mnBLL,11q exists besides supposedly sporadic cases.

For a correct lymphoma diagnosis, it is necessary to correlate immunophenotype data with genetic alterations. In light of this and considering the complexity of lymphomas, we performed ImmunoFISH, a method to detect, at the same time, immunolabeling and cytogenetic alterations.

Fixation and preparation techniques were optimised to best preserve nuclear morphology and protein epitopes without the need for any antigen retrieval. We also report a case of 79- a year-old man with a history of atrial fibrillation presenting with progressive fatigue and dyspnea. PET-CT identified multiple lymphadenopathies localized in the anterior mediastinum. Bone marrow biopsy showed a lymphoid infiltrate composed of small to medium-sized cells with irregular nuclear contours. Lymph node biopsy showed two different lymphoid populations: the major was CD3+, CD5+ CD10+, PAX5- and Tdt+ with 80% of ki67 while the minor was: CD5+, CD19+, CD20+, CYCLIN-D1+, BCL2+, PAX5+ and 30% of ki-67. FISH analysis with Dual Fusion for IGH/CCND1 was performed, revealing the t (11;14) in both lymphoid population cells**.**

The combination of immunolabeling for CD3 and Interphase FISH with IGH/CCND1Dual Fusion probe, allowed us to identify t (11;14-table 6) in both lymphoid populations: mantle B cell lymphoma phenotype and lymphoblastic T cell phenotype. This case may represent a T-lymphoblastic transformation of Mantle Cell lymphoma, probably due to methylation of PAX-5, a key regulator in the development and differentiation of B-cell (53-54).

We also applied Double Immunofluorescence in HLs to study chromosomal instability in CD30+ cells and morphological alterations of the mitotic spindle, using gamma-tubulin and Acetylated alpha-tubulin antibodies. Gamma-tubulin in CD30+ cells showed a granular pattern, probably because of their genetic instability than the surrounding microenvironment, whose expression was point-like. Acetylated alpha-tubulin showed a filamentous distribution limited to HRS. Atypical and not polarized mitotic fuses, characterized by three centrosomes, are not standard in all HLs examined.

CONCLUSION

Cytogenetic analysis of lymphomas is essential to identify recurring translocations and establishing the principle that translocations cause deregulation of genes at the breakpoints, leading to aberrant cell function and initiation of neoplastic proliferation. Genetic analysis is a powerful approach to resolve the biological complexity of tumors and gain insights into their behaviour, leading to a better understanding of disease and better patient management. Cytogenetic data must be integrated with clinical and immunophenotypic data to correct the classification of lymphoma and correct patient management.

TABLE 1: an example of a case of LNH from routine diagnostics in which, using a break-apart probe, we observed co-localization of red and green signals (63X magnification), indicative of the normal gene status.

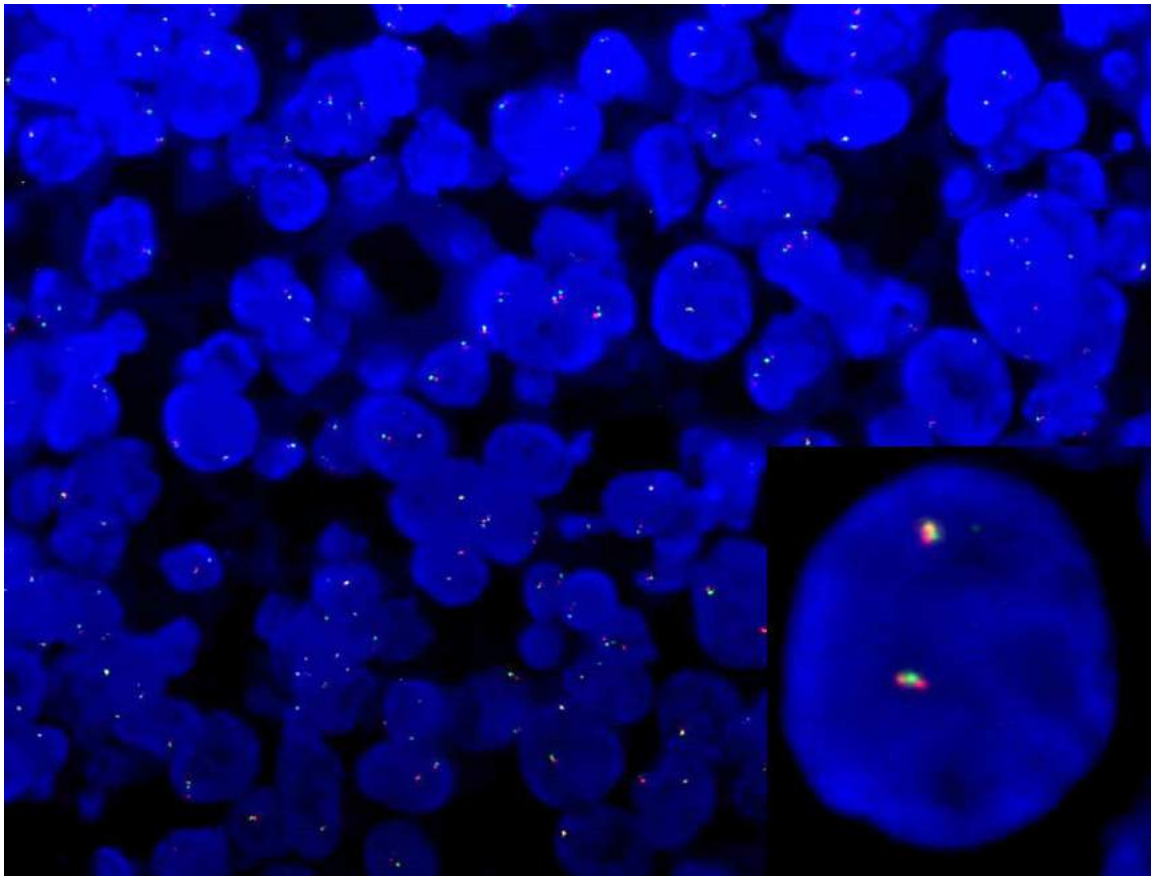

TABLE 2: a routine diagnostic case of LNH with rearrangement. We can notice one signal of fusion (yellow) and one single red and gren (63x magnification)

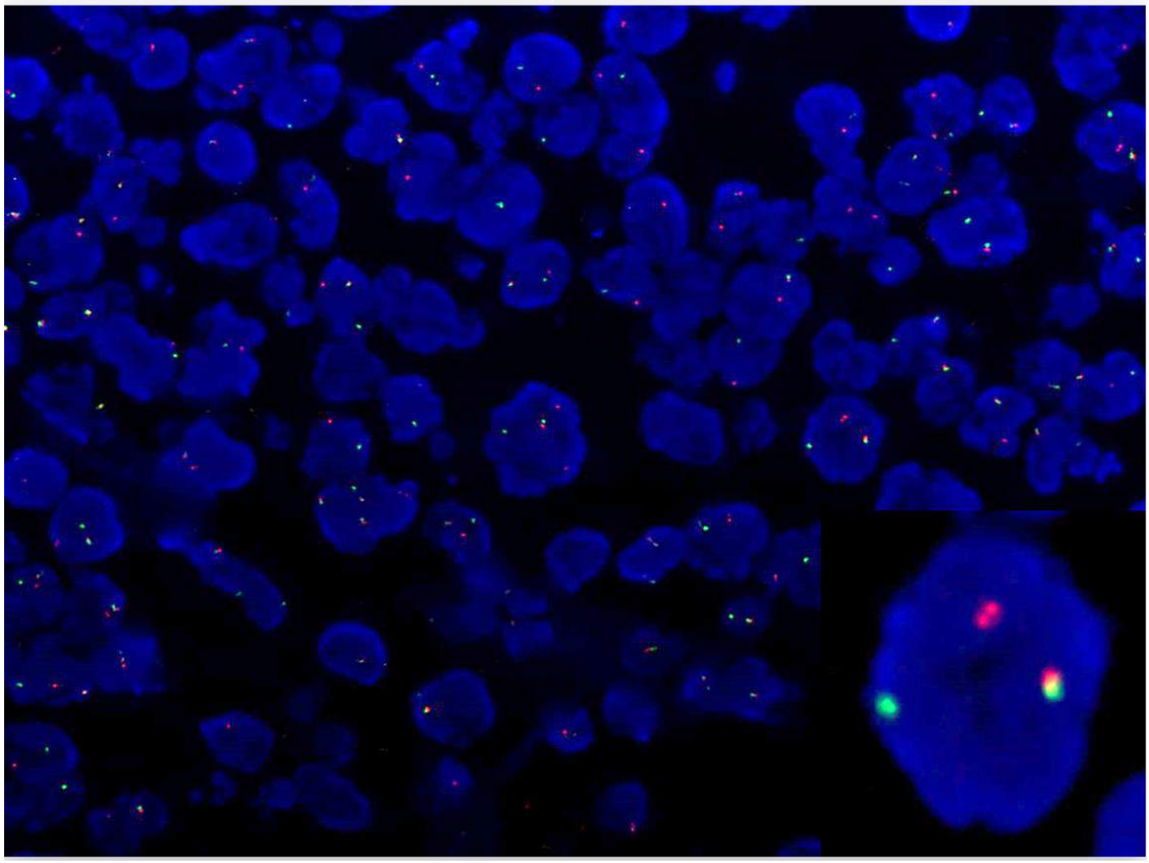

TABLE3: a routine diagnostic case of LNH in which we use dual-fusion probe. We observe nuclei with two single-color that suggest a pattern of normality (63x magnification).

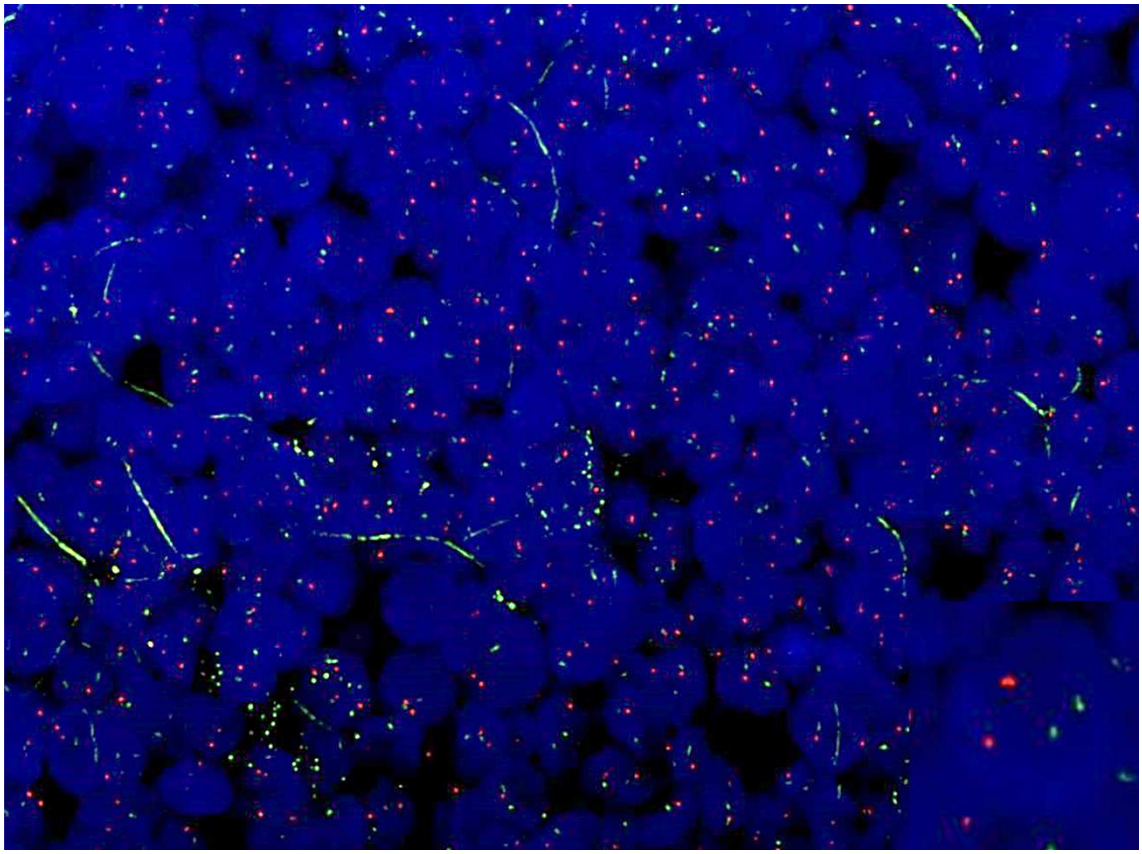

TABLE 4: a routine diagnostic case of LNH in which we use a dual-fusion probe displaying some nuclei with one fusion and two single-color that suggest a pattern of translocation (63x magnification).

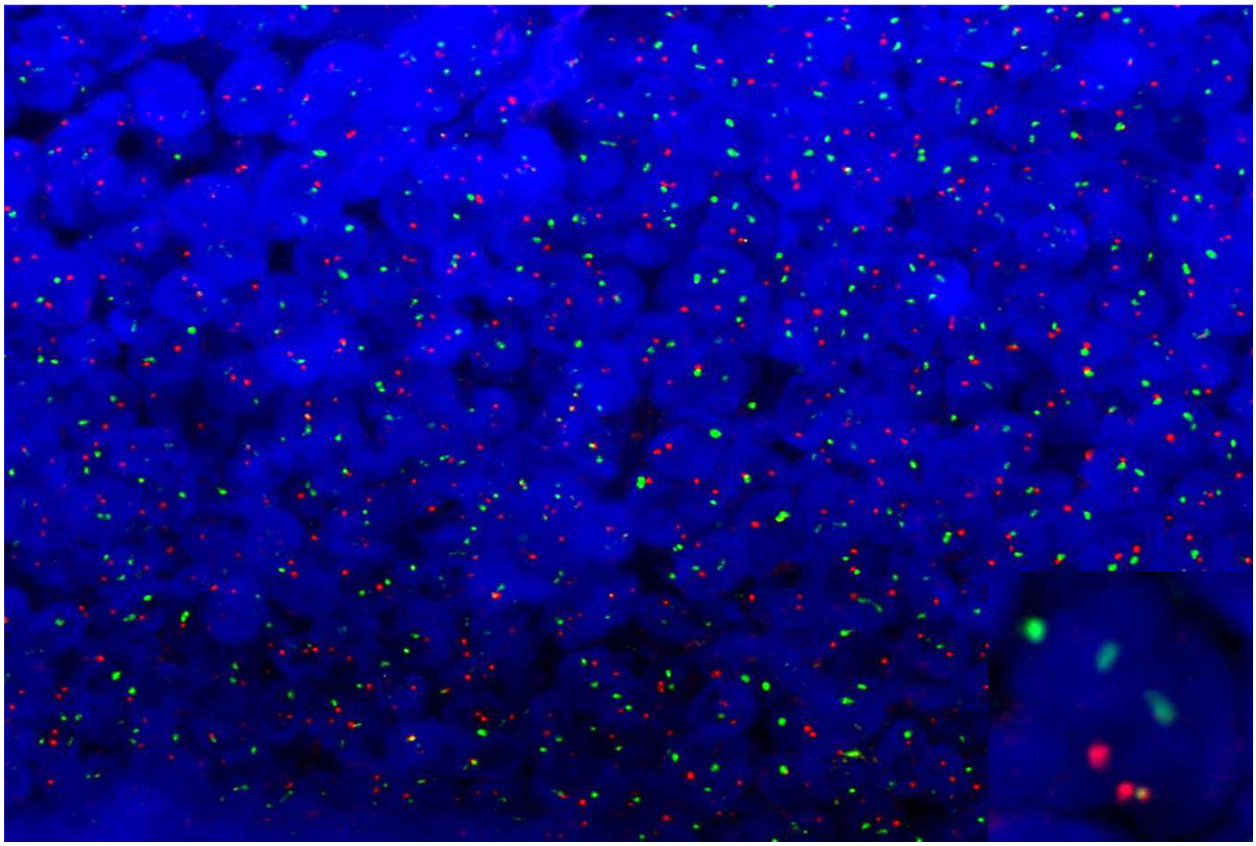

TABLE 5: 11q evaluation

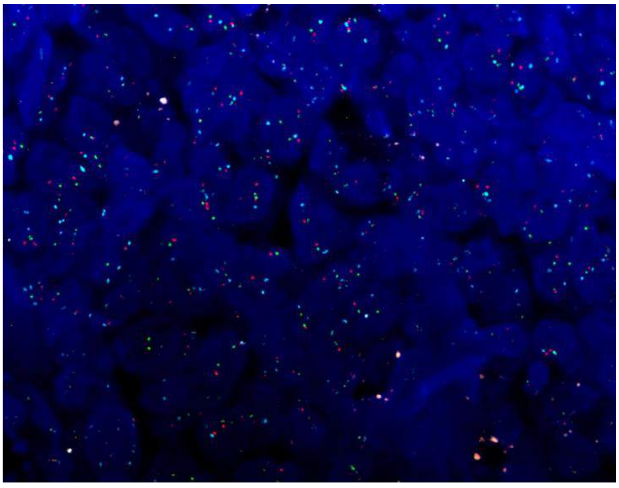

11q gain/loss: normal pattern with 2 signals of MGR (green), 2 signals of MLR (orange) and 2 signals of CEP11 (blu). (63x magnification)

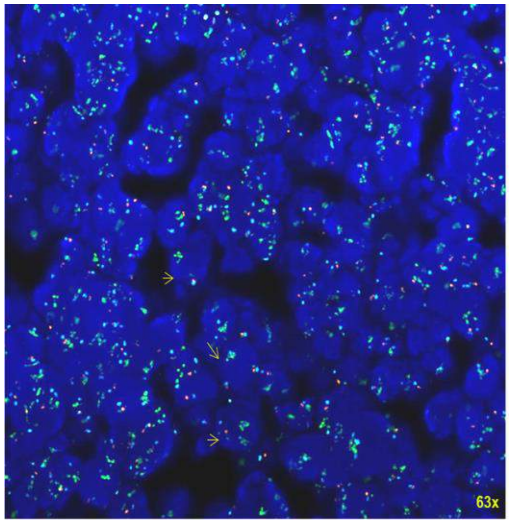

Biopsy of cervical lymph node: FISH using 11q gain / loss triple color probes showed 3 to clustered green signals in the 11q23.3 region but only one orange signal in the 11q24. 3 region, confirming the presence of the typical loss pattern of gain 11q.

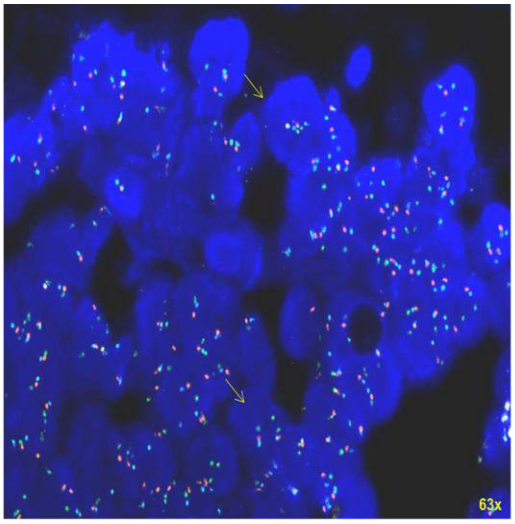

Papillary carcinoma: FISH using 11q gain/loss triple color probes showed 2 to 3 green signals in the 11q23.3 region, 2 to 3 orange signals in the 11q24. 3 region and 2 to 3 blu signals in the 11p11.1-q11 region.

TABLE 6: t (11;14) in B-cells and in T-cells

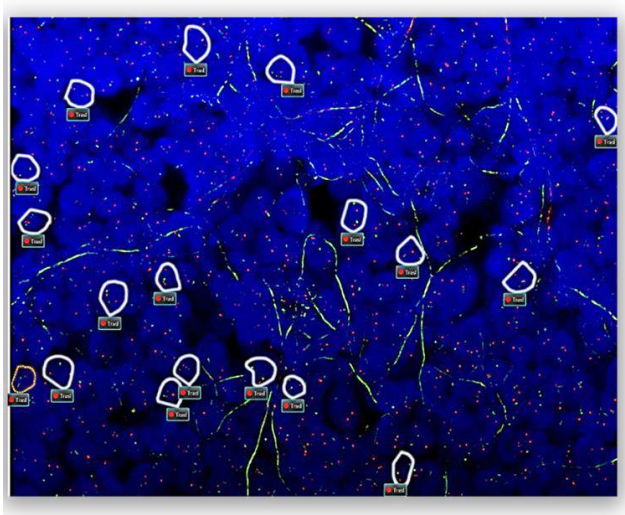

B-CELL POPULATION (63X magnification)

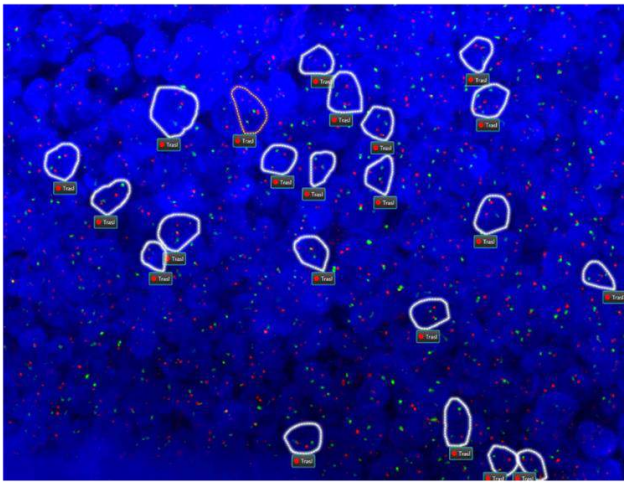

T-CELL POPULATION (63X magnification)

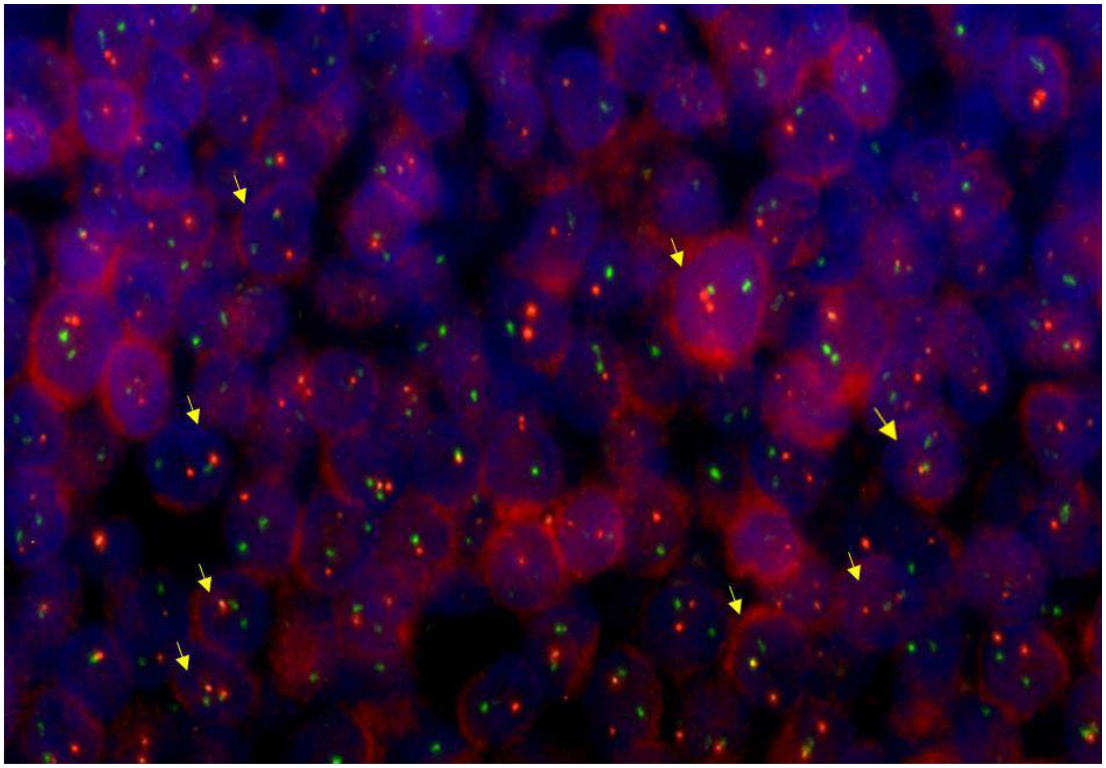

ImmunoFISH for CD3 (red) and IGH/CCND1 (63x magnification)

TABLE 7: atypical mitosis in HL

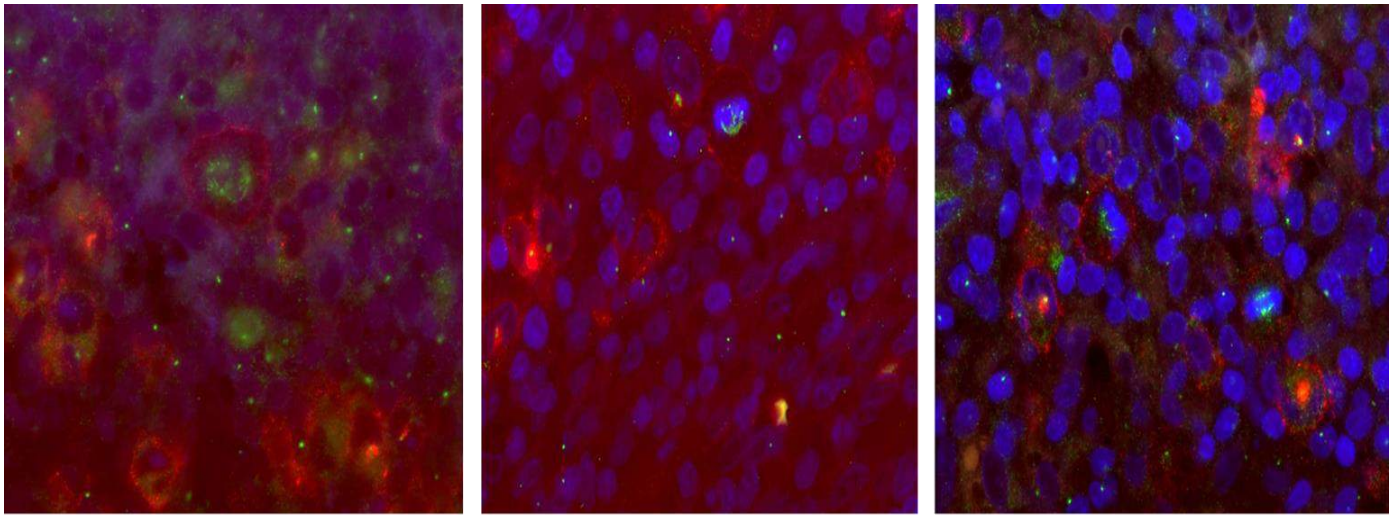

Immunofluorescence for CD30 and gamma tubulin

TABLE 8: typical mitotis in HL

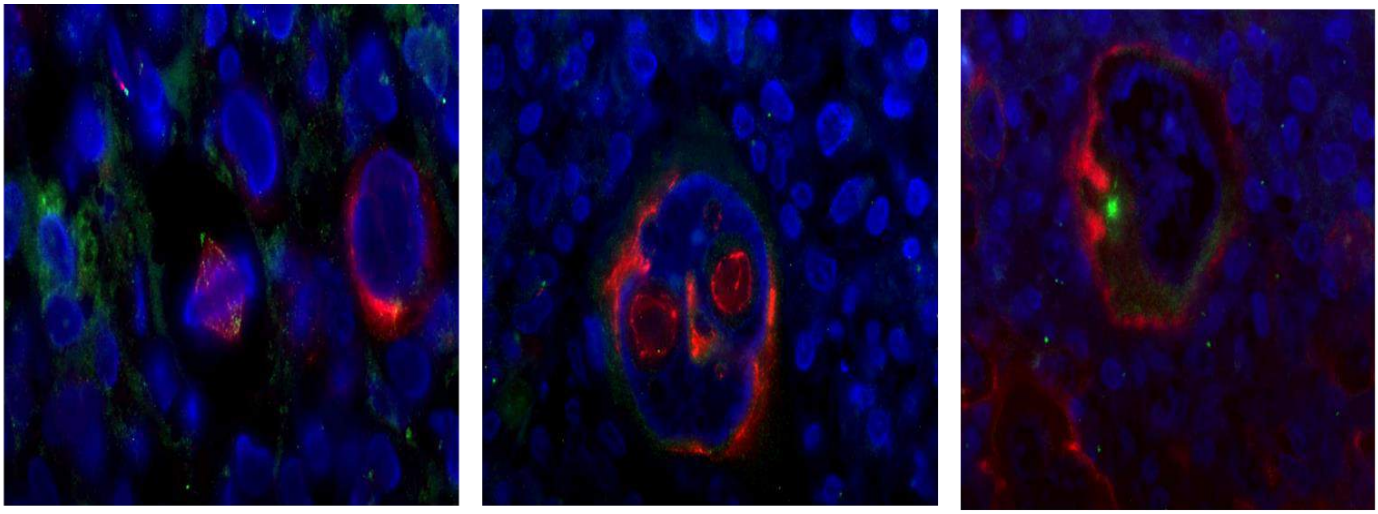

IF for gamma tubulin (green) and alpha tubulin (red), shows typical mitotic fuse. (63x magnification)

Immunofluorescence for CD30 and gamma tubulin

REFERENCES

1. Edelman GM; Antibody structure and molecular immunology; Science 1973.
2. Yong-Jun Liu et al; Sites of specific B cell activation in primary and secondary responses to T cell-dependent and T cell-independent antigens; Immunology 1991.
3. MacLennan C.; Germinal centers; Immunol 1994.
4. Taher E. et al; Intracellular B Lymphocyte Signalling and the Regulation of Humoral Immunity and Autoimmunity; Clinic Rev Allerg. Immunol 2017.
5. Hozumi N. et al; Evidence for somatic rearrangement of immunoglobulin genes coding for variable and constant regions. Proc Natl Acad Sci USA 1976.
6. Bassing CH. et al; The mechanism and regulation of chromosomal V(D)J recombination. Cell 2002.
7. Schatz DG. et al; V(D)J recombination: mechanisms of initiation. Annu Rev Genet 2011.
8. Busslinge Meinrad; Transcriptional control of early B cell development. Annu Rev Immunol 2004.
9. Oettinger M A et al; RAG-1 and RAG-2, adjacent genes that synergistically activate V(D)J recombination; Science 1990.
10. Gellert Martin; V(D)J recombination: RAG proteins, repair factors, and regulation; Annu Rev Biochem 2002.
11. Herzog Sebastian at al; Regulation of B-cell proliferation and differentiation by pre-B-cell receptor signalling; Nat Rev Immunol 2009.
12. Davis A C, et al; IgM-molecular requirements for its assembly and function; Immunol 1989.
13. Sarafova Sophia et al; Modulation of Coreceptor Transcription during Positive Selection Dictates Lineage Fate Independently of TCR/Coreceptor Specificity; Immunity 2005.
14. Skibola Christine F. et al; Genetic Susceptibility to Lymphoma; Haematologica 2007.
15. De Leval et al; Lymphoma Classification; The Cancer Journal 2020.
16. Jiang Manli et al; Lymphoma classification update: T-cell lymphomas, Hodgkin lymphomas, and histiocytic/dendritic cell neoplasms; Expert Rev Hematol. 2018.
17. Global Cancer Observatory: Cancer Today. Lyon, France: International Agency for Research on Cancer 2019.
18. Rodney R. et al; Molecular genetics of childhood, adolescent and young adult non-Hodgkin

lymphoma; Br J Haematol. 2016.
19. Heim S, et al. Cancer Cytogenetics, Wiley-Liss, 1995
20. Steven H; The 2016 revision of the World Health Organization classification of lymphoid neoplasms.
21. Pardue ML. et al; Molecular hybridization of radioactive RNA to the DNA of cytological preparations. Proc Natl Acad Sci; 1969.
22. Shakoo Rauf Abdul. Fluorescence In Situ Hybridization (FISH) and its application, chromosome structure and aberrations; 2017.
23. Saxe DF, et al. Cytogenetics Resource Committee of the College of American Pathologists. Validation of fluorescence in situ hybridization using an analyste-specific reagent for detection of abnormalities involving the mixed lineage leukemia gene. Arch Pathol Lab Med. 2012.
24. Wan TS, et al. Complex cytogenetic abnormalities in T-lymphoblastic lymphoma:resolution by spectral karyotyping. Cancer Genet Cytogenet. 2000.
25. Ma SK, et al. Trisomy 8 as a secondary genetic change in acute megakaryoblastic leukemia associated with Down's syndrome; Leukemia 1999.
26. Ma SK, et al; Characterization of additional genetic events in childhood acute lymphoblastic leukemia with TEL/AML1 gene fusion: a molecular cytogenetics study; Leukemia 2001.
27. Roland A. Ventura et al; FISH Analysis for the Detection of Lymphoma-Associated Chromosoma Abnormalities in Routine Paraffin-Embedded Tissue; the journal of molecular diagnostic 2006.
28. Valera Alexandra et al. Definition of MYC genetic heteroclonality in diffuse large B-cell lymphoma with 8q24 rearrangement and its impact on protein expression; Modern Pathology 2016.
29. Salaverria I., et al. A recurrent 11q aberration pattern characterizes a subset of MYC negative high-grade B-Cell lymphomas resembling burkitt lymphoma; Blood; 2014.
30. Dayang Sharyati Datu Abdul Salam et al. C-MYC, BCL2 and BCL6 Translocation in B-cell Non-Hodgkin Lymphoma Cases; Journal of Cancer 2020.
31. Vega F, et al; Chromosomal translocations involved in non-Hodgkin lymphomas; Arch Pathol Lab Med. 2003.
32. Iqbal J, et al; BCL2 expression is a prognostic marker for the activated B-cell-like type of diffuse large B-cell lymphoma; J Clin Oncol. 2006.
33. Wlodarska I, et al; Frequent occurrence of BCL6 rearrangements in nodular lymphocyte predominance Hodgkin lymphoma but not in classical Hodgkin lymphoma; Blood 2003.
34. Chong Lauren C. et al; High-resolution architecture and partner genes of MYC rearrangements in lymphoma with DLBCL morphology; Blood 2018.

35. Aukema SM, et al. Double-hit B-cell lymphomas; Blood 2011.
36. Ott G, et al. Understanding MYC-driven aggressive B-cell lymphomas: pathogenesis and classification; Blood 2013.
37. Lin P, et al. Prognostic value of MYC rearrangement in cases of B-cell lymphoma, unclassifiable, with features intermediate between diffuse large B-cell lymphoma and Burkitt lymphoma; Cancer 2012.
38. Li S, et al. B-cell lymphomas with MYC/8q24 rearrangements and IGH/BCL2 (14;18) (q32; q21): an aggressive disease with heterogeneous histology, germinal center B-cell immunophenotype and poor outcome. Mod Pathol. 2012.
39. Swerdlow SH.et al; WHO Classification of Tumours of Haematopoietic and Lymphoid Tissues; IARC 2008.
40. Salaverria I.et al. High resolution copy number analysis of IRF4 translocation-positive diffuse large B cell and follicular lymphomas; Genes Chromosomes Cancer 2013.
41. Salaverria I. et al; Molecular Mechanisms in Malignant Lymphomas Network Project of the Deutsche Krebshilfe; German High-Grade Lymphoma Study Group; Berlin FrankfurtMünster-NHL Trial Group. Translocations activating IRF4 identify a subtype of germinal center-derived B- cell lymphoma affecting predominantly children and young adults; Blood 2011.
42. Jian-Yong Li et al; Detection of Translocation t (11;14) (q13; q32) in Mantle Cell Lymphoma by Fluorescence in Situ Hybridization; Am J Pathol. 1999.
43. Tsuyama Naoko et al; Anaplastic large cell lymphoma: pathology, genetics, and clinical aspects; J Clin Exp Hematop. 2017.
44. Foss H.D.et al. Anaplastic large-cell lymphomas of T-cell and null-cell phenotype express cytotoxic molecules; Blood 1996.
45. Xing X.,et al; Anaplastic large cell lymphomas: ALK positive, ALK negative, and primary cutaneous. Adv. Anat. Pathol. 2015.
46. Swerdlow SH. et al, WHO Classification of Tumours of Haematopoietic and Lymphoid Tissues. Revised 4th edition. Lyon: IARC, 2017.
47. Itziar Salaverria et al; A recurrent 11q aberration pattern characterizes a subset of MYC- negative high-grade B-cell lymphomas resembling Burkitt lymphoma; lymphoid neoplasia 2014.
48. Ferreiro JF.et al; Post-transplant molecularly defined Burkitt lymphomas are frequently MYC-negative and characterized by the 11q-gain/loss pattern. Haematologica 2015.
49. Grygalewicz Beata et al; The 11q-Gain/Loss Aberration Occurs Recurrently in MYC-Negative Burkitt-like Lymphoma with 11q Aberration, as Well as MYC-Positive Burkitt Lymphoma and MYC-Positive High-Grade B-Cell Lymphoma, NOS; Am J Clin Pathol 2018.

50. Havelange V, et al. The peculiar 11q-gain/ loss aberration reported in a subset of MYC-negative high-grade B-cell lymphomas can also occur in a MYC-rearranged lymphoma; Cancer Genet. 2016.
51. Granai Massimo et al; MYC protein expression scoring and its impact on the prognosis of aggressive B-cell lymphoma; blood 2018.
52. Mundo Lucia et al; Molecular switch from MYC to MYCN expression in MYC protein negative Burkitt lymphoma cases; Blood Cancer Journal 2019.
53. Zhang Xianglan et al; Pax5 expression in Non-Hodgkin's Lymphomas and Acute Leukemias;J Korean Med Sci 2003.
54. Lazzi S. et al; Rare lymphoid neoplasms coexpressing B- and T-cell antigens. The role of PAX-5 gene methylation in their pathogenesis; Human Pathology 2009.

MYC protein expression scoring and its impact on the prognosis of aggressive B-cell lymphoma patients

This study examined the reproducibility of MYC and BCL-2 immunohistochemical scoring as well as the impact of higher expression of both proteins (double expressor status, DE) on survival and progression in a large retrospective cohort of aggressive B-cell lymphoma patients treated with rituximab *plus* cyclophosphamide, doxorubicin, vincristine and prednisone (R-CHOP) or R-CHOP-like regimens with a median follow up of 67 months (range 0-138). We also investigated possible MYC protein expression cut offs with the highest reproducibility among pathologists and predictability of gene translocation. We showed that immunohistochemistry (IHC) for MYC and BCL-2 is highly reproducible when cut-off values of >70% for MYC and >50% for BCL-2 are used. This threshold not only predicts the presence of rearrangements (with respect to *MYC*), but is also clinically valuable. In fact, it identifies a subset of patients who are poor responders and who may benefit from alternate therapeutic strategies.

Several investigators have demonstrated that diffuse large B-cell lymphomas (DLBCL) with MYC and BCL-2 double expression (DE-LBCL) have adverse prognosis when treated by conventional immunochemotherapies.[1] Therefore, evaluation of MYC and BCL-2 protein expression by IHC is an important tool in the prognostic stratification of patients.[2] Although expression of MYC-IHC in ≥40% neoplastic cells and the BCL-2 in ≥50% have been indicated as prognostically significant cut offs in many reports, among hematopathologists, some disagreement about these thresholds remains.[3,4] Standardizing cut offs to define positivity for MYC-IHC and BCL-2-IHC with higher reproducibility and prognostic impact is thus highly desirable in order to optimize patient management.[5,6]

We analyzed 753 aggressive B-cell lymphoma patients. These included: Burkitt lymphomas (BL, n=223); DLBCL not otherwise specified (DLBCL-NOS, n=456); high grade B-cell lymphomas (HGBCL) with *MYC* and *BCL-2* and/or *BCL-6* rearrangement [HG double hit (HGDH), n=51, including 8 blastoid, 16 diffuse monomorphic and 27 intermediate morphology]; and HGBCL, NOS (n=23).[7-9] All cases belonging to these categories, except for BL, will be referred to hereon as non-BL. The following clinical data were collected for non-BL: sex, age at diagnosis, ECOG performance status, stage (Ann Arbor), lactate dehydrogenase (LDH) level, International Prognostic Index (IPI), bulky disease, extranodal *versus* nodal, bone marrow involvement. Original MYC-IHC and BCL-2-IHC slides were re-evaluated by 3 trained pathologists blinded as to the original scores. Although aware that immunohistochemical interpretation may be affected by technical issues, we intentionally decided not to re-stain all slides in only one laboratory, but instead to confront original slides from different laboratories which apply different unmasking procedures and use different clones on a "real-life" basis (Table 1). Scores were reported in 5% intervals rounded up to the nearest 10%. Any discrepancies in MYC-IHC and BCL-2-IHC scoring was resolved by consensus on a multi-head microscope until an agreement of >95% concordance was reached. Discrepancy was defined as 10% deviation. Our findings confirm that BCL-2-IHC scoring is highly reproducible across the different institutions and that a ≥50% cut off is reliably assessable [agreement >90%; k=0.97; standard error (SE):=0.018; 95% confidence interval (CI): 0.765-0.901]. On the contrary, scoring MYC-IHC staining was confirmed to be critical, mainly because of the variability of staining intensity, percentage of positivity, presence of necrosis and crush artifacts. Concordance was high only for MYC-IHC positivity >70%, while a larger discrepancy was observed in the range 40-69%[10] (Figure 1). The latter can have a crucial impact on clinical decision making

Table 1. Immunohistochemical and FISH analysis of MYC* and BCL-2* proteins and genes in the different institutions.

	MYC clone/source	MYC antigen retrieval/dilution	BCL-2 clone/source	BCL-2 antigen retrieval/dilution
Berlin	EP121, Epitomics, Germany	Pressure cooker, citrate buffer pH 6.0	124, Agilent, Germany	Pressure cooker, citrate buffer pH 6.0
Bologna	EP121, Epitomics, Milan	PT link 92°C /1:100	124, Agilent, Milan	PT link 90°C /1:100
Firenze	Y69, Roche, Milan	Ready to use	SP124, Roche, Milan	Ready to use
London	Y69, Abcam, UK	Ready to use	124, Dako, UK	PT link 90°C /1:100
Siena & Nairobi	Y69, Roche, Milan	Ready to use	SP124, Roche, Milan	Ready to use
	MYC BAP probe/source	**MYC FUSION probe/source**		**BCL-2 BAP probe/source**
Berlin	Split Signal MYC, Agilent, Germany	Dual fusion IGH/MYC, Zytomed, Germany		Splits Signal BCL-2, Agilent, Germany
Bologna	ZytoLight SPEC MYC Dual Color Break Apart Probe, Bio-Optica, ZitoVision GmbH, Germany	ZytoLight SPEC MYC/IgH Dual Color Dual Fusion Probe , Bio-Optica, ZitoVision GmbH, Germany		ZytoLight SPEC BCL-2 Dual Color Break Apart Probe, Bioptica, ZitoVision GmbH, Germany
Firenze	ZytoLight SPEC MYC Dual Color Break Apart Probe, Bio-Optica, ZitoVision GmbH, Germany	ZytoLight SPEC MYC/IgH Dual Color Dual Fusion Probe, Bio-Optica, ZitoVision GmbH, Germany		ZytoLight SPEC BCL-2 Dual Color Break Apart Probe, Bioptica, ZitoVision GmbH, Germany
London	Kreatech, Leica, UK	Kreatech, Leica, UK		Kreatech, Leica, UK

Siena & NairobiZytoLight SPEC MYC Dual Color Break Apart Probe, Bio-Optica, ZitoVision GmbH, Germany ZytoLight SPEC MYC/IgH Dual Color Dual Fusion Probe, Bio-Optica, ZitoVision GmbH, GermanyZytoLight SPEC BCL-2 Dual Color Break Apart Probe, Bioptica, ZitoVision GmbH, Germany. *On 4 m thick formalin-fixed paraffin-embedded sections; BAP: break-apart probe.

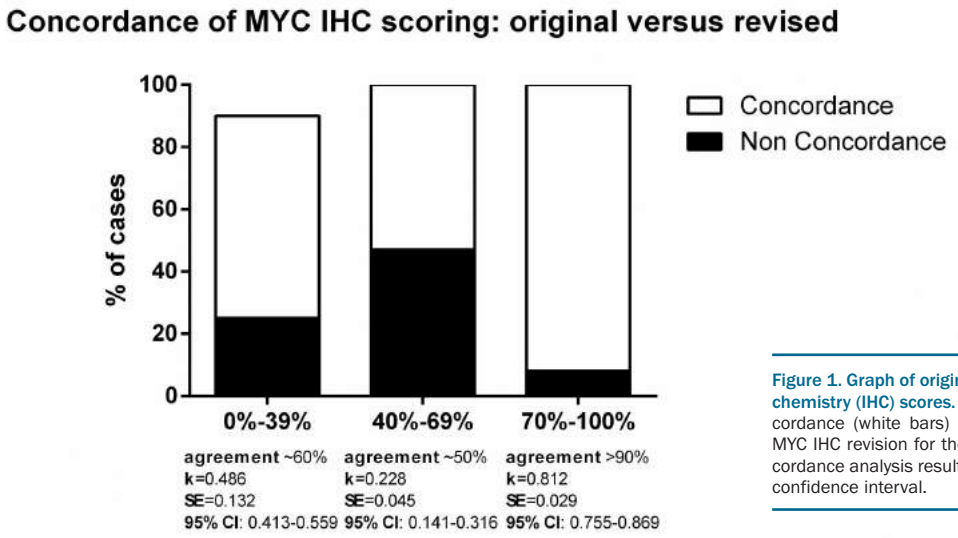

Figure 1. Graph of original and revised MYC immunohistochemistry (IHC) scores. The percentage of cases with concordance (white bars) or discordance (black bars) after MYC IHC revision for the three ranges is shown. The concordance analysis results are listed. SE: standard error; CI: confidence interval.

and patient care, as well as on the comparison between different studies. Therefore, we propose the threshold of MYC-IHC 70-100% to define non-BL cases with high expression of MYC and 0-39% to classify samples with low expression of MYC protein. Samples with MYC-IHC scores between 40% and 69% could not be categorized as MYC protein negative or positive with acceptable accuracy in routine practice and should be termed as cases with intermediate MYC expression. Moreover, we suggest scoring should preferably be defined on moderately to strongly stained nuclei and in hot spot areas, if present. After revision, in the non-BL series, prevalence of DE-LBCL as defined by the cut offs proposed by the literature (MYC-IHC ≥40% and BCL-2-IHC ≥50%) was 32% (n=176/530);[7] of these 100 showed MYC-IHC ≥70% (DE 70% in the following).

A second end point of this study was to investigate the relation between MYC-IHC and *MYC* gene alterations, trying to identify parameters potentially applicable in a value-for-money approach. When using the threshold of MYC-IHC ≥80% in BL and ≥70% in non-BL, around 99% BL and 88% non-BL cases with *MYC* rearrangements can be predicted. Therefore, considering the high correlation between *MYC* gene rearrangement and MYC protein expression in BL, FISH analysis could theoretically be limited to cases with atypical morphology and/or immunophenotype and MYC-IHC <80%. In non-BL, a cut off of MYC-IHC ≥70% would identify cases at higher probability of MYC rearrangement. However, it should be noted that roughly 10% of HGDH have a lower expression of MYC; in these cases, FISH should be recommended.[11]

The third end point was to perform a survival analysis in cases of HGDH, DE, nonDH/nonDE patients for whom overall survival (OS) and progression-free survival (PFS) data were available. HGDH lymphomas are known to be very aggressive neoplasms that do not respond to standard therapy and they have a dismal prognosis.[12] However, it has recently been reported that the adverse prognosis may be mitigated by other factors such as lack of BCL-2 protein, and absence/low MYC protein expression.[5] The clinical significance of MYC-IHC and BCL-2-IHC expression has been extensively studied but the results have not been consistent; hence, there is still no clear use for protein expression evaluation in the clinic.[13,14]

Univariate Cox analysis showed that the factors significantly associated with OS and PFS were: age [Odds Ratio (OR): 4.8% each year; confidence interval (CI): 1.03-1.066; P<0.001], LDH >150 UI/L (OR: 187%, CI: 1.756-4.715; P<0.001), IPI (OR: 71%, CI: 1.422-2.056; P<0.001), bone marrow involvement (OR: 86.2%, CI: 1.102-3.145; P=0.02), *MYC* translocation (OR: 71%, CI: 1.281-2.297; P<0.001), *BCL-2* translocation (OR: 97%, CI: 1.389-2.795; P=0.002), MYC-IHC ≥70% (OR: 65%, CI: 0.22-0.539; P<0.001), DH status (OR: 310%, CI: 2.529-6.662; P<0.001), DE 70% status (OR: 61.5%, CI: 1.976-2.67; P=0.04). Stepwise multivariate analysis demonstrated that IPI (OR: 62.2%, CI: 1.225-2.146; P=0.001), MYC-IHC ≥70% (OR: 224.8%, CI: 1.714-6.155; P<0.001), DH status (OR: 131.7%, CI: 1.003-5.350; P=0.049), DE 70% status (OR: 177.5%, CI: 1.020-1.080; P=0.006) were independent prognostic factors that influence patients' outcome.

A comparison of HGDH, DE-LBCL [according to World Health Organization (WHO) criteria, i.e. MYC-IHC ≥40% and BCL-2-IHC ≥50%] and nonDH/nonDE subsets of non-BL in terms of OS and PFS confirmed that HGDH patients showed significantly worse survival than the other two groups (P<0.001; χ^2 39.24 for OS and 13.13 for PFS) (Figure 2A and *Online Supplementary Figure S1A*).

By stratifying DE-LBCL according to MYC protein expression (70-100%, 40-69%,) the prognosis turned out to be poorer in the former (P<0.001, $\chi^2$13.152 for OS and 10.723 for PFS) (Figure 2B and *Online Supplementary Figure S1B*).

Dividing HGDH cases according to MYC protein positivity revealed that those with MYC-IHC ≥70% had a worse prognosis than cases with MYC-IHC ≤69% (P<0.001, $\chi^2$48.215 for OS and 35.549 for PFS) (Figure 2C and *Online Supplementary Figure S1C*). This supports prior observations that patients with *MYC* rearrangements or DH lymphomas devoid of MYC-IHC expression might exhibit less aggressive clinical behaviors.[13]

Given that the highest concordance and reproducibility of MYC-IHC was >70%, we compared OS and PFS of DE-LBCL showing MYC-IHC >70% and BCL-2-IHC >50% with HGDH cases; we found no significant differ-

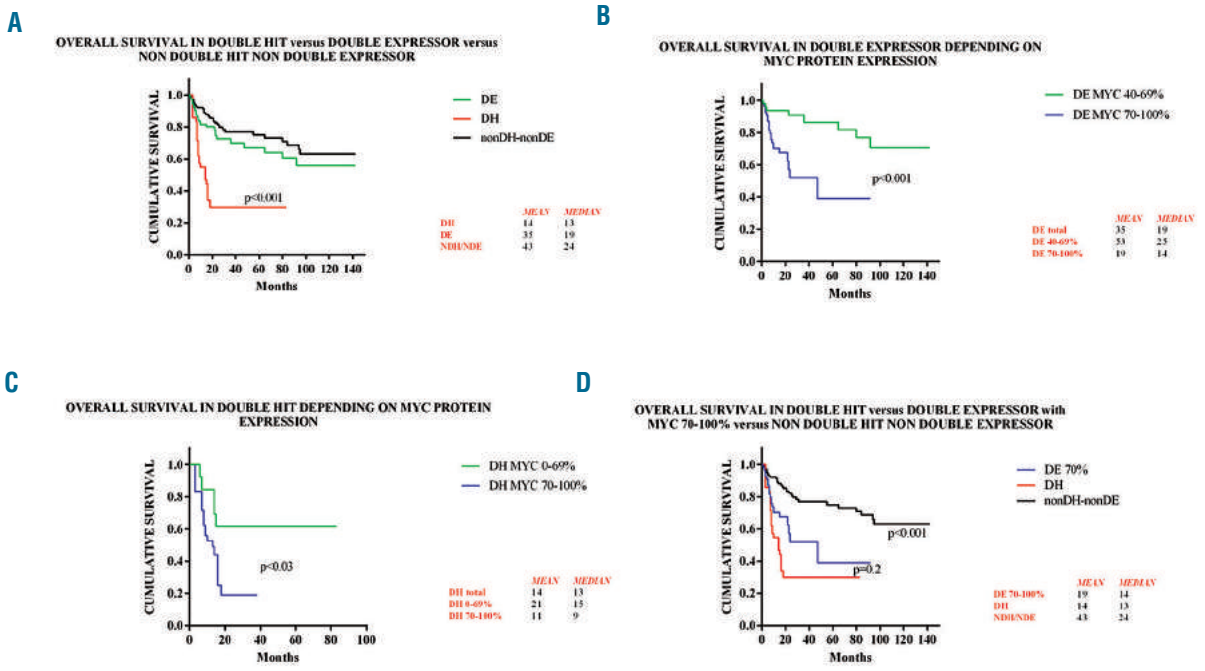

Figure 2. Kaplan-Meier curves of overall survival (OS) in the different patient groups. (A) Kaplan-Meier curve of OS in double hit (DH) *versus* double expressor (DE) *versus* non-double hit/non-double expressor (nonDH/nonDE) lymphomas. There was a significant difference in OS between the DH and the other two groups (log rank test, *P*<0.001). DH lymphomas were defined by having both *MYC* and *BCL-2* rearrangements; DE were characterized by showing MYC-immunohistochemistry (IHC) ≥40% and BCL-2-IHC ≥50%; nonDH/nonDE included cases without double hits or with one only single hit, and with none or only one protein expression between MYC and BCL-2. (B) Kaplan-Meier curve of OS in DE depending on MYC protein expression. OS was significantly lower in the group showing MYC-IHC ≥70% than in the group with MYC-IHC 40-69% (log rank test, *P*<0.001) indicating that a MYC-IHC ≥70% cut off defines a clinically relevant subgroup of DE cases. (C) Kaplan-Meier curve of OS in DH depending on MYC protein expression. There was a significant difference in OS between the two groups (MYC-IHC 0-69% and BCL-2-IHC ≥50%, and MYC-IHC ≥70% and BCL-2-IHC ≥50%) with MYC ≥70% cases having the lower survival rate (log rank test, *P*<0.001). Noteworthy, among HGDH with MYC-IHC 0-69%, the 3 cases showing MYC-IHC <40% had a mean OS of 44 months (*data not shown*). These findings indicate that adverse survival in HGDH is highly impacted by high MYC-IHC expression (≥70%). (D) Kaplan-Meier curve of OS in DH *versus* DE as defined by MYC-IHC ≥70% and BCL-2-IHC ≥50% *versus* nonDH/nonDE. OS overlaps in DH and DE with MYC-IHC ≥70% and BCL-2-IHC ≥50% (log rank test, *P*=0.2 for DH *versus* DE with MYC ≥70% and BCL-2-IHC ≥50%;), this is worse than the OS of the nonDH/nonDE (log rank test, *P*<0.001 for either DH or DE with MYC ≥70% and BCL-2-IHC ≥50% *versus* nonDH/nonDE).

ences in prognosis (*P*=0.2, $\chi^2$0.777 for OS and 3.441 for PFS) (Figure 2D and *Online Supplementary Figure S1D*).

Interestingly, the OS and the PFS of HGBCL, NOS strictly depended on *MYC* expression being 30 and 28 months in HGBCL, NOS with MYC 40-69%, 10 and 14 months in those with MYC 70-100%.

These findings again highlight the need to establish more widely reproducible cut-off values for IHC assays with higher predictive value, to safely stratify high-risk patients. Moreover, they may also, at least in part, explain the above mentioned inconsistencies in published data.

Finally, since the cell-of-origin (COO) classification of LBCL exerts a prognostic impact, with non-GCB lymphomas showing a poorer prognosis than GCB ones, we stratified HGDH and DE-LBCL according to COO defined by Hans' algorithm.[15] A poorer prognosis was demonstrated only in patients with MYC-IHC ≥70%, with no differences according to the COO. However, no conclusions can be drawn due to both the limited number of cases examined per group and to the IHC assessment of COO which is known to misclassify a subset of samples.

Different molecular mechanisms may be responsible for the same disease entity and neoplastic phenotype. FISH currently represents the gold standard for identifying rearrangements, but it is not capable of detecting genetic deregulation affecting gene expression at transcriptional and post-transcriptional levels that might result in protein overexpression and neoplastic transformation.[4] Our results support the role of MYC protein as the active trigger of the MYC-mediated oncogenic effects since protein expression levels likely represent a more direct measure of the activity of a particular gene[16] and MYC-IHC should be undertaken in all cases. However, the last WHO criteria assessed that MYC staining is not reliable enough to select cases for FISH analysis.[7] According to our results, the cut off of MYC-IHC ≥70%, based both on reproducibility among pathologists and clinical impact, is a good indicator of underlying *MYC* gene rearrangement. Nonetheless, our promising data need further validation in an independent cohort of patients. In addition, given the highest scoring efficiency, the cut offs of MYC-IHC ≥70% and BCL-2-IHC ≥50% could be applied when FISH is not available (due to issues of practicability, cost, short turn-around-time, quality control) to select a subset of patients who are poor responders and who may benefit from alternate therapeutic strategies.

Maria R. Ambrosio,[1] Stefano Lazzi,[1] Giuseppe Lo Bello,[1] Raffaella Santi,[2] Leonardo Del Porro,[1] Maria M. de Santi,[3] Raffaella Guazzo,[1] Lucia Mundo,[1] Luigi Rigacci,[4] Sofia Kovalchuck,[4] Noel Onyango,[5] Alberto Fabbri,[6] Emanuele Cencini,[6] Pier Luigi Zinzani,[7] Francesco Zaja,[8] Francesco Angrilli,[9] Caterina Stelitano,[10] Maria G. Cabras,[11] Giuseppe Spataro,[12] Roshanak Bob,[13] Thomas Menter,[14,15]

Massimo Granai,[1] Gabriele Cevenini,[1] Kikkeri N. Naresh,[15] Harald Stein,[13] Elena Sabattini[16] and Lorenzo Leoncini[1]

[1]Department of Medical Biotechnologies, University of Siena, Italy; [2]Division of Pathological Anatomy, University of Florence, Italy; [3]Unit of Pathological Anatomy, AOU Siena, Italy; [4]Hematology Division, AOU Careggi, University of Firenze, Italy; [5]Department of Clinical Medicine and Therapeutics, Unit of Medical Oncology, University of Nairobi, Kenya; [6]Haematology Unit, Azienda Ospedaliera Universitaria Senese, Siena, Italy; [7]Institute of Hematology "L. e A. Seràgnoli", University of Bologna, Italy; [8]Clinica Ematologica ed Unità di Terapie Cellulari "Carlo Melzi", DAME, University of Udine, Italy; [9]Ematologia Ospedale Civile dello Spirito Santo, Pescara, Italy; [10]Ematologia, Ospedale Bianchi Melacrino Morelli, Reggio Calabria; [11]Hematology, Cagliari Hospital, Italy; [12]Post Graduate School of Public Health, University of Siena, Italy; [13]Pathodiagnostik Lab. Berlin, Germany; [14]Institute of Pathology and Medical Genetics, University Hospital of Basel, Switzerland; [15]Department of Cellular and Molecular Pathology, Hammersmith Hospital Campus, Imperial College Healthcare NHS Trust, London, UK and [16]Unit of Haemolymphopathology, Department of Hematology and Oncology, University Hospital of Bologna, Italy

Acknowledgments: the Authors would like to thank additional hematological centers that contributed with clinical data: Di Raimondo F. - Hematology, Catania University, Italy, Cimino G. and Centra N. Hematology, Latina Hospital, Galieni P. – Hematology, Ascoli Piceno Hospital, Martelli M. and Di Rocco A. – Hematology, Roma University "La Sapienza", Italy, Vigna E. – Hematology, Cosenza Hospital, Italy, Taratini G. – Hematology, Barletta Hospital, Italy, Scalone R. – Hematology, casa di Cura La Maddalena, Palermo, Italy, Mannina D. – Hematology, Papardo Hospital, Messina, Italy

Correspondence: lorenzo.leoncini@dbm.unisi.it
doi:10.3324/haematol.2018.195958

Information on authorship, contributions, and financial & other disclosures was provided by the authors and is available with the online version of this article at www.haematologica.org.

References

1. Sarkozy C, Traverse-Glehen A, Coiffier B. Double-hit and double-protein-expression lymphomas: aggressive and refractory lymphomas. Lancet Oncol. 2015;16(15):e555-567.
2. Miura K, Takahashi H, Nakagawa M, et al. Clinical significance of co-expression of MYC and BCL-2 protein in aggressive B-cell lymphomas treated with a second line immunochemotherapy. Leuk. Lymphoma. 2016;57(6):1335-1341.
3. Kluk MJ, Ho C, Yu H, et al. MYC Immunohistochemistry to Identify MYC-Driven B-Cell Lymphomas in Clinical Practice. Am. J. Clin. Pathol. 2016;145(2):166-179.
4. Mahmoud AZ, George TI, Czuchlewski DR, et al. Scoring of MYC protein expression in diffuse large B-cell lymphomas: concordance rate among hematopathologists. Mod. Pathol. 2015;28(4):545-551.
5. Kawashima I, Inamoto Y, Maeshima AM, et al. Double-Expressor Lymphoma Is Associated with Poor Outcomes after Allogeneic Hematopoietic Cell Transplantation. Biol Blood Marrow Transplant. 2018;24(2):294-300.
6. Rosenthal A, Younes A. High grade B-cell lymphoma with rearrangements of MYC and BCL-2 and/or BCL6: Double hit and triple hit lymphomas and double expressing lymphoma. Blood Rev. 2017; 31(2):37-42.
7. Swerdlow S.H, Campo E, Harris NL, et al. WHO classification of Tumours of Haematopoietic and Lymphoid, 4th ed. Lyon, France, IARC Press, 2017.
8. Naresh KN, Hazem AHI, Lazzi S, et al. Diagnosis of Burkitt Lymphoma using an algorithmic approach applicable in both resource-poor and resource-rich countries. Br J Haematol. 2011; 154(6):770-776.
9. Menter T, Medani H, Ahmad R, Flora R, Trivedi P, Reid A, Naresh KN. MYC and BCL2 evaluation in routine diagnostics of aggressive B-cell lymphomas - presentation of a work-flow and the experience with 248 cases. Br J Haematol. 2017;179(4):667-688.
10. Landis JR, Koch GG. The measurement of observer agreement for categorical data. Biometrics. 1977;33(1):159-174.
11. Scott, DW, King RL, Staiger AM, et al. High-grade B-cell lymphoma with MYC and BCL2 and/or BCL6 rearrangements with diffuse large B-cell lymphoma morphology. Blood. 2018;131(18):2060-2064.
12. Friedberg JW. How I treat "Double Hit" lymphoma. Blood. 2017; 130(5):590-596.
13. Herrera AF, Mei M, Low L, et al. Relapsed or Refractory Double-Expressor and Double-Hit Lymphomas Have Inferior Progression-Free Survival After Autologous Stem-Cell Transplantation. J Clin Oncol. 2017;35(1):24-31.
14. Green TM, Young KH, Visco C, et al. Immunohistochemical double-hit score is a strong predictor of outcome in patients with diffuse large B-cell lymphoma treated with rituximab plus cyclophosphamide, doxorubicin, vincristine, and prednisone. J Clin Oncol. 2012;30(28):3460-3467.
15. Staiger AM, Ziepert M, Horn H, et al. Clinical Impact of the Cell-of-Origin Classification and the MYC/ BCL-2 Dual Expresser Status in Diffuse Large B-Cell Lymphoma Treated Within Prospective Clinical Trials of the German High-Grade Non-Hodgkin's Lymphoma Study Group. J Clin Oncol. 2017;35(22):2515-2526.
16. Ott G, Rosenwald A, aCampo E. Understanding MYC-driven aggressive B-cell lymphomas: pathogenesis and classification. Blood. 2013; 122(24):3884-3891.

Mundo et al. *Blood Cancer Journal* (2019)9:91
https://doi.org/10.1038/s41408-019-0252-2

Blood Cancer Journal

ARTICLE Open Access

Molecular switch from MYC to MYCN expression in MYC protein negative Burkitt lymphoma cases

Lucia Mundo[1], Maria Raffaella Ambrosio[1], Francesco Raimondi[2], Leonardo Del Porro[1], Raffaella Guazzo[1], Virginia Mancini[1], Massimo Granai[1], Bruno Jim Rocca[1], Cristina Lopez[3], Susanne Bens[3], Noel Onyango[4], Joshua Nyagol[4], Nicholas Abinya[4], Mohsen Navari[5], Isaac Ndede[6], Kirkita Patel[6], Pier Paolo Piccaluga[7,8], Roshanak Bob[9], Maria Margherita de Santi[1], Robert B. Russell[2], Stefano Lazzi[1], Reiner Siebert[3], Harald Stein[9] and Lorenzo Leoncini[1]

Abstract

MYC is the most altered oncogene in human cancer, and belongs to a large family of genes, including *MYCN* and *MYCL*. Recently, while assessing the degree of correlation between *MYC* gene rearrangement and MYC protein expression in aggressive B-cell lymphomas, we observed few Burkitt lymphoma (BL) cases lacking MYC protein expression despite the translocation involving the *MYC* gene. Therefore, in the present study we aimed to better characterize such cases. Our results identified two sub-groups of MYC protein negative BL: one lacking detectable MYC protein expression but presenting MYCN mRNA and protein expression; the second characterized by the lack of both MYC and MYCN proteins but showing *MYC* mRNA. Interestingly, the two sub-groups presented a different pattern of SNVs affecting *MYC* gene family members that may induce the switch from *MYC* to *MYCN*. Particulary, MYCN-expressing cases show MYCN SNVs at interaction interface that stabilize the protein associated with loss-of-function of MYC. This finding highlights MYCN as a reliable diagnostic marker in such cases. Nevertheless, due to the overlapping clinic, morphology and immunohistochemistry (apart for MYC versus MYCN protein expression) of both sub-groups, the described cases represent bona fide BL according to the current criteria of the World Health Organization.

Introduction

MYC, a proto-oncogene located on chromosome 8q24, is the most commonly altered oncogene in human cancer[1,2]. The encoded protein (MYC) is a multifunctional, nuclear phosphoprotein that plays a key role in cell cycle progression, apoptosis, cellular differentiation, and metabolism[3]. It functions as a transcription factor that regulates expression of about 15% of all human genes[3] through binding on enhancer box sequences (E-boxes) and recruiting histone acetyl-transferases (HATs). In addition to its role as a classical transcription factor, *MYC* also acts to regulate global chromatin structure by modifying histone acetylation both in gene-rich regions and at sites far from known genes[4]. A strict check of MYC expression is physiologically accomplished by controlling it at multiple levels, i.e. transcription, translation, and mRNA and protein stability. *MYC* belongs to a large family of genes, also including *MYCN* and *MYCL1* in human[5]. Despite the *MYC* family members display notable differences in the patterns of expression, they function in a similar manner and have similar genomic structures. In particular, the the *MYC* and *MYCN* loci are similarly organized and both genes comprise three exons. Most of the first exon and the 3′ portion of the third exon contain untranslated regions that carry transcriptional or post-transcriptional regulatory sequences[5,6]. Since, they present high homology in their sequences and protein binding sites and largely share their target genes, they can compensate and substitute for each other in both physiological and pathological conditions[5–8]. Previous studies

Correspondence: Lorenzo Leoncini (lorenzo.leoncini@dbm.unisi.it)
[1]Department of Medical Biotechnology, University of Siena, Siena, Italy
[2]Cell Networks, Bioquant, University of Heidelberg, Heidelberg, Germany
Full list of author information is available at the end of the article.

demonstrated a cross regulating expression of MYC family members; in particular, it has been shown that MYC and MYCN reciprocally control their expression via regulatory loops and via repressing each other at defined promoter sites[9–12].

Concerning human lymphoid neoplasms, MYC is typically expressed in Burkitt lymphoma (BL), as a consequence of the t(8;14)(q24;q32) translocation or its variants. Moreover, a variable proportion of plasmablastic lymphomas (PBLs), diffuse large B-cell lymphomas (DLBCLs), mantle cell lymphomas (MCLs), and plasma cell myelomas express MYC[13]. In contrast, MYCN expression has not been systematically studied so far in lymphoid neoplasms. It has been recently shown that MYC and MYCN are both required for hematopoietic stem cell (HSC) proliferation, metabolic growth, differentiation, long-term self-renewal activity, and survival[14]. Moreover, MYCN is expressed in self-renewing, quiescent stem cells, also including the hematopoietic ones that switch to higher MYC expression in transit-amplifying progenitors that further differentiate[14–16].

Interestingly, in a previous study on the standardization of MYC protein expression by immunohistochemistry (IHC) and its correlation with *MYC* gene rearrangements by fluorescent in situ hybridization (FISH) in BL and DLBCL, we detected few BL cases lacking MYC protein expression despite carrying a translocation involving the *MYC* gene[17].

Therefore, in the present study we aimed to (1) better characterize such BL cases lacking MYC protein expression, (2) evaluate whether a cross-talk between the *MYC* gene family members does also exist in BL, and (3) explore the genetic landscape of this subset of BL cases.

Materials and methods

Cases selection, immunophenotype and FISH

We studied 92 morphologically and immunophenotypically typical BL cases (82 pediatric and 10 adult; median age: 12 years (range 3–79)). All cases have been diagnosed according to the updated World Health Organization (WHO) classification of tumors of haematopietic and lymphoid tissues[12]. The cases were retrieved from the archives of four institutions, namely Siena University Hospital (Italy, $n = 8$), Pathodiagnostik Laboratory Berlin (Germany, $n = 4$), Nairobi University (Kenya, $n = 50$), and Moi University, Eldoret (Kenya, $n = 30$) and considering their regional derivation by definition included 12 sporadic and 80 endemic samples. Before enrolling the cases in this study, they were re-evaluated by expert hematopathologists (LL, HS) and diagnoses were confirmed by morphology on histological slides stained with haematoxylin and eosin (H&E) or giemsa, and by immunophenotyping. The main clinical features of our cohort are summarized in Supplementary Table 1. All the procedures were carried out automatically on representative paraffin sections from each case by Bench Mark Ultra (Ventana, Monza, Italy) using extended antigen retrieval and with DAB as chromogen. MYC detection was performed by exploiting the clone Y69 (Ventana and Epitomics, Germany)[18]. For MYCN we employed the ab198912 (Abcam, Cambridge, UK). Both antibodies produced a strictly nuclear staining. As positive control, a BL case expressing MYC protein at high level and characterized by *MYC* gene rearrangement by FISH analysis, was used; for MYCN, human brain tissue was used as control. Negative control was provided by replacing the two antibodies with non-immune mouse serum. The intensity of staining and the percentage of positive neoplastic cells for MYC and MYCN were evaluated by two hematopathologists (MRA and SL) independently and scored according to previous published data[17]. Scoring was evaluated on strongly stained nuclei and in hot spot areas, if present[19]. FISH analysis for *MYC* gene rearrangements was performed using break-apart probes in all cases (ZytoLight SPEC MYC Dual Color Break Apart Probe, Bio-Optica, Germany) following the manufacturer's instructions. In addition, we used dual-fusion probes (ZytoLight SPEC MYC/IGH Dual Color Dual Fusion Probe, Bio-Optica, Germany) in *MYC* translocation negative samples and in the MYC protein-negative cases following the manufacturer's instructions. The IGH-MYC negative cases were further evaluated by IGK-MYC and IGL-MYC probes (Supplementary Table 1)[20]. FISH analysis of chromosome 2p24/CEP2 for *MYCN* amplification [Vysis LSI MYCN (2p24) Spectrum Green/Vysis CEP2 Spectrum Orange Probe, Abbott, USA] was also performed as previously described[21]. A *MYCN* break apart FISH assay was applied, containing four clones, which flank the *MYCN* gene, RP11-105P20 (spectrum green), RP11-422A6 (spectrum green), RP11-355H10 (spectrum orange) and RP11-744F11 (spectrum orange). For each specimen, at least 100 intact non-overlapping non nuclei were analyzed manually on a Leika DM 600B (Leica Microsystems, Switzerland) or Zeiss fluorescence microscope equipped with DAPI, SpectrumGreen, SpectrumOrange filters. DNA preparation from bacterial clones and fluorescent labeling were performed following recently described protocols (Supplementary Table 1)[22]. Appropriate negative and positive controls were used[22]. In situ hybridization (ISH) for Epstein-Barr virus encoded RNAs (EBER) was carried out in each sample on 5 mm thick section as previously described[23–25]. A control slide prepared from a paraffin-embedded tissue block containing metastatic nasopharyngeal carcinoma in a lymph node accompanied each hybridization run.

The study was approved by the institutional ethical committees of the institutions submitting the cases, and written permission and informed consent have been

obtained before samples collection in accordance with the Declaration of Helsinki.

RNA extraction

RNA was extracted from FFPE sections of primary tumors and reactive lymph nodes using the FFPE RNA Easy kit (Qiagen, CA), and from cell lines using the RNA Easy Kit (Qiagen, CA), according to the manufacturer's instructions. The amount and quality of RNA were evaluated by measuring the OD at 260 nm and the 260/230 and 260/280 ratios using a Nanodrop spectrophotometer (Celbio, Milan, Italy). The quality of RNA was also checked using a Bioanalyzer 2100 (Agilent, CA, USA).

In situ detection of MYC and MYCN mRNA by RNAscope assay

RNA ISH was performed to investigate the expression of *MYC* gene family members at mRNA level. RNAscope 2.5 HD Red Detection Kit (Advanced Cell Diagnostics, Hayward, CA, USA) and RNAscope Probes for MYC and MYCN mRNA (Hs-MYC, Cat # 311761; Hs-MYCN, Cat # 417501) were applied, according to the manufacturer's instructions[26]. Briefly, sections of formalyn-fixed paraffin-embedded (FFPE) tissue were baked for 1 h at 60 °C prior to use. After de-paraffinization and dehydration, the tissues were air dried and treated with a peroxidase blocker before boiling in a pre-treatment solution for 10 min. Protease was then applied for 30 min at 40 °C. Target probes were hybridized for 2 h at 40 °C, followed by a series of signal amplification and washing steps. Probes are hybridized and followed by a cascade of signal amplification which enhances the signal for low expressing gene and mRNA present in archived samples and partial degraded specimens. Hybridization signals were detected by chromogenic reactions using Fast Red. mRNA staining signal was identified as cytoplasm and nuclear red punctate dots. Each sample was quality controlled for mRNA integrity with a probe specific to the housekeeping *PPIB* mRNA. Negative control background staining was evaluated by using a probe specific to bacterial *dapB* gene; all cases did not show any signals in the neoplastic tissue, therefore they were included in the analysis.

Reverse transcription-quantitative PCR (RT-qPCR)

In primary tumors, the expression of *MYC* has been investigated by RT-qPCR using two different approaches: by using primers designed with the help of Primer-BLAST service (Supplementary Table 2) and by using specific Taqman probes for *MYC* gene detecting all the three *MYC* gene exons (Cat. # 4331182, ThermoFisher Scientific, USA). This approach aimed to rule out possible technical failures due to splicing variants in these cases. The measures obtained from all assays were used to calculate the mean value of MYC mRNA. Thus, the resulting *MYC* expression is a merge of all exons studied. MYCN mRNA has been checked by using the specific Taqman probe (Cat. # 4331182, ThermoFisher Scientific, USA) according to the manufacturer's instructions. Four endogenous controls (hypoxanthine-guanine phosphoribosyltransferase, *HPRT*; Phosphoglycerate kinase, *PGK*; Beta-2-Microglobulin, *b2m*; TATA-Box Binding Protein, *TBP*) were included in the experiment. Considering that *HPRT* housekeeping gene showed the higher and more constant expression in all our cases, we selected it for relative quantification of each target gene.

Reactive lymph nodes have been used as control and the relative expression is expressed as $2^{-\Delta\Delta Ct}$.

Next generation sequencing (NGS)

Targeted NGS of 409 cancer related genes was performed on 40 ng tumoral DNA using the IonAmpliSeq Comprehensive Cancer Panel (Thermo Fisher Scientific, USA) according to the manufacturer's protocol. Alignment, variant calling and filtering were performed with Ion Reporter 4.4 (Thermo Fisher Scientific, USA). The following filter chain was used: "Location in utr_3, splicesite_3, exonic, splicesite_5, utr_5" in, "variant effect in stoploss, nonsense, missense, frameshift Insertion, non-frameshift Insertion, non-frameshift Block Substitution, frameshift Deletion, non-frameshift Deletion, frameshift Block Substitution. The base coverage was minimum 60.80% and maximum 70.36%, with average equal to 65.71%. The mean of reads with >Q20 was equal to 92.59%.

Sanger sequencing

To further explore the MYCN locus, primers were designed to amplify 200 bp fragments covering all exons of *MYCN* gene. PCR products were purified and subjected to Sanger sequencing in two reactions, one with the forward and one with the reverse primer (Thermo Fisher Scientific, USA, Catalog # A15629, A15630).

Functional in vitro studies

The human BL cell line Namalwa (ATCC CRL-1432) and a human B lymphoblastoid cell line (LCL; GK-5 (ATCC® CRL-183)) were used to perform the in vitro experiments. Namalwa was characterized by *MYC*-rearrangements and strong expression of MYC mRNA. The LCL has been investigated to better appreciate the effect of *MYC* silencing. Both cell lines were EBV-positive. Briefly, cells were cultured in RPMI-1640 medium supplemented with 10% Fetal Bovine Serum (FBS), 1% L-glutamine, 1% penicillin/streptomycin (CARLO ERBA Reagents, Milan, Italy), with 5% CO_2, at 37 °C. Transient transfections were performed by nucleofection, using an Amaxa Nucleofector device (Lonza, Cologne, Germany), program A23 and solution V (Lonza, Cologne, Germany)

as a buffer solution, following the manufacturer's instructions. 5 × 106 cells were transfected with 0.5 and 1 µg small interfering RNA (siRNA) targeting MYC, esiRNA human MYC (MISSION esiRNA Human MYC (esiRNA1), Sigma Aldrich, St. Louis, USA) or with 1 µg esiRNA targeting RLUC (esiRNA1) used as negative control of gene inhibitor (MISSION esiRNA RLUC (esiRNA1), Sigma Aldrich, St. Louis, USA); transfection solution was used as a mock. Transfection efficiency was assessed transfecting 2 µg of pmaxGFP and detecting both fluorescence and cell viability by flow cytometry; RNA was extracted 48 and 72 h after nucleofection. *MYC* and *MYCN* expression was checked by RT-qPCR as described above.

Statistical analyses

Statistical analyses were performed using IBM SPSS Statistics 20.0 (IBM, Armonk, NY, USA) and Prism (GraphPad Softwares, La Jolla, CA, USA). ANOVA, unpaired T-tests, and linear regression were used for continuous variable analysis. Chi-square was used for non-continuous variable analysis. Two-sided tests were used in all calculations. The limit of significance for all analyses was defined as $p < 0.05$.

Modeling predicted effects

We annotated SNVs on *MYCN* and *MYC* canonical amino acid sequence through Ensembl Variant Effect Predictor (VEP)[27] and graphically displayed through the lollipos software[28]. We used ELM (http://elm.eu.org/)[29] to predict mutation effects on linear motives, while we employed Mechismo (http://mechismo.russelllab.org/)[30], using default settings[31] to predict mutations effects at 3D interaction interfaces. Similarly to what we did in a previous study[32], we analyzed SNVs in the exon 2 of *MYC* gene for enrichment in phosphosite area, considered a window of −/−4 aminoacids close to phosphosite residues. Frequency of observed SNVs in phosphosite was obtained dividing the observed number of SNVs in phosphosite area (12 and 9 for MYCN positive and MYCN negative, respectively) for its length ($n = 78$), while the expected frequency was done by dividing the total number of SNVs (34 and 31, respectively) in exon 2 for its length ($n = 252$) (Supplementary Tables 3, 4). For the statistical analysis Fisher's exact test was done.

Results

Rare BL cases lack MYC expression despite MYC gene translocation

Ninety out of ninety-two cases (98%) showed a translocation involving *MYC* gene detectable by FISH analysis (Supplementary Table 1). At immunohistochemistry, eighty-three out of ninety-two cases (90%) did present with intense and diffuse nuclear MYC protein expression in more than 80% of neoplastic cells (Fig. 1a), including the two cases lacking an identifiable *MYC* gene translocation by commercial probes, suggesting the presence of a *MYC* juxtaposition to one of the not tested light chain loci or an alternative means of MYC activation, like cryptic insertion of *MYC* into IG loci[20,33–36].

Remarkably, 9/90 (7 endemic BL-eBL, 2 sporadic BL-sBL) cases carrying a translocation involving *MYC* gene did not

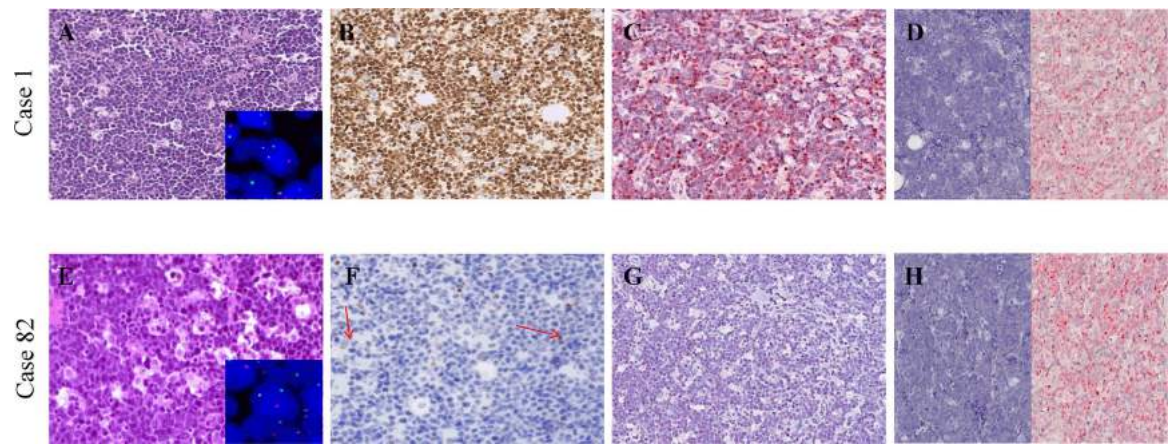

Fig. 1 Morphology, immunophenotype and cytogenetics of our cohort. a A BL case with the typical morphology carrying MYC gene translocation (inset) and expressing MYC at protein and mRNA level. **b** An example of those cases that despite MYC gene translocation (inset), did not express MYC at protein level and showed a heterogeneous staining for MYC mRNA; these cases presented the characteristic cohesive growth, squared-off cytoplasm and starry-sky appearance; scattered positive non-neoplastic cells (red arrows) served as internal control to ensure a successful immunohistochemical reaction. A–B, from left to right: haematoxyin and eosin (H&E), MYC protein staining (brown chromogen; Y69 clone), RNAscope assay for MYC mRNA (red chromogen). dapB and PPIB probes were applied as negative and positive controls, respectively. A–B, Original magnification (O.M.): ×20.

Table 1 Clinical data and representative mutation sites located on MYC and MYCN genes.

Case	Age	Sex	Epidemiology	Biopsy site	EBER	*MYC* FISH			PROTEIN		SNVs position	AA switch
						MYC B.A.	MYC-IGH	MYC-IGK/IGL	MYC	MYCN		
BL 8	14	F	endemic	lymph node	–	+	+	n.p.	–	+	g.chr2:16086085G>A	V421I
BL 82	7	M	endemic	ileum	–	+	–	+ (IGL)/-(IGK)	–	+	g.chr2:16086115C>T g.chr8:128753056C>T	H431Y P406L
BL 83	8	M	endemic	soft tissue	+	+	+	n.p.	–	–	g.chr8:128750542T>G g.chr8:128750610G>T g.chr8:128750607G>A	Y27D Q49H Q48Q
Bl 84	9	F	endemic	maxilla	+	+	+	n.p.	–	+	g.chr2:16086046G>A g.chr8:128752981G>A	V408M R381K
BL 85	11	M	endemic	oral cavity	+	+	+	n.p.	–	+	g.chr2:16086104C>T	T427I
BL 86	4	F	endemic	lymph node	+	+	+	n.p.	–	+	g.chr2:16086208C>T g.chr8:128753079G>A	R462W A414T
BL 87	10	M	endemic	maxilla	+	+	–	+ (IGL) / -(IGK)	–	+	g.chr2:16086076G>A g.chr8:128753064G>A	A418T V409I
BL 91	45	M	sporadic	stomach	–	+	+	n.p.	–	–	g.chr8:128750540A>G g.chr8:128750543A>C	N26S Y27S
BL 92	79	F	sporadic	vagina	–	+	+	n.p.	–	–	g.chr8:128750543A>G	Y27C

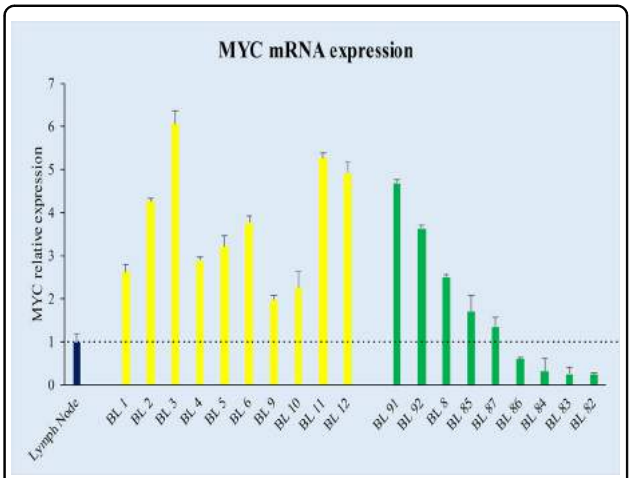

Fig. 2 Comparison of MYC protein positive with MYC protein-negative BL cases in terms of mRNA by RT-qPCR. The merge of measures obtained by applying different assays detecting all MYC exons demonstrated a heterogeneous MYC mRNA expression (*y* axis) among the different samples (*x* axis). The threshold is represented by black dotted line. Specifically, some BL cases without MYC protein expression showed a MYC mRNA expression overlapping that detected in MYC protein-positive cases; whereas, others showed a very low expression with a value below that detected in the normal lymph node used as control (lymph node in blue, MYC protein-positive cases in yellow, MYC protein-negative cases in green).

express MYC at the protein level, showing a weak positivity in only 0–5% cells (Fig. 1b; Table 1). All the nine cases presented a *MYC* gene translocation by break apart probes, seven out of nine showed an MYC/IGH fusion; the 2 cases in which the *IGH/MYC* fusion probes did not demonstrated a juxtaposition of *MYC* to *IGH*, were tested by IGK and IGL probes, revealing a translocation involving the light chain lambda gene locus (Table 1). To evaluate whether the lack of MYC protein observed in 9/90 cases with *MYC* breakpoint was related to transcriptional or post-transcriptional issues, MYC mRNA was investigated by RNAscope and RT-qPCR. Strong expression of MYC mRNA visualized as punctate red dot signals was detected in BL cases characterized by a marked expression of MYC protein by immunohistochemistry (Fig. 1a), whereas the cases with the absence of MYC protein showed a heterogeneous staining for MYC mRNA with few cases being almost completely negative (Fig. 1b). These findings overlapped the RT-qPCR results (Fig. 2) that showed a heterogeneous MYC mRNA level ranging from 1.98 to 6.06 for MYC protein-positive BL cases and from 0.24 to 4.68 for MYC protein-negative specimens (Fig. 2).

Small subset of BL cases present MYCN expression

The heterogeneous expression of MYC mRNA and protein level in our cohort raised the question of how cases lacking MYC mRNA and/or protein could maintain

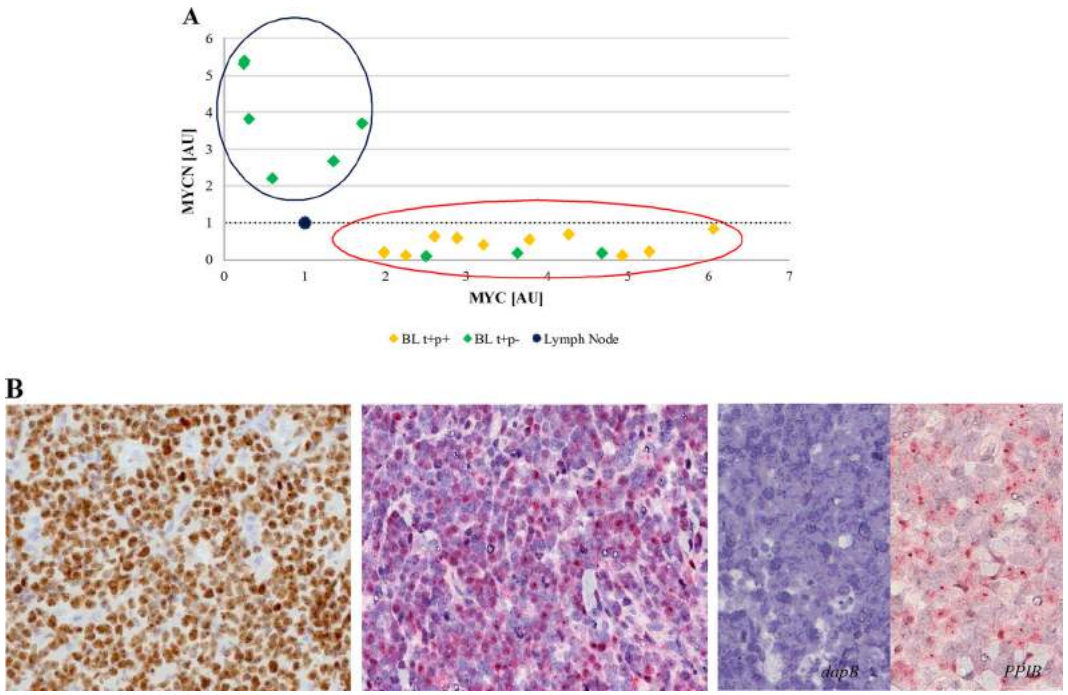

Fig. 3 Correlation between MYC and MYCN expression at mRNA by RT-qPCR and protein level by IHC. An almost mutual exclusivity between MYC and MYCN was identified at mRNA and protein level. Specifically, MYCN transcript was clearly detectable almost exclusively in MYC gene/protein-negative cases. **a** The regression analysis comparing the expression of MYC (*x* axis) and MYCN (*y* axis) mRNA identified two different clusters: one consisting of six cases characterized by very low MYC mRNA level and higher MYCN mRNA expression (circle blue); the second contains all the other cases, including the MYC translocation-positive/protein-positive samples and the cases being MYC translocation-positive/protein negative but expressing MYC at mRNA level (circle red). The threshold is represented by black dotted line. **b** Immunohistochemical evaluation and RNAscope assay for MYCN protein and mRNA expression showed a strong MYCN nuclear staining identified respectively as brown and red nuclear signals, in almost 90% of neoplastic cells only in the six MYCN mRNA positive samples. Probes detecting dapB and PPIB were used as negative and positive controls, respectively.

a complete BL phenotype. Previous studies have demonstrated a regulatory loop among *MYC* gene family members, specifically, between *MYC* and *MYCN*[9–12,37]. Accordingly, we evaluated MYCN mRNA and protein expression in such BL cases. Interestingly, we detected an almost mutual exclusivity between the expression of the two genes in our series at mRNA level by RNAscope and RT-qPCR, with cases expressing MYCN mRNA lacking MYC mRNA and vice versa ($p = 0.0003$, Student's t test, unpaired). The regression analysis identified two different clusters: one consisting of six cases characterized by very low MYC mRNA level and higher MYCN mRNA expression; the second cluster contains all the other cases, including the typical BLs and those cases characterized by MYC protein negativity but showing MYC mRNA (Fig. 3a). Then we validated our results at protein level by evaluating MYCN protein expression. A strong MYCN nuclear staining in almost 90% of neoplastic cells was detected in the six MYCN mRNA positive samples (Fig. 3b) while the remaining cases showing only MYC mRNA did not express MYCN at protein level. In such cases we investigated all the mechanisms responsible of MYCN over-expression (i.e. amplification, translocation and proviral insertion)[38]. Specifically, by FISH analysis of chromosome 2p24/CEP2, no amplification or translocation of the *MYCN* gene was detected. In addition, sequencing of *MYCN* gene did not provide evidence for a possible proviral insertion (by EBV, cytomegalovirus, HHV8) that could explain an enhanced *MYCN* transcription in the absence of increased copy number. We also investigated the association with EBV by applying EBER-ISH assay. Seventy-three cases (70 eBL, 3 sBL) resulted EBV-positive while nineteen (10 eBL, 9 sBL) were negative. The statistical analysis did not show a significant difference between the MYCN negative (69% EBV-positive) and MYCN positive (66% EBV-positive) cases.

Genomic analysis supports the presence of two subsets of BL depending on MYCN expression

We then explored the genetic landscape of eight out of the nine MYC protein-negative cases for which enough DNA was available by an ultra-deep sequencing analysis targeted on 409 cancer associated genes. Since we found SNVs affecting genes previously reported in BL and other

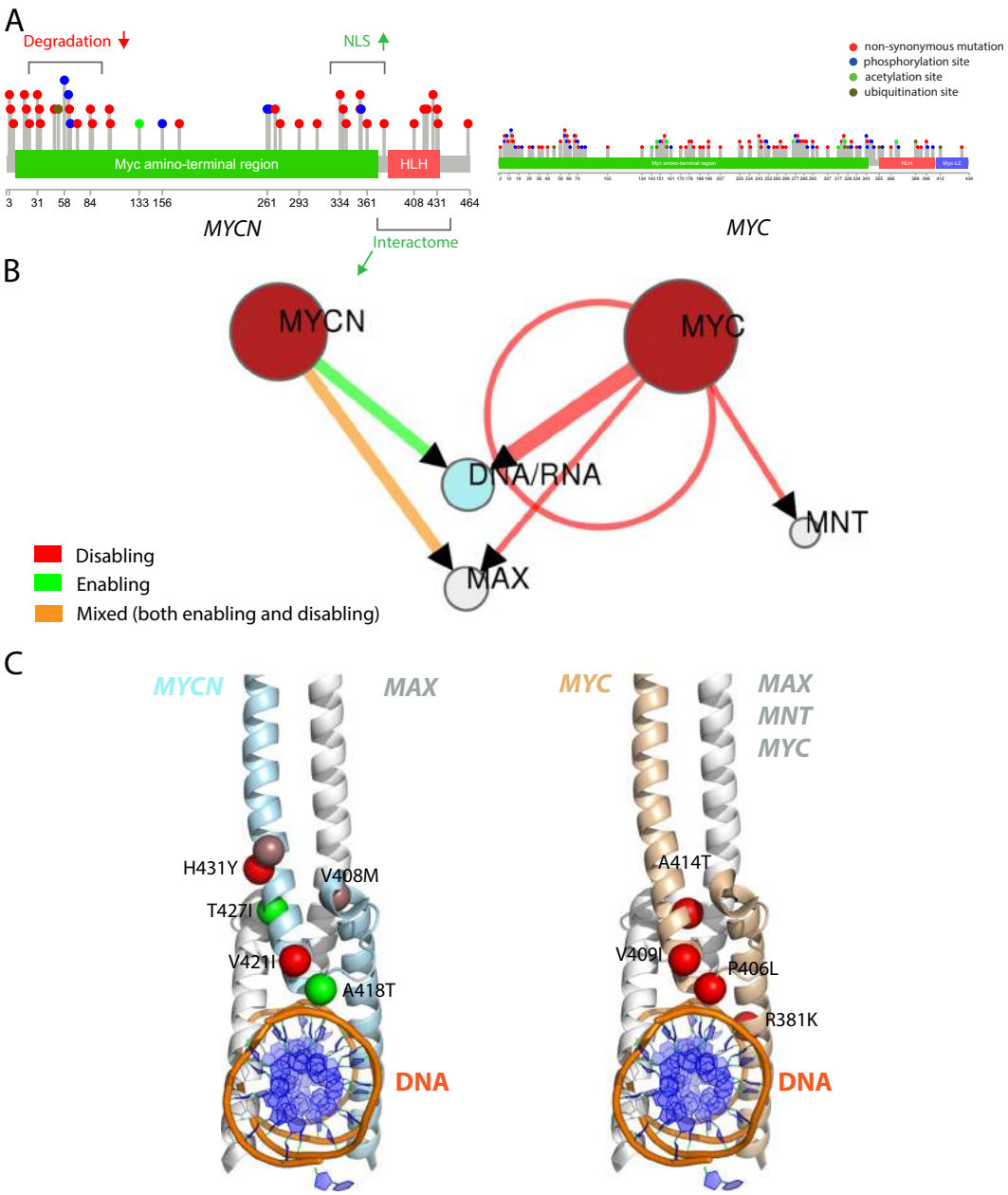

Fig. 4 MYC and MYCN non-synonymous mutations comparison. Mutations (red lollipops) annotated on protein primary sequence with additional information regarding post-translational modifications (PTMs) and domain composition. Linear motif annotations have been obtained from ELM (http://elm.eu.org/cgimodel.py?fun=smartResult&userId=QiKSrcdQR9&EXPECT_CUTOFF=100&r=1&bg=on). MYC mutations have been mapped to the canonical (isoform 1 from Swissprot, ID: P01106) protein isoform. Only mutations for MYCN positive cases are displayed. **b** Network representation of predicted effects at 3D interaction interfaces through Mechismo (http://mechismo.russelllab.org/). Predicted disabling, enabling and mixed effects are in indicated by red, green and orange arrows. **c** 3D cartoon representation (PDB ID: 1NKP) of mutations perturbing interaction interfaces. Sphere coloring is the same as for arrows in B. For MYC, we show mutation numberings referred to both the canonical amino acid sequence as well as to the isoform 2.

lymphomas[39–46] we decide to focus our attention on the mutational landscape of *MYC* family genes. Remarkably, in cases lacking *MYCN* expression, we identified SNVs only in *MYC* gene; specifically, we detected SNVs within the region coding for the N-terminus domain (NTD) of MYC. In particular, we reported SNVs in the MYC gene resulting in amino acid changes at position 27 (chr8:128,750,543A>C, p.Y27S; chr8:128,750,543A>G, p.Y27C; chr8:128,750,542T>G, p.Y27D) of the MYC protein (Supplemenatry Table S3). It is likely that these

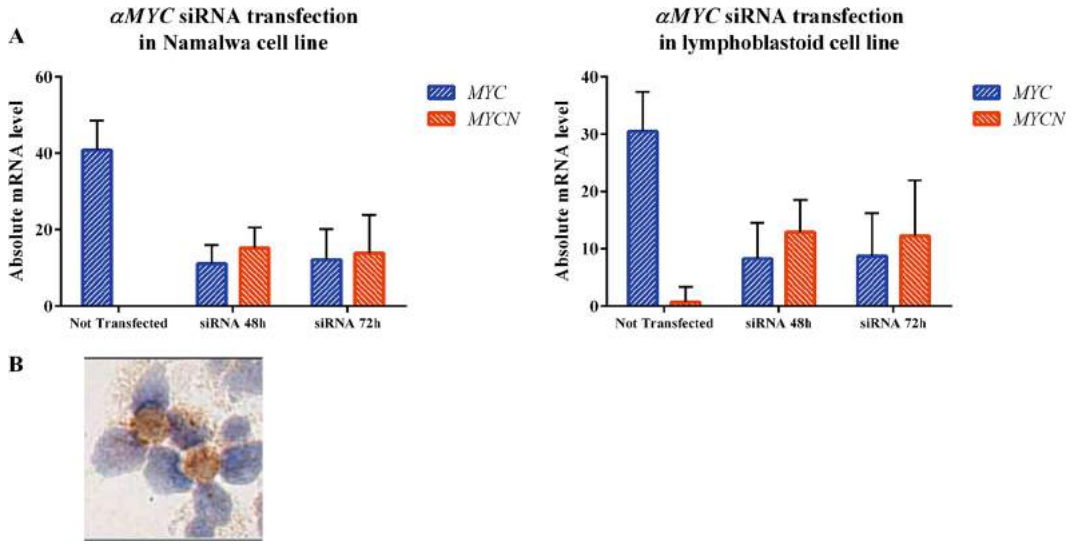

Fig. 5 Regulatory loop between MYC and MYCN exists also in Namalwa and lymphoblastoid cell lines. a Silencing of MYC mRNA expression by siRNA nucleofection in Namalwa and lymphoblastoid (B) cell lines resulted in a lower expression of MYC mRNA along with higher expression of MYCN. MYC mRNA has been investigated by RT-qPCR applying designed and Taqman primers. **b** Transfected cells collected after MYC silencing showed MYCN protein expression by immunohistochemistry.

SNVs, adjacent to N11 polymorphism and within the Y69 target epitope, may interfere with antibody binding and explain the MYC protein-negative staining.

On the other hand, MYCN positive samples, carried MYCN SNVs concentrated at the N-and C-terminus of the MYC amino-terminal region and at the helix-loop-helix (HLH) domain (Fig. 4a), where they likely perturb regulatory or functional motives of the protein. Indeed, while the first region (a.a. 20–90) is a segment important for post-translational modifications (PTMs) and binding events (e.g. GSK3, p38 MAPK, WW binding domains and FBXW7) leading to MYCN degradation[47], the second one (approximately a.a. 300–370), contains nuclear localization sequences (NLSs) (Fig. 4a; http://elm.eu.org/). The overall electrostatic charge switch caused by non-synonymous mutations in MYCN, with nearly 40% of SNVs leading to an increase of positive charge (Supplementary Table 3), is likely to affect the binding and signaling properties mediated by these motives. Along this line, SNVs affecting the C-terminal HLH domain are predicted to positively affect MYCN interactome in these cases, in contrast to MYC, which is overall disabled (Fig. 4b, c). Taken together, MYCN mutations in MYCN expressing cases are predicted to lead to an overall stabilization of its activity, by ultimately perturbing degradation signals while enhancing nuclear localization and mediated interactions. Interestingly, we found no significant enrichment of SNVs in *MYC*'s exon 2 phosphosite regions (Supplemetary Tables 3, 4), which is a hallmark of MYC up-regulation in sporadic BL[32]. Finally, to further support the hypothesis of a cross-talk between MYC and MYCN in BL, we silenced *MYC* gene in BL Namalwa and LCLs cell lines by shRNA and evaluated MYCN mRNA and protein expression after 48 and 72 h. We found that silencing of *MYC* gene results in higher expression of both MYCN mRNA and protein (Fig. 5a). Particularly, after siRNA nucleofection, MYC mRNA levels in Namalwa cell line dropped down from 40.79 arbitrary units (AU) to 11.03 AU at 48 h and 12.11 AU at 72 h, while *MYCN* increased from 0 to 15.2 at 48 and 13.89 at 72 h ($p < 0.0001$). In LCLs cell line *MYC* dropped down from 30.5 to 8.28 at 48 h and 8.75 at 72, while *MYCN* raised from 0.75 to 12.9 and 12.26 (48 and 72 h respectively). Consistently, MYCN protein expression was recorded after transfection by RT-qPCR (Fig. 5b).

Discussion

In this paper we describe a rare subset of BL cases characterized by the lack of MYC protein expression and the presence of MYCN protein. These rare cases, despite FISH analysis documenting *MYC* gene translocation to one of the immunoglobulin loci, lacked MYC protein expression and expressed another MYC family member, MYCN. Noteworthy, we observed an inverse correlation between the expression of MYC and MYCN at mRNA and protein level. It has been previously demonstrated that MYCN is able to compensate MYC activity in neuroblastoma cell lines and primary tumors, a mutual regulatory loop existing between them[7–13]. NGS analysis showed a different mutational fingerprint of *MYC* family genes in cases expressing or not MYCN at mRNA and protein level. Specifically, *MYCN* negative cases presented

SNVs in *MYC* genes localized within the region coding for the NTD. It is conceivable that such SNVs prevented an effective antigen-antibody reaction, as recently reported[34], thus determining the negative results at immunohistochemistry. By contrast, in MYCN positive samples analysis of MYCN SNVs at linear motives and interaction interfaces suggests converging effects towards an overall stabilization of protein activity, by either perturbation of degradation signals, enhancement of nuclear localization, or interactome stabilization. On the other hand, multiple somatic mutations affecting *MYC* suggest an overall loss-of-function phenotype, differently from sporadic BL, where SNVs cluster at exon 2 phosphosite regions leading to *MYC* up-regulation[32]. It is intriguing to speculate that the SNVs present in *MYC* and *MYCN* in the respective cases may activate and switch on *MYCN* gene and simultaneously switch off *MYC* gene by inducing their regulatory loop[48]. Interestingly, we found that silencing of *MYC* gene results in higher expression of both MYCN mRNA and protein. In particular, after siRNA nucleofection, MYC mRNA levels decreased while MYCN ones increased and MYCN protein expression was detectable in cell lines.

In conclusion, it is conceivable that *MYCN* determined molecular effects, in terms of transcriptional regulation, similar to those exerted by *MYC* in BL cells thanks to a cross-talk between the two genes involving a significant number of targets shared by MYC and MYCN[9–11,15,16]. This mirrors what is already known in neuroblastoma cell lines and primary tumors in which the expression of MYC and MYCN are mutually exclusive[9,11,15,16]. Remarkably, we have yet only detected the switch from MYC to MYCN expression in MYC-translocation-positive BL in the pediatric age group and only in eBL. Nevertheless, the genetic composition of the tumors suggests that the switch occurs in the presence and probably subsequently to the *IG-MYC* translocation. Therefore and considering that the clinical presentation, morphologic appearance and immunohistochemical profile of these MYC protein negative/MYCN protein-positive *MYC*-translocated tumors is not different from MYC protein-positive BL we think that this does not affect the diagnostic work-up as such cases might be easily diagnosed as BL based on current WHO criteria[13].

Author details
[1]Department of Medical Biotechnology, University of Siena, Siena, Italy. [2]Cell Networks, Bioquant, University of Heidelberg, Heidelberg, Germany. [3]Ulm University and Ulm University Medical Center, Ulm, Germany. [4]University of Nairobi, Nairobi, Kenya. [5]Department of Medical Biotechnology & Research Center of Advanced Technologies in Medicine, Torbat Heydariyeh University of Medical Sciences, Torbat Heydariyeh, Iran. [6]Moi Eldoret University, Eldoret, Kenya. [7]Department of Experimental, Diagnostic, and Specialty Medicine Bologna University Medical School, S. Orsola Malpighi Hospital, Bologna and Euro-Mediterranean Institute of Science and Technology (IEMEST), Palermo, Italy. [8]Jomo Kenyatta University of Agriculture and Technology, Nairobi, Kenya. [9]Pathodiagnostik Lab, Berlin, Germany

Conflict of interest
The authors declare that they have no conflict of interest.

Publisher's note
Springer Nature remains neutral with regard to jurisdictional claims in published maps and institutional affiliations.

Supplementary Information accompanies this paper at (https://doi.org/10.1038/s41408-019-0252-2).

Received: 4 March 2019 Revised: 29 July 2019 Accepted: 19 August 2019
Published online: 20 November 2019

References

1. Dang, C. V. MYC on the path to cancer. *Cell* **149**, 22–35 (2012).
2. Ambrosio, M. R. et al. MYC protein expression scoring and its impact on the prognosis of aggressive B-cell lymphoma patients. *Haematologica* **104**, e25–e28 (2019).
3. Sewastianik, T., Prochorec-Sobieszek, M., Chapuy, B. & Juszczyński, P. MYC deregulation in lymphoid tumors: molecular mechanisms, clinical consequences and therapeutic implications. *Biochim. Biophys. Acta* **1846**, 457–467 (2014).
4. Kieffer-Kwon, K. R. et al. Myc regulates chromatin decompaction and nuclear architecture during B cell activation. *Mol Cell* **67**, 566–578 (2017).
5. Beltran, H. The N-myc oncogene: maximizing its targets, regulation, and therapeutic potential. *Mol Cancer Res.* **12**, 815–822 (2014).
6. Facchini, L. M. & Penn, L. Z. The molecular role of Myc in growth and transformation: recent discoveries lead to new insights. *FASEB J.* **12**, 633–651 (1998).
7. Malynn, B. A. et al. N-myc can functionally replace c-myc in murine development, cellular growth, and differentiation. *Genes Dev.* **14**, 1390–1399 (2000).
8. Westermann, F. et al. Distinct transcriptional MYCN/c-MYC activities are associated with spontaneous regression or malignant progression in neuroblastomas. *Genome Biol.* **9**, R150 (2008).
9. Breit, S. & Schwab, M. Suppression of MYC by high expression of NMYC in human neuroblastoma cells. *J. Neurosci. Res.* **24**, 21–28 (1989).
10. Sivak, L. E. et al. Autoregulation of the human N-myc oncogene is disrupted in amplified but not single-copy neuroblastoma cell lines. *Oncogene* **15**, 1937–1946 (1997).
11. Delgado, M. D. & León, J. Myc roles in hematopoiesis and leukemia. *Genes Cancer* **1**, 605–616 (2010).
12. Aubry, S. & Charron, J. N-Myc shares cellular functions with c-Myc. *DNA Cell Biol* **19**, 353–364 (2000).
13. Swerdlow S. H. et al. (eds). *WHO classification of Tumours of Haematopoietic and Lymphoid Tissues* 4th edn. (IARC Press, Lyon, France, 2017).
14. Rickman, D. S., Schulte, J. H. & Eilers, M. The expanding world of N-MYC–driven tumors. *Cancer Discov* **8**, 150–163 (2018).
15. King, B. et al. The ubiquitin ligase Huwe1 regulates the maintenance and lymphoid commitment of hematopoietic stem cells. *Nat. Immunol.* **17**, 1312–1321 (2016).
16. Kawagoe, H., Kandilci, A., Kranenburg, T. A. & Grosveld, G. C. Overexpression of N-Myc rapidly causes acute myeloid leukemia in mice. *Cancer Res.* **67**, 10677–10685 (2007).
17. Ambrosio, M. R. et al. Standardization of MYC protein expression by immunohistochemistry and its correlation with MYC gene rearrangements in Burkitt lymphoma and diffuse large B-cell lymphoma. *Haematologica* **104**, e25–e28 (2019).
18. Zhu, W., Aihua, L. & Chen, T. In *Handbook of Practical Immunohistochemistry* 2nd edn (eds Lin F. & Prichard, J.) 77–84 (Springer, New York, NY, USA, 2015).
19. De Falco, G. et al. Burkitt lymphoma beyond MYC translocation: N-MYC and DNA methyltransferases dysregulation. *BMC Cancer* **15**, 668 (2015).
20. Hummel, M. et al. A biologic definition of Burkitt's lymphoma from transcriptional and genomic profiling. *N. Engl. J. Med.* **354**, 2419–2430 (2006).
21. Mathew, P. et al. Detection of MYCN gene amplification in neuroblastoma by fluorescence in situ hybridization: a pediatric oncology group study. *Neoplasia* **3**, 105–109 (2001).
22. Ventura, R. A. et al. FISH analysis for the detection of lymphoma-associated chromosomal abnormalities in routine paraffin-embedded tissue. *J. Mol. Diagn.* **8**, 141–151 (2006).

23. Ambrosio, M. R. et al. Plasmablastic transformation of a pre-existing plasmacytoma: a possible role for reactivation of Epstein Barr virus infection. *Haematologica* **99**, e235–e237 (2014).
24. Ambrosio, M. R. et al. A look into the evolution of Epstein-Barr virus-induced lymphoproliferative disorders: a case study. *Am. J. Clin. Pathol.* **144**, 817–822 (2015).
25. Mundo, L. et al. Unveiling another missing piece in EBV-driven lymphomagenesis: EBV-encoded MicroRNAs expression in EBER-negative Burkitt lymphoma cases. *Front Microbiol* **8**, 229 (2017).
26. Wang, F. et al. RNAscope: a novel in situ RNA analysis platform for formalin-fixed, paraffin-embedded tissues. *J Mol Diagn* **14**, 22–29 (2012).
27. McLaren, W. et al. The ensembl variant effect predictor. *Genome Biol* **1**, 122 (2016).
28. Jay, J. J. & Brouwer, C. Lollipops in the clinic: information dense mutation plots for precision medicine. *PLoS ONE* **11**, e0160519 (2016).
29. Dinkel, H. et al. ELM 2016-data update and new functionality of the eukaryotic linear motif resource. *Nucleic Acids Res.* **44**, D294–300 (2016).
30. Betts, M. J. et al. Mechismo: predicting the mechanistic impact of mutations and modifications on molecular interactions. *Nucleic Acids Res.* **43**, e10 (2015).
31. Raimondi, F. et al. Insights into cancer severity from biomolecular interaction mechanisms. *Sci Rep* **6**, 34490 (2016).
32. López, C. et al. Genomic and transcriptomic changes complement each other in the pathogenesis of sporadic Burkitt lymphoma. *Nat Commun* **10**, 1459 (2019).
33. Leucci, E. et al. MYC translocation-negative classical Burkitt lymphoma cases: an alternative pathogenetic mechanism involving miRNA deregulation. *J. Pathol.* **216**, 440–450 (2008).
34. Wagener, R. et al. Cryptic insertion of MYC exons 2 and 3 into the IGH locus detected by whole genome sequencing in a case of MYC-negative Burkitt lymphoma. *Haematologica* https://doi.org/10.3324/haematol.2018.208140 (2019).
35. Boxer, L. M. & Dang, C. V. Translocations involving c-myc and c-myc function. *Oncogene* **20**, 5595–5610 (2001).
36. Haralambieva, E. et al. Interphase fluorescence in situ hybridization for detection of 8q24/MYC breakpoints on routine histologic sections: validation in Burkitt lymphomas from three geographic regions. *Genes Chromosomes Cancer* **40**, 10–18 (2004).
37. Kapeli, K. & Hurlin, P. J. Differential regulation of N-Myc and c-Myc synthesis, degradation, and transcriptional activity by the Ras/mitogen-activated protein kinase pathway. *J. Biol. Chem.* **286**, 38498–38508 (2011).
38. van Lohuizen, M., Breuer, M. & Berns, A. N-myc is frequently activated by proviral insertion in MuLV-induced T cell lymphomas. *EMBO J* **8**, 133–136 (1989).
39. Abate, F. et al. Distinct viral and mutational spectrum of endemic Burkitt lymphoma. *PLoS Pathog* **11**, e1005158 (2015).
40. Amato, T. et al. Clonality analysis of immunoglobulin gene rearrangement by next-generation sequencing in endemic Burkitt lymphoma suggests antigen drive activation of BCR as opposed to sporadic Burkitt lymphoma. *Am. J. Clin. Pathol.* **145**, 116–127 (2016).
41. Dave, S. S. et al. Molecular diagnosis of Burkitt's lymphoma. *N. Engl. J. Med.* **354**, 2431–2442 (2006).
42. Schmitz, R., Ceribelli, M., Pittaluga, S., Wright, G. & Staudt, L. M. Oncogenic mechanism in Burkitt lymphoma. *Cold Spring Harb Perspect. Med.* **4**, a014282 (2014).
43. Schmitz, R. et al. Burkitt lymphoma pathogenesis and therapeutic targets from structural and functional genomics. *Nature* **490**, 116–20 (2012).
44. Love, C. et al. The genetic landscape of mutations in Burkitt lymphoma. *Nat. Genet.* **44**, 1321–5 (2012).
45. Richter, J. et al. Recurrent mutation of the ID3 gene in Burkitt lymphoma identified by integrated genome, exome and transcriptome sequencing. *Nat. Genet.* **44**, 1316–20 (2012).
46. Grande, B. M. et al. Genome-wide discovery of somatic coding and noncoding mutations in pediatric endemic and sporadic Burkitt lymphoma. *Blood* https://doi.org/10.1182/blood-2018-09-871418 (2019)
47. Otto, T. et al. Stabilization of N-Myc is a critical function of Aurora A in human neuroblastoma. *Cancer Cell* **15**, 67–78 (2009).
48. Cotterman, R. et al. N-Myc regulates a widespread euchromatic program in the human genome partially independent of its role as a classical transcription factor. *Cancer Res* **68**, 9654–9662 (2008).

Brief Communication to Cancer Genetics

Immuno-deficiency related high-grade B-cell lymphoma with 11q aberration: Further evidence for a lymphoma entity from a patient with simultaneous Papillary Renal Cell Carcinoma occurring after pediatric kidney transplant

Raffaella Guazzo[1], Anja Pfaus[2], Alberto Fabbri[3], Guido Garosi[4], Massimo Granai[1], Sergio Antonio Tripodi[1] Kathrin Oehl-Huber[2], Susanne Bens[2], Abukabar Moawia[2], Emanuele Cencini[3], Stefano Lazzi[1], Reiner Siebert[2], Lorenzo Leoncini[1]

[1] Department of Medical Biotechnology, Siena University

[2] Institute of Human Genetics, Ulm University and Ulm University Medical Center, Albert-Einstein-Allee 11, D-89081 Ulm, Germany

[3] Haematology Unit, Siena University

[4] Nephrology, Dyalisis and Transplantation Unit, Siena University

Corresponding Author:

Professor Lorenzo Leoncini

ABSTRACT

Burkitt-like lymphoma (BLL) with 11q aberration is characterized by morphological features and an immunophenotypic profile resembling those of Burkitt lymphoma but lacks the IG-*MYC* translocation. It is cytogenetically characterized by a peculiar pattern of an 11q aberration consisting of a gain in 11q23.2-23.3 followed by a telomeric loss in 11q24.1-qter. BLL-11q cases occur over a wide age range but are more common in children and young adults.

Here, we report the case of a 25-year-old patient developing a *MYC*-negative BLL (**LBL11q**), after kidney transplant in childhood and presenting with simultaneous papillary renal cell carcinoma of the kidney. Interphase FISH for the detection of 11q alteration was performed both on lymph node and renal cell carcinoma. At the same time, array-based copy number analyses were carried out.

In lymph node, FISH in line with array-based copy number analyses showed amplifications in 11q23.3q24.1 and loss in 11q24.1q25, while a gain of whole chromosome 11 was detected in the papillary renal cell carcinoma.

Our findings support the view, that similarly to classical Burkitt lymphoma besides supposedly sporadic cases a subgroup of immunodeficiency-related **LBL11q**, exists.

Introduction

Historically, Burkitt lymphoma has been a frontrunner and model disease with regard to somatic cancer genetics and virus driven tumorigenesis. After the initial discovery of the Burkitt translocation t(8;14)(q24;q32) (Manolov&Manolova, 1972; Zech et al,, 1976), the subsequent description of the variant Burkitt translocation t(8;22) and t(2;8) and the identification of the *MYC* oncogene deregulated by juxtaposition next to one of the IG-enhancers, it is nowadays widely accepted that the *IG::MYC* translocation is the genetic hallmark of Burkitt lymphomas. Indeed, an *IGH:MYC*, *IGK::MYC* or *IGL::MYC* translocation can be observed by cytogenetic and molecular cytogenetic techniques in more than 90% of Burkitt lymphomas. Moreover, a subset of formerly supposedly *MYC*-translocation negative Burkitt lymphomas has meanwhile shown to carry *IG:MYC* alterations cryptic to metaphase and interphase cytogenetics but well detectable by modern sequencing technologies (Wagener et al., 2020). Nevertheless, a small subset of high-grade B-cell lymphomas with features of Burkitt lymphomas remain which bona fide lack a genomic event deregulating the *MYC* gene. A good subset of these cases has been recently shown to carry a peculiar pattern of chromosome 11 aberration, namely a gain in 11q23 and a more telomeric loss in 11q (Rymkiewicz et al., 2018; Salaverria et al., 2014; Wagener et al., 2019). These cases have been named Burkitt like lymphoma with 11q aberration in the 2016 edition of WHO classification (Swerdlow et al., 2016). Despite showing a similar morphology with Burkitt lymphomas, the genetic alterations of these cases with 11q aberration differ quite strongly from those of Burkitt lymphomas (Rymkiewicz et al., 2018; Salaverria et al., 2014; Wagener et al., 2019) and until further naming by the next WHO classification they can be referred to as *MYC*-negative high-grade B-cell lymphomas with 11q aberration (hgBCL, 11q) as initially described.

Classical Burkitt lymphomas are historically divided into three epidemiologic subgroups: sporadic Burkitt lymphoma, endemic Burkitt lymphoma and immunodeficiency related Burkitt-lymphoma (Swerdlow et al., 2016). With regard to the latter, the immunodeficiency can be inborn or acquired. Inborn immunodeficiencies include rare genetic disorders like ataxia telangiectasia (AT, OMIM #208900), Nijmegen breakage syndrome (NBS, OMIM #251260) or X-linked lymphoproliferative disease (Purtillo or Duncan’s syndrome, OMIM #308240). Acquired immunodeficiencies include among others therapeutic immunosuppression after organ-transplant or HIV-associated immunodeficiency. Remarkable, already the first description of hgBCL, 11q, by our group reported the disease in a patient with ataxia telangiectasia (Salaverria et al., 2014). Subsequently, Ferreiro et al. (2015) provided evidence that the typical 11q aberration pattern is particularly frequent in BL in immunodeficient hosts. Indeed, these authors showed that the typical 11q pattern is significantly more frequent in BL occurring in the setting of transplantation and immunosuppression (43% of all post-

transplant-mBL and 60% of EBV-negative post-transplant-mBL) than in immunocompetent patients (3%) (Ferreiro et al, 2015).

Here, we report another patient developing hgBCL,11q, after kidney transplant in childhood and presenting with simultaneous papillary renal cell carcinoma of the kidney. Both tumors share gains on chromosome 11 but due to different mechanisms, which can be a diagnostic pitfall. Our findings support the view that similarly to classical Burkitt lymphoma besides supposedly sporadic cases a subgroup of immunodeficiency-related hgBCL, 11q, exists.

Case report.

We here report a male renal transplant recipient with developmental delay and hypogonadism . He had suffered from lupus nephropathy since early childhood. Despite immunosuppressive therapy since age of 8 years that condition worsened over time ultimately leading to renal insufficiency. At the age of 17 years the patient had received a deceased-donor kidney transplant (male) with subsequent standard triple immunosuppressive maintenance therapy (tacrolimus, mycophenolatemofetil and steroid). The graft functionality was excellent with average creatinine values of around 1,2 mg/dl (ClCr 80 ml/min). At presentation, a routine abdominal echography followed by total body CT scan with contrast and PET scan demonstrated a right native kidney mass and massive lymphadenopathy.

A biopsy of the kidney mass showed type 2 papillary renal cell carcinoma (pRCC). Additionally, a through cut biopsy of a cervical lymph node was performed to exclude metastasis form the pRCC. Remarkably, the histologic and cytogenetic analyses detailed below revealed the diagnosis of a hgBCL,11q. Bone marrow biopsy and cerebral spinal fluid analysis were negative for lymphomatous involvement. (IIIA Ann Arbor staging, IPI 2 with LDH increased) The lymphoma was treated with 4 cycles of chemotherapy (IVAC regimen). The control PET and CT imaging 5 month after diagnosis were negative. Seven months after diagnosis, robot-assisted right nephrectomy surgery was performed. At time of writing (approximately 3 years after diagnosis), the lymphoma appears in regression and the follow-up of the kidney cancer is negative; kidney function was normal at last follow-up (Supplementary Figure 1).

Materials and methods

Histopathology

Lymph node and renal tissues were fixed in formalin and embedded in paraffin. They were stained with HE and with Giemsa staining for lymphoma.

Immunohistochemical staining for both lymphoma and renal cell carcinoma diagnosis using a panel of antibodies listed in Supplementary Table 1a and 1b was performed on a Ventana platform, following the manufacturer's instructions.

Fluorescence in situ Hybridization (FISH)

FISH on FFPE sections of the tumors was conducted according to standard procedures (Ventura et al., 2006). Briefly, 4-mm-thick tissue embedded in paraffin was cut, the slides were incubated in heat pretreatment solution, washed, digested, dehydrated, hybridized with probes.

On the lymph node biopsy, interphase cytogenetic analysis was performed using commercial break apart probes LSI BCL2 BAP, LSI BCL6 BAP and LSI MYC BAP (all Abbott), as well as a commercial triple color LSI IGH/MYC/CEP8 probe (Abbott). In addition, recently described double-color double-fusion probes for the detection of *IGK:MYC* and *IGL:MYC* fusions as well as for the typical 11q aberration pattern were applied (Hummel et al., 2006; Martín-Subero et al., 2002; Salaverria et al., 2014). For the latter, in addition a commercial 11q gain/loss Triple Color Probe (Bio-Optica) was applied.

Genome-wide copy number and loss-of-heterozygosity mapping using OncoScan

DNA from tumor tissues was extracted using the GeneRead DNA FFPE Kit (Qiagen, Hilden, Germany) and from blood using MagCore Genomic DNA Whole Blood Kit (Diatech, Pharmacogenetics, Jesi, Italy). DNA was hybridized to an OncoScan CNV assay (Thermo Fisher Scientific, Waltham, MA, USA). Analysis was performed using the Chromosome Analysis Suite Software version 4.0 (Thermo Fisher Scientific, Waltham, MA, USA). Only copy number alterations larger than 50kb, encompassing at least 20 informative probes with a median log2ratio of >0.2 or <-0.2 and copy number neutral losses of heterozygosity larger than 5 Mb were considered for further analyses. All variants were manually inspected and curated considering the B-allele-frequency and the sample quality.

Tumor and Germline Exome Sequencing

DNA from both tumors and blood was subjected to exome sequencing using XXX … was analysed using targeted enrichment (TruSight Rapid Capture Kit) followed by Next Generation Sequencing (Illumina: TruSight One®, >4800 genes). Sequencing was conducted using a MiSeq Reagent Kit v.3 Flow Cell (600 cycles). The minimal coverage was set to 20x. Analysis was performed using the hg19 genome version and exclusively for a list of genes associated with cancer predisposition and immune defects (see Supplementary Tables XXX). Only coding exonic regions of the genes as well as 10bp

of the flanking intronic regions were evaluated using the in silico prediction tools SIFT, PolyPhen-2, MutationTaster and Align GVGD as well as the clinical databases HGMD professional, ClinVar and LOVD.

Nextera: Exome sequencing was performed on ≈ 50 ng of genomic DNA isolated from fresh frozen tissue using the NextSeq High Output Kit v2.5 (300 cycles; Illumina: Nextera™ Exome Kit) and sequenced on a NextSeq platform. Data was analyzed with Varvis-Software Version 1.18.4 (Limbus Medical Technologies GmbH, Rostock).

Results

Histopathology

The histological examination of cervical lymph node biopsy revealed sheets of medium to large-sized tumor cells with fine or vesicular chromatin, one or multiple prominent nucleoli, frequent mitosis and few tingible body macrophages with 'starry sky' appearance. Tumor cells were diffusely positive for CD20, CD10, BCL6 and Ki67 (almost 100%) and MYC protein expression but negative (fig.2) for TDT, BCL2, and CyclinD1.Though >40% of cells was positive for MYC immunostaining, staining intensity was weaker than the typical for Burkitt Lymphoma (BL) and suggested the possibility of the diagnosis of hgBCL,11q (i.e. MYC-negative Burkitt-like lymphoma with 11q aberration according to the revised 4th Edition of the WHO Classification of Tumors of the Haematopoietic and Lymphatic Tissue).

Gross and microscopic examination of the recipient renal mass revealed a pigmented renal carcinoma with type 2 papillary architecture (nuclear grade 3, pT3a TNM eight edition; Moch et al., 2016) The immunophenotype was positive for CDAE1-AE3, CD10, CK7, AMACR, HMB45, MELAN-A, TFE-3 and PAX8. Morphology and immunophenotype were suspicious for a Microphthalmia family of transcription factors associated renal cell carcinoma (MiT family). (fig.3)

Interphase Cytogenetics

FISH analyses in the lymph node biopsy showed no evidence of a breakpoint in the MYC locus (8q24) or of any kind *IG:MYC* fusion. Thus, a structural variant at the *MYC* locus involving one of the three *IG* loci as typical for BL could be widely excluded. Nevertheless, around 50-60% of nuclei per probe showed three signals indicating a gain at the MYC locus, whereas the probes for the centromeric region of chromosome 8 and the three *IG* loci shows diploid patterns. Breakpoints or imbalances affecting the *BCL2* (18q21) or *BCL6* (3q27) loci were also not detectable by FISH. Interphase FISH analyses using two different 11q assays consistently detected signals patterns

indicating gain in the 11q23.3 region and loss in 11q24 in around 80% of nuclei examined, with a normal diploid signal pattern for the centromeric region of chromosome 11 (Figure 1a). In the papillary RCC, FISH analysis showed an average of three copies for all probes on chromosome 11 (Figure 1b).

Array-based copy number analyses were in line with the FISH analyses and showed gain of chromosome whole chromosome 11 in the papillary RCC, in contrast to amplifications (7-8 copies) in 11q23.3q24.1 and loss in 11q24.1q25 (1 copy) in the lymphoma sample (Figure 1c,d). The regions of imbalance in 11q in the lymphoma sample contained previously discussed candidate genes in hgBCL,11q, like *POU2F3* and *KMT2A* in the gained and *ETS1* and *NFRKB* in the lost region (Salaverria et al., 2014; Wagener et al., 2019) (Supplementary Table 2). Thus, both the papillary RCC and the lymphoma sample share gain in 11q23.3q24.1, but due to different mechanisms. Whereas the papillary RCC displays the typical pattern of gains and losses of multiple whole chromosomes as typical for this entity, the lymphoma exhibits a more restricted set of additional imbalances, including complex rearrangements of chromosome 6, gain in 8q22q24 containing the *MYC* gene locus, trisomy 12 and copy-neutral loss of heterozygosity encompassing major parts of chromosome 17 including the TP53 gene locus. Chromosome 6, besides a large deletion in the long arm encompassing well-known tumor suppressors in lymphomas like *PRDM1* and *TNFAIP3* carried a complex pattern of focal gains and losses resembling chromothripsis in the short arm. Whereas the most highly gained region (6 copies) in 6p contained the lymphoma-related oncogene *PIM1*, the deleted region encompassed the HLA locus but also tumor suppressors like *CDKN1A*.

No clinically relevant imbalance was detected in the blood sample of the patient. Nevertheless, it is remarkable to note, that all samples, including the blood sample, shared a long stretch of homozygosity of over 5Mb in 20p11.23p12.2 (Genes listed in Supplementary Table 3). This locus contains the *MACROD2* gene, which has been associated with the NF-kB pathway, chromosome instability and was found focally deleted in several cancer types resembling a common fragile site (Sakthianandeswaren et al., 2018; Palazzo et al., 2019; Rajaram et al., 2013). Additionally, *MACROD2* is included in the list of SLE associated genes of the Harmonize project (Rouillard et al., 2016).

Exome sequencing

Exome sequencing was performed for both tumors and the germline blood sample and revealed 42 sequencing variants shared between all three samples (Table 1). Pathogenic variants included a missense variant in *INPP5E*, a frameshift variant in *MPO* and a missense variant in *PRKN*.

Of note, germline variants with unknown significance (VUSs) further include a missense mutation in *INPP5D* (also known as *SHIP1*), which was predicted to be damaging. B cells of Ship deficient mice show lower thresholds for activation and are not properly selected for high-affinity antibodies leading to spontaneous lupus development (Leung et al., 2013). Additionally, the *TNFα/MiR-155/INPP5D* pathway was shown to influence proliferation of DLBCL cells (Pedersen et al., 2009). Moreover, VUS germline variants affected several genes associated with the immune system, such as *CD5*, *RNF31, CR1, C8B, MS4A1, TGFB2, C1QB* and *DOCK8*.

Variants specific to the lymphoma (n = 22) and classified as likely pathogenic included recurrently mutated genes in mnBLL, 11q, such as *PIK3R1* and *TP53* (Gonzales-Farre et al., 2019) (Table 1). A VUS was further reported in *MTA3*, a BCL6-associated transcriptional co-repressor in GCB cells and lymphomas (Jaye et al., 2007).

Amongst the 6 variants exclusively found in the renal cell carcinoma, a pathogenic variant in *SNX14* was found. An additional VUS was identified in *EPHA5*, which was shown to be associated with tumor stage in ccRCC (Wang et al., 2017).

When comparing all identified variants to recurrently mutated genes in mnBLL, 11q (Wagener et al., 2019; Gonzales-Farre et al., 2019), only *MUC5B*, found as germline variant, was detected in addition to *PIK3R1* and *TP53*. However, mutations in *MUC5B* were considered as dubious hit in earlier publications (Wagener et al., 2019; Lawrence et al., 2013).

No germline variants were detected in genes located in the homozygously deleted region at 20p11.23p12.2. Only in the lymphoma sample 5 variants with very low read numbers and quality scores were detected in genes in this region (*RIN2, SLC24A3, POLR3F, PET117, KIF16B*).

Discussion

In the present report we provide further evidence for the existence of an immune-deficiency associated subtype of high-grade B-cell lymphomas with 11q aberration and features of Burkitt lymphomas. Our findings corroborate prior reports, including our initial description of this lymphoma entity and the extensive analyses by Ferreiro et al. suggesting an increased incidence of hgBCL, 11q, particularly in patients with inborn or acquired errors of immunodeficiency. A potential reasons could for this increased incidence of hgBCL, 11q, in immunocompromised patients could be the existence of a peculiar cell-of-origin population. Indeed, we have recently proposed for BL, that the cell population at risk could be a germinal center derived B-cell population poised to express IgA which experiences a first microbial challenge in a primary immune response (Lopez et al., 2019; ElGafaary et al., 2021). Indeed, inborn and acquired immunodeficiencies lead to the loss of immunologic

memory, and, thus, to a higher rate of primary immune responses extending the cell population at risk to develop BL as well as hgBCL, 11q. In contrast to BL, considering the predominant nodal presentation of disease, hgBCL, 11q, seem not to have a preponderance for the mucosa-associated tissue lymphatic system. Also in the present cases there was predominant nodal involvement. Thus, hgBCL, 11q, might derive from a mislead primary B-cell response not poised for IgA expression, as typical for the gastrointestinal tract, but more poised to a systemic (e.g. IgG) response. This might explain the different body sites affected as well as the different pattern of somatic mutations in hgBCL,11q as compared to BL with the prior more resembling mutational patterns typical for primary lymphomas not presenting in the gut, like DLBCL (REFs hier zu diversen papern Wagener, Schmitz, Chapuy, Dave). Also the present case matches in this pattern both with regard to clinical presentation somatic mutation pattern.

The current case is of particular interest, as it displays features of inborn errors and acquired disturbancies of immunity, as well as two synchronous malignancies. The latter forces the hypothesis, that there could be a (cancer stem) cell common to both malignancies. Indeed, the tumor cells of the lymphoma and the pRCC shared regions of imbalance, particularly gains in 8q encompassing the MYC oncogene and the name-giving gain in 11q23.3. Nevertheless, the mechanism of gain was different in both lymphomas, being whole chromosome gain in the pRCC and structural variation in the hgBCL,11q. The only chromosomal aberration truly in common between both was trisomy (i.e. gain of whole chromosome) 12, which was not detected in the blood sample of the patient. Thus, we cannot rule out that this event has been present in an early ancestor cell.

With regard to the immunodeficiency, the patient received immune-modulating treatment before and after renal transplant, which is a sufficient cause for immune-dysregulation. Nevertheless, immune dysregulation (immunodeficiency instead of immune dysregulation) is also the cause of immune dysregulation. Thus, we evaluated the exome sequencing data also with regard to genetic variants linked to immune-disorders and cancer predisposition.

Acknowledgements

Contributions

References

[1] Manolov G, Manolova Y. Marker band in one chromosome 14 from Burkitt lymphoma. Nature. 1972; 237:33–34

[2] L. Zech, U. Haglund, K. Nilsson, G. Klein. Characteristic chromosomal abnormalities in biopsies and lymphoid-cell lines from patients with burkitt and non-burkitt lymphomas. International Journal of Cancer. 1976; 47-56

[3] Salaverria I, Martin-Guerrero I, Wagener R, et al. A recurrent 11q aberration pattern characterizes a subset of MYC-negative high-grade B-cell lymphomas resembling Burkitt lymphoma. Blood. 2014;123:1187-11*98.*

[4] Ferreiro J., Julie Morscio, et al. Post-transplant molecularly defined Burkitt lymphomas are frequently MYC -negative and characterized by the 11q-gain/loss pattern. Haematologica.2015; 100:e275-9.

[5] Leticia Quintanilla-Martinez. The 2016 updated WHO classification of lymphoid neoplasias. Hematological Oncology. 2017;35(S1):37–45.

Leung WH, Tarasenko T, Biesova Z, Kole H, Walsh ER, Bolland S. Aberrant antibody affinity selection in SHIP-deficient B cells. Eur J Immunol. 2013 Feb;43(2):371-81. doi: 10.1002/eji.201242809. Epub 2012 Dec 12. PMID: 23135975; PMCID: PMC3903325.

Pedersen IM, Otero D, Kao E, Miletic AV, Hother C, Ralfkiaer E, Rickert RC, Gronbaek K, David M. Onco-miR-155 targets SHIP1 to promote TNFalpha-dependent growth of B cell lymphomas. EMBO Mol Med. 2009 Aug;1(5):288-95. doi: 10.1002/emmm.200900028. PMID: 19890474; PMCID: PMC2771872.

Wang X, Xu H, Wu Z, Chen X, Wang J. Decreased expression of EphA5 is associated with Fuhrman nuclear grade and pathological tumour stage in ccRCC. Int J Exp Pathol. 2017 Feb;98(1):34-39. doi: 10.1111/iep.12219. Epub 2017 Apr 19. PMID: 28421649; PMCID: PMC5447857.

Palazzo L, Mikolčević P, Mikoč A, Ahel I. ADP-ribosylation signalling and human disease. Open Biol. 2019 Apr 26;9(4):190041. doi: 10.1098/rsob.190041. PMID: 30991935; PMCID: PMC6501648.

Rajaram M, Zhang J, Wang T, Li J, Kuscu C, Qi H, Kato M, Grubor V, Weil RJ, Helland A, Borrenson-Dale AL, Cho KR, Levine DA, Houghton AN, Wolchok JD, Myeroff L, Markowitz SD, Lowe SW, Zhang M, Krasnitz A, Lucito R, Mu D, Powers RS. Two Distinct Categories of Focal Deletions in Cancer Genomes. PLoS One. 2013 Jun 21;8(6):e66264. doi: 10.1371/journal.pone.0066264. PMID: 23805207; PMCID: PMC3689739.

Sakthianandeswaren A, Parsons MJ, Mouradov D, MacKinnon RN, Catimel B, Liu S, Palmieri M, Love C, Jorissen RN, Li S, Whitehead L, Putoczki TL, Preaudet A, Tsui C, Nowell CJ, Ward RL, Hawkins NJ, Desai J, Gibbs P, Ernst M, Street I, Buchert M, Sieber OM. *MACROD2* Haploinsufficiency Impairs Catalytic Activity of PARP1 and Promotes Chromosome Instability and Growth of Intestinal Tumors. Cancer Discov. 2018 Aug;8(8):988-1005. doi: 10.1158/2159-8290.CD-17-0909. Epub 2018 Jun 7. PMID: 29880585.

Jaye DL, Iqbal J, Fujita N, Geigerman CM, Li S, Karanam S, Fu K, Weisenburger DD, Chan WC, Moreno CS, Wade PA. The BCL6-associated transcriptional co-repressor, MTA3, is selectively expressed by germinal centre B cells and lymphomas of putative germinal centre derivation. J Pathol. 2007 Sep;213(1):106-15. doi: 10.1002/path.2199. PMID: 17573669.

Lawrence MS, Stojanov P, Polak P, Kryukov GV, Cibulskis K, Sivachenko A, Carter SL, Stewart C, Mermel CH, Roberts SA, Kiezun A, Hammerman PS, McKenna A, Drier Y, Zou L, Ramos AH, Pugh TJ, Stransky N, Helman E, Kim J, Sougnez C, Ambrogio L, Nickerson E, Shefler E, Cortés ML, Auclair D, Saksena G, Voet D, Noble M, DiCara D, Lin P, Lichtenstein L, Heiman DI, Fennell T, Imielinski M, Hernandez B, Hodis E, Baca S, Dulak AM, Lohr J, Landau DA, Wu CJ, Melendez-Zajgla J, Hidalgo-Miranda A, Koren A, McCarroll SA, Mora J, Crompton B, Onofrio R, Parkin M, Winckler W, Ardlie K, Gabriel SB, Roberts CWM, Biegel JA, Stegmaier K, Bass AJ, Garraway LA, Meyerson M, Golub TR, Gordenin DA, Sunyaev S, Lander ES, Getz G. Mutational heterogeneity in cancer and the search for new cancer-associated genes. Nature. 2013 Jul 11;499(7457):214-218. doi: 10.1038/nature12213. Epub 2013 Jun 16. PMID: 23770567; PMCID: PMC3919509.

Rouillard AD, Gundersen GW, Fernandez NF, Wang Z, Monteiro CD, McDermott MG, Ma'ayan A. The harmonizome: a collection of processed datasets gathered to serve and mine knowledge about genes and proteins. Database (Oxford). 2016 Jul 3;2016:baw100. doi: 10.1093/database/baw100. PMID: 27374120; PMCID: PMC4930834.

Wagener R, Bens S, Toprak UH, Seufert J, López C, Scholz I, Herbrueggen H, Oschlies I, Stilgenbauer S, Schlesner M, Klapper W, Burkhardt B, Siebert R. Cryptic insertion of *MYC* exons 2 and 3 into the immunoglobulin heavy chain locus detected by whole genome sequencing in a case of "*MYC*-negative" Burkitt lymphoma. Haematologica. 2020 Apr;105(4):e202-e205. doi: 10.3324/haematol.2018.208140. Epub 2019 May 9. PMID: 31073073; PMCID: PMC7109723.

Rymkiewicz G, Grygalewicz B, Chechlinska M, Blachnio K, Bystydzienski Z, Romejko-Jarosinska J, Woroniecka R, Zajdel M, Domanska-Czyz K, Martin-Garcia D, Nadeu F, Swoboda P, Rygier J, Pienkowska-Grela B, Siwicki JK, Prochorec-Sobieszek M, Salaverria I, Siebert R, Walewski J. A comprehensive flow-cytometry-based immunophenotypic characterization of Burkitt-like lymphoma with 11q aberration. Mod Pathol. 2018 May;31(5):732-743. doi: 10.1038/modpathol.2017.186. Epub 2018 Jan 12. PMID: 29327714.

Salaverria I, Martin-Guerrero I, Wagener R, Kreuz M, Kohler CW, Richter J, Pienkowska-Grela B, Adam P, Burkhardt B, Claviez A, Damm-Welk C, Drexler HG, Hummel M, Jaffe ES, Küppers R, Lefebvre C, Lisfeld J, Löffler M, Macleod RA, Nagel I, Oschlies I, Rosolowski M, Russell RB, Rymkiewicz G, Schindler D, Schlesner M, Scholtysik R, Schwaenen C, Spang R, Szczepanowski M, Trümper L, Vater I, Wessendorf S, Klapper W, Siebert R; Molecular Mechanisms in Malignant Lymphoma Network Project; Berlin-Frankfurt-Münster Non-Hodgkin Lymphoma Group. A recurrent 11q aberration pattern characterizes a subset of MYC-negative high-grade B-cell lymphomas resembling Burkitt lymphoma. Blood. 2014 Feb 20;123(8):1187-98. doi: 10.1182/blood-2013-06-507996. Epub 2014 Jan 7. PMID: 24398325; PMCID: PMC3931189.

Wagener R, Seufert J, Raimondi F, Bens S, Kleinheinz K, Nagel I, Altmüller J, Thiele H, Hübschmann D, Kohler CW, Nürnberg P, Au-Yeung R, Burkhardt B, Horn H, Leoncini L, Jaffe ES, Ott G, Rymkiewicz G, Schlesner M, Russell RB, Klapper W, Siebert R. The mutational landscape of Burkitt-like lymphoma with 11q aberration is distinct from that of Burkitt lymphoma. Blood.

2019 Feb 28;133(9):962-966. doi: 10.1182/blood-2018-07-864025. Epub 2018 Dec 19. PMID: 30567752; PMCID: PMC6396176.

Swerdlow S, et al. in WHO Classification of Haematopoietic and Lymphoid Tissues (ed Swerdlow S, et al.), International Agency for Research on Cancer, Lyon, France, 2017.

Swerdlow SH, Campo E, Pileri SA, Harris NL, Stein H, Siebert R, Advani R, Ghielmini M, Salles GA, Zelenetz AD, Jaffe ES. The 2016 revision of the World Health Organization classification of lymphoid neoplasms. Blood. 2016 May 19;127(20):2375-90. doi: 10.1182/blood-2016-01-643569. Epub 2016 Mar 15. PMID: 26980727; PMCID: PMC4874220.

Ventura RA, Martin-Subero JI, Jones M, McParland J, Gesk S, Mason DY, Siebert R. FISH analysis for the detection of lymphoma-associated chromosomal abnormalities in routine paraffin-embedded tissue. J Mol Diagn. 2006 May;8(2):141-51. doi: 10.2353/jmoldx.2006.050083. PMID: 16645199; PMCID: PMC1867591.

Hummel M, Bentink S, Berger H, Klapper W, Wessendorf S, Barth TF, Bernd HW, Cogliatti SB, Dierlamm J, Feller AC, Hansmann ML, Haralambieva E, Harder L, Hasenclever D, Kühn M, Lenze D, Lichter P, Martin-Subero JI, Möller P, Müller-Hermelink HK, Ott G, Parwaresch RM, Pott C, Rosenwald A, Rosolowski M, Schwaenen C, Stürzenhofecker B, Szczepanowski M, Trautmann H, Wacker HH, Spang R, Loeffler M, Trümper L, Stein H, Siebert R; Molecular Mechanisms in Malignant Lymphomas Network Project of the Deutsche Krebshilfe. A biologic definition of Burkitt's lymphoma from transcriptional and genomic profiling. N Engl J Med. 2006 Jun 8;354(23):2419-30. doi: 10.1056/NEJMoa055351. PMID: 16760442.

Martín-Subero JI, Harder L, Gesk S, Schlegelberger B, Grote W, Martinez-Climent JA, Dyer MJ, Novo FJ, Calasanz MJ, Siebert R. Interphase FISH assays for the detection of translocations with breakpoints in immunoglobulin light chain loci. Int J Cancer. 2002 Mar 20;98(3):470-4. doi: 10.1002/ijc.10169. PMID: 11920602.

Gonzalez-Farre B, Ramis-Zaldivar JE, Salmeron-Villalobos J, Balagué O, Celis V, Verdu-Amoros J, Nadeu F, Sábado C, Ferrández A, Garrido M, García-Bragado F, de la Maya MD, Vagace JM, Panizo CM, Astigarraga I, Andrés M, Jaffe ES, Campo E, Salaverria I. Burkitt-like lymphoma with 11q aberration: a germinal center-derived lymphoma genetically unrelated to Burkitt lymphoma. Haematologica. 2019 Sep;104(9):1822-1829. doi: 10.3324/haematol.2018.207928. Epub 2019 Feb 7. PMID: 30733272; PMCID: PMC6717587.

Groot N, Shaikhani D, Teng YKO, de Leeuw K, Bijl M, Dolhain RJEM, Zirkzee E, Fritsch-Stork R, Bultink IEM, Kamphuis S. Long-Term Clinical Outcomes in a Cohort of Adults With Childhood-Onset Systemic Lupus Erythematosus. Arthritis Rheumatol. 2019 Feb;71(2):290-301. doi: 10.1002/art.40697. PMID: 30152151; PMCID: PMC6590133.

Moch H, Cubilla AL, Humphrey PA, Reuter VE, Ulbright TM. The 2016 WHO Classification of Tumours of the Urinary System and Male Genital Organs-Part A: Renal, Penile, and Testicular Tumours. Eur Urol. 2016 Jul;70(1):93-105. doi: 10.1016/j.eururo.2016.02.029. Epub 2016 Feb 28. PMID: 26935559.

Figure 1: FISH and OncoScan

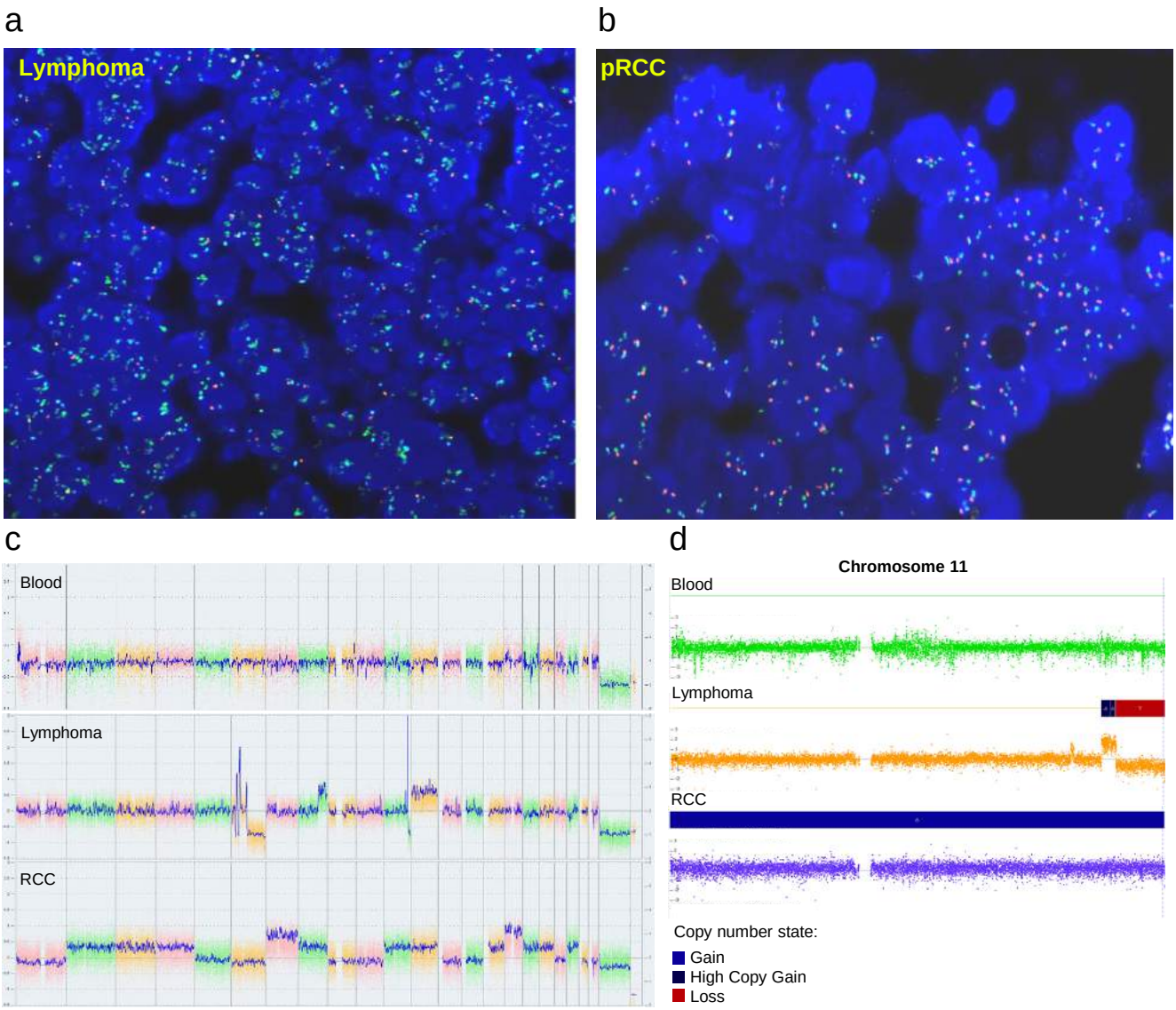

Figure 1: Cytogenetic and copy-number analyses of lymphoma and pRCC. a, FISH analysis of cervical lymph node biopsy using the 11q gain / loss triple color probe showed clustered green signals in the 11q23.3 region but only one orange signal in the 11q24.3 region, confirming the presence of the typical loss pattern of gain 11q. The centromeric region of chromosome 11 is indicated by the blue signal **b,** FISH analysis of the pRCC using 11q gain/loss triple color probe showed 2 to 3 for all regions on chromosome 11 investigated. **c,** OncoScan analysis showing whole genome views of copy-number alterations in the blood, the lymphoma and the pRCC sample. **d,** Copy number states of chromosome 11 of blood, lymphoma and pRCC sample indicating a balanced genotype in the blood, the typical gain/loss pattern in the lymphoma and trisomy of the complete chromosome 11 in the pRCC .

Figure 2: HE and immunostaining of lymphoma

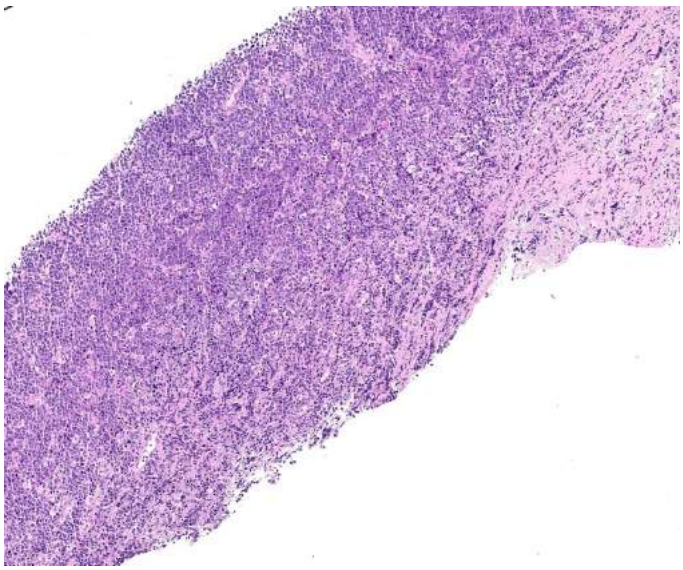

HE (10x)

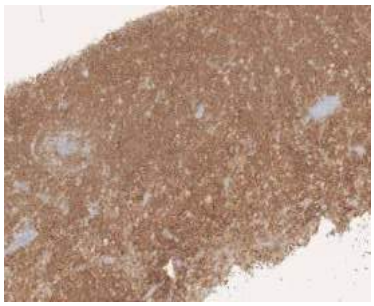

CD10 immunostaining (4X)

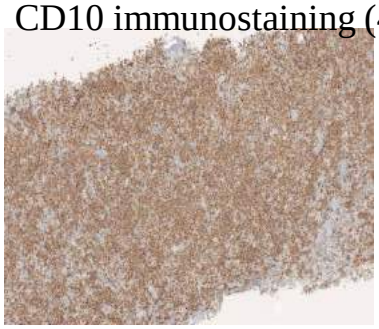

BCL6 immunostaining (4X)

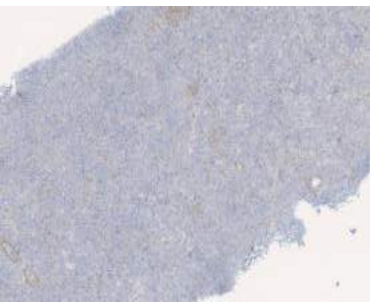

BCL2 immunostaining (4X)

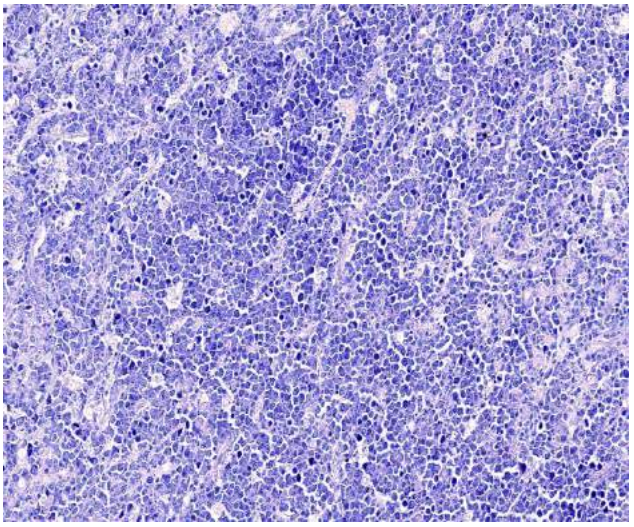

Giemsa (20X)

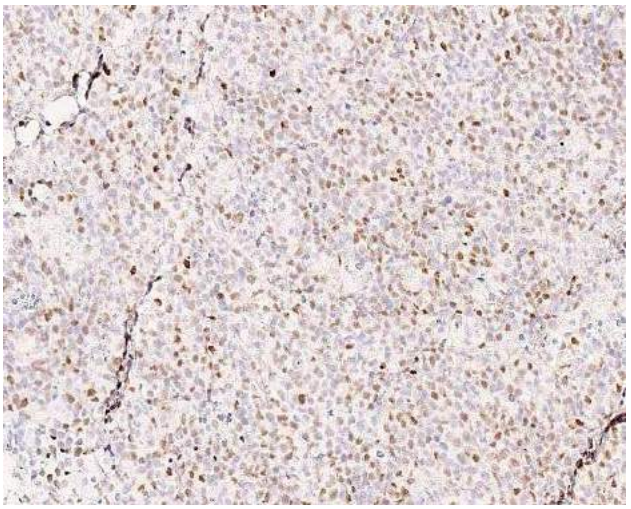

MYC immunostaining (20X)

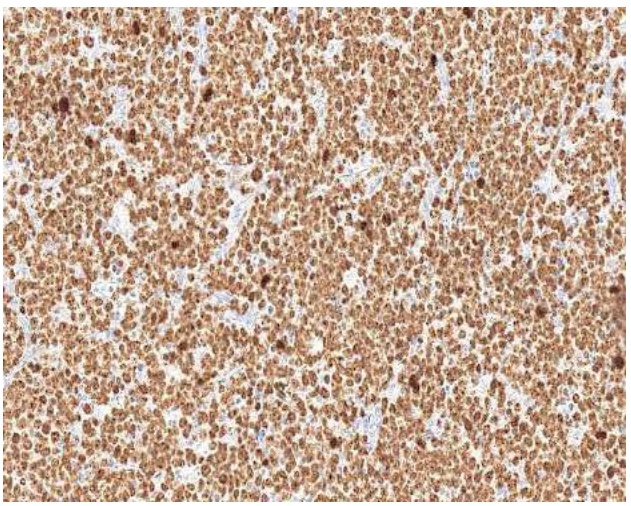

Ki-67 immunostaining (20X)

Figure 3: Papillary Renal Cell Carcinoma

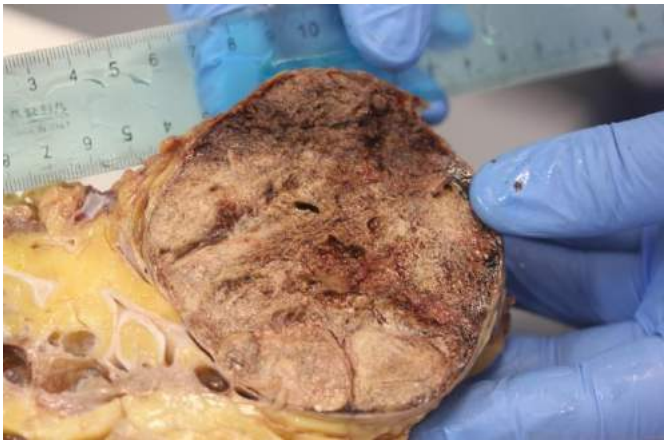

Gross image of the melanocytic Renal Cancer

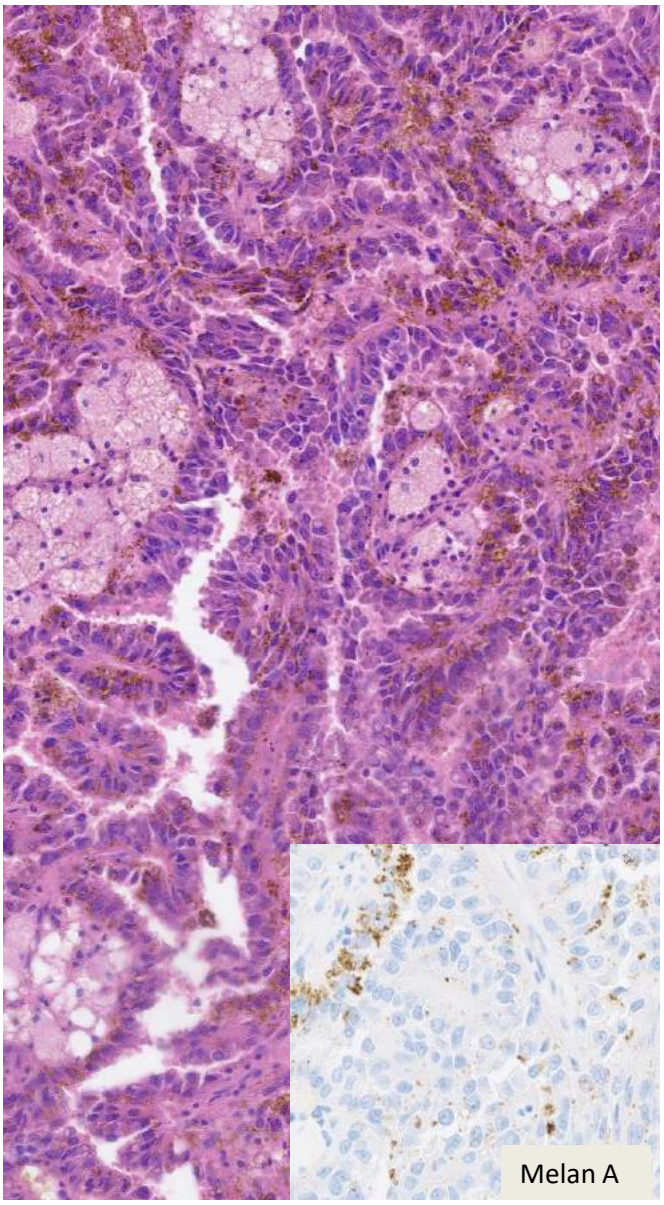

HE and Melan A immunostaing (20X)

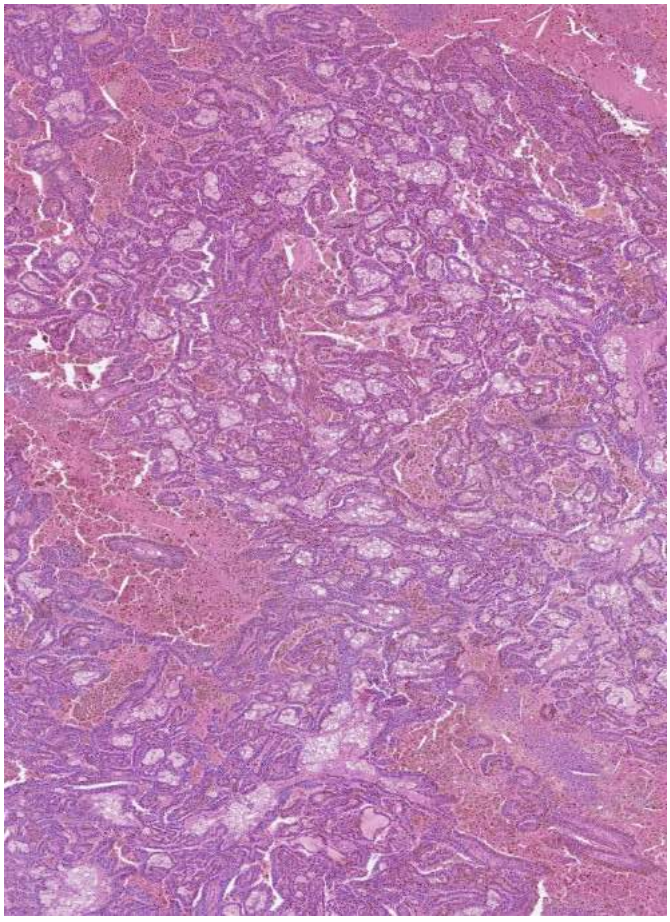

HE (10X)

Gross an microscopic examination of the recipient renal mass revealed a pigmented renal carcinoma with type 2 papillary architecture and immunoexpression of melanocytic markers (MELAN-A)

Table 1:Genetic variants detected in Exome sequencing

Blood/Lymphoma/RCC							
Gene	**Variant nature**	**c. HGVS**	**Exon**	**Reads quality (G/L/R)**	**Zygosity**	**ClinVar**	**OMIM Phenotype+Inheritence**
ATM	Missense	c.4388T>G	7	167/57/41	Het/Het/Het	Likely Benign/VUS	Lymphoma, B-cell non-Hodgkin
HMCN1	Missense	c.15926T>C	103	312/77/47	Het/Het/Het	Absent	Macular degeneration (AD)
RNF31	Missense	c.2432A>C	14	139/41/15	Het/Het/Het	Absent	NA
INPP5E	Missense	c.1132C>T	4	320/76/46	Het/Het/Het	Pathogenic	Joubert syndrome (AR)
MPO	Frameshift	c.1555_1568del	9	34/65/112	Het/Homo/Het	Pathogenic	Myeloperoxidase deficiency (AR)
INPP5D	Missense	c.2804C>T	26	54/23/97	Het/Het/Het	Absent	NA
CHD6	Missense	c.146A>T	3	350/103/56	Het/Het/Het	Absent	Hallermann-Streiff syndrome
PABPC1	Missense	c.1267_1268delTAinsCC	9	130/116/71	Het/Het/Het	Absent	NA
ARHGAP25	Splice site	c.881+22C>T	7	103/36/18	Het/Het/Het	Absent	NA
TLK1	Splice site	c.549+21T>A	6	114/63/66	Het/Het/Het	Absent	NA
NID1	Missense	c.435C>G	2	224/16/9	Het/Het/Het	Absent	NA
KLHL24	Missense	c.95A>G	3	178/56/48	Het/Het/Het	Absent	Epidermolysis bullosa simplex 6 (AD)
COL4A4	Splice site	c.975+4A>C	16	87/53/75	Het/Het/Het	Absent	Hematuria (AD)/Alport syndrome2 (AR)
ADCYAP1R1	Missense	c.950T>C	12	187/41/397	Het/Het/Het	Absent	NA
ALOX5	Missense	c.29C>G	1	34/272/48	Het/Het/Het	Absent	Asthma (AD)/Atherosclerosis
CD5	Missense	c.1381_1382delCAinsTG	9	163/44/77	Het/Het/Het	Absent	NA
CD5	Missense	c.1221G>C	7	28/22/49	Het/Het/Het	Absent	NA
GBX2	Missense	c.862G>A	2	189/63/62	Het/Het/Het	Absent	NA
HERC5	Missense	c.723C>G	5	52/11/15	Het/Het/Het	Absent	NA
CHFR	Missense	c.1618A>C	14	184/87/41	Het/Het/Het	Absent	NA
GRAMD2A	LOF	c.49C>T	2	278/61/54	Het/Het/Het	Absent	NA
RTN2	Splice site	c.35-11C>T	1	202/72/92	Het/Het/Het	Absent	Spastic paraplegia 12 (AD)
DDX27	Missense	c.1880A>G	15	203/61/30	Het/Het/Het	Absent	NA
VIRMA	Missense	c.3571A>G	14	178/56/49	Het/Het/Het	Absent	NA
ANGPT1	Missense	c.994G>A	6	89/50/50	Het/Het/Het	Absent	Angioedema (AD)
ZHX3	Missense	c.1115G>A	3	318/23/32	Het/Het/Het	Absent	NA
MUC5B	MNV	c.12950_12952delAATinsCAC	31	137/113/84	Het/Het/Het	Absent	Pulmonary fibrosis (AD)
CCDC169-SOHLH2	Splice site	c.556+6T>C	8	119/76/44	Het/Het/Het	Absent	NA
ZNF629	Missense	c.214G>A	3	56/19/21	Het/Het/Het	Absent	NA
PPIG	inframe_deletion	c.2125_2127del	14	148/34/33	Het/Het/Het	Absent	NA
ABAT	Splice site	c.367-16T>C	6	373/95/90	Het/Het/Het	Absent	NA
CR1	Missense	c.5218G>A	31	112/46/18	Het/Het/Het	Absent	Blood group, Knops system
C8B	Missense	c.1331C>T	9	271/39/31	Het/Het/Het	Absent	C8 deficiency, type II (AR)
CORO1A	Splice site	c.322-4G>A	4	86/67/169	Het/Het/Het	Likely benign	Immunodeficiency 8 (AR)
MS4A1	Missense	c.50T>C	3	376/51/48	Het/Het/Het	VUS	Immunodeficiency, common variable, 5 (AR)
TGFB2	Splice site	c.594+12_594+17del	3	93/20/29	Het/Het/Het	VUS	Loeys-Dietz syndrome 4 (AD)
C1QB	Missense	c.223G>A	3	165/34/29	Het/Het/Het	VUS	C1q deficiency (AR)
MUTYH	Missense	c.715G>A	9	110/49/44	Het/Het/Het	VUS	Adenomas, multiple colorectal (AR)
PRKN	Missense	c.823C>T	7	560/75/70	Het/Het/Het	Pathogenic	Parkinson disease/Adenocarcinoma of lung
DOCK8	Missense	c.4283A>G	34	210/76/51	Het/Het/Het	VUS	Hyper-IgE recurrent infection syndrome (AR)
RHD	Missense	c.809T>G	6	188/34/?	Homo/Homo/Het	Pathogenic	Hemolytic disease of fetus and newborn
IPO11	Missense	c.2991G>A	30	108/19/14	Het/Het/Het	Absent	NA
Blood/Lymphoma							
Gene	**Variant nature**	**c. HGVS**	**Exon**	**Reads quality (G/L/R)**	**Zygosity**	**ClinVar**	**OMIM Phenotype+Inheritence**
POU2F1	Splice donor variant	c.1269+2T>C	11	86/28/0	Het	Absent	NA
PISD	LOF	c.175C>T	3	197/34/0	Het	Absent	Liberfarb syndrome (AR)

Supplementary Figure 1: Overview Case Report

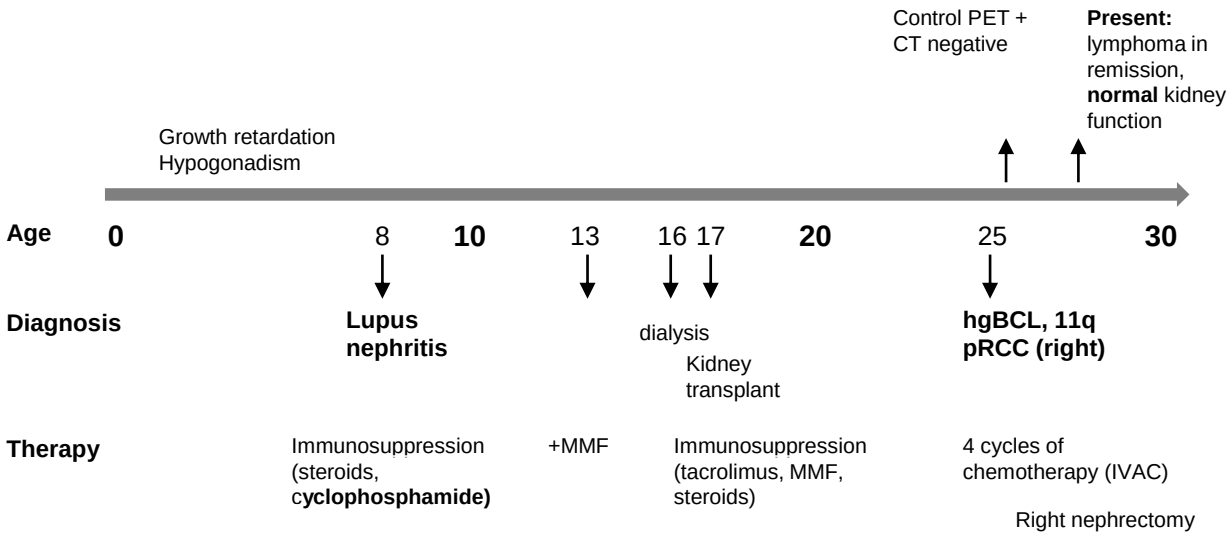

Supplementary Figure 2: OncoScan Whole Genome View including B-allele frequency

Blood

Log2-Ratio

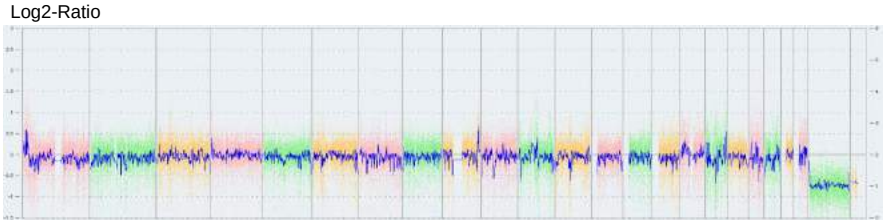

B-allele-frequency

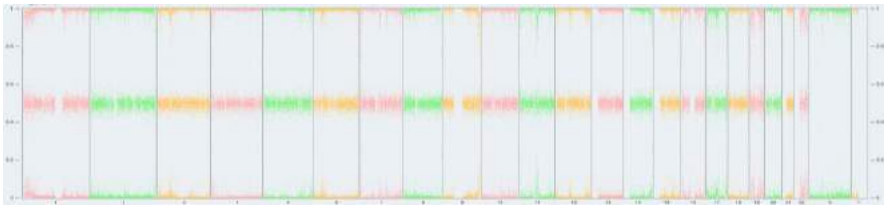

Lymphoma

Log2-Ratio

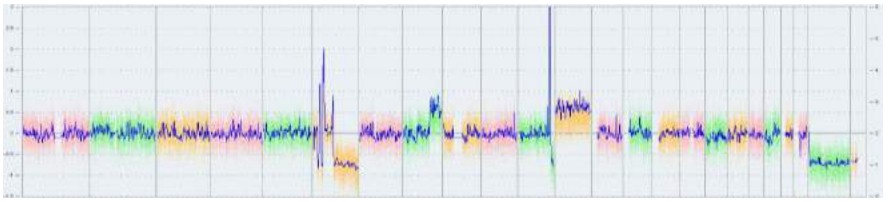

B-allele-frequency

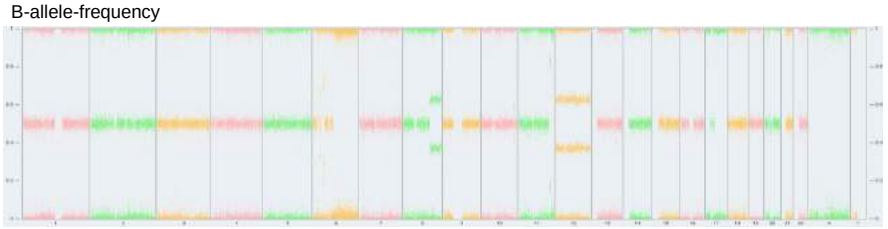

Renal cell carcinoma

Log2-Ratio

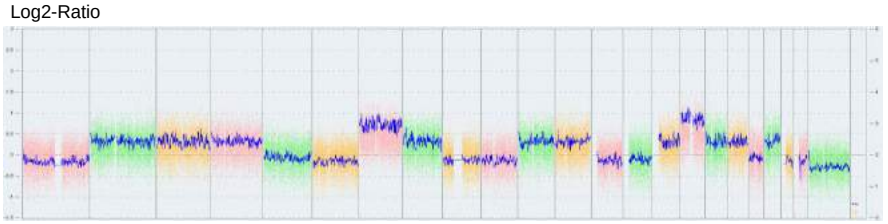

B-allele-frequency

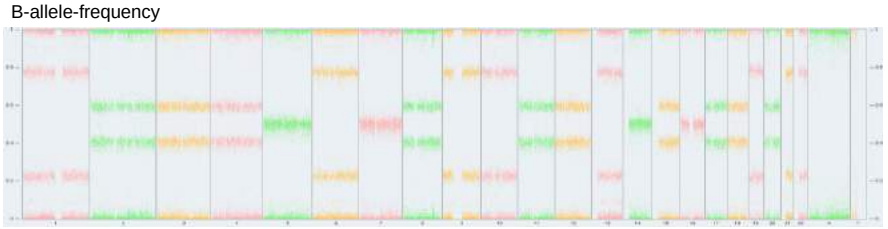

Supplementary Figure 3: OncoScan Chromosome 11 including B-allele frequency

Chromosome 11

Blood

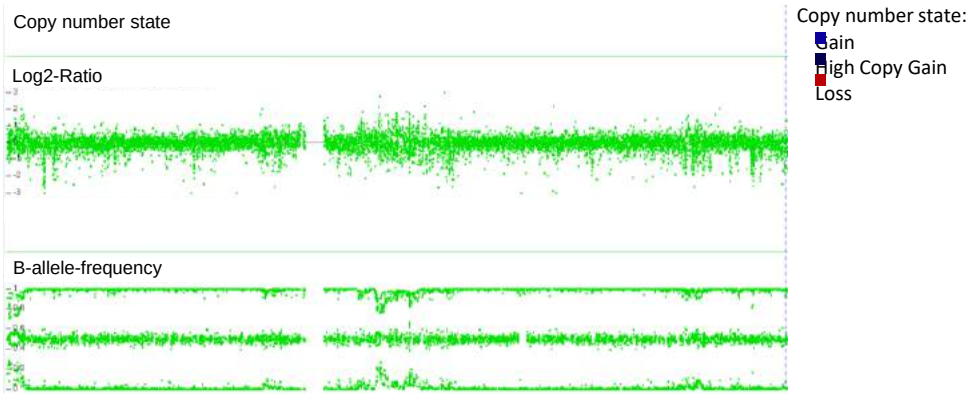

Lymphoma

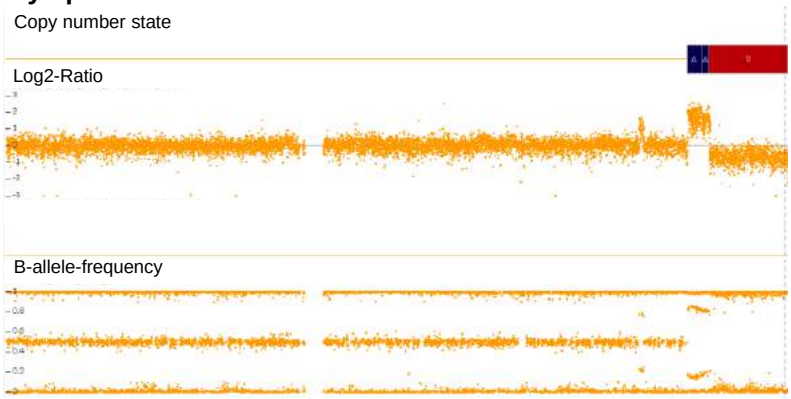

Renal cell carcinoma

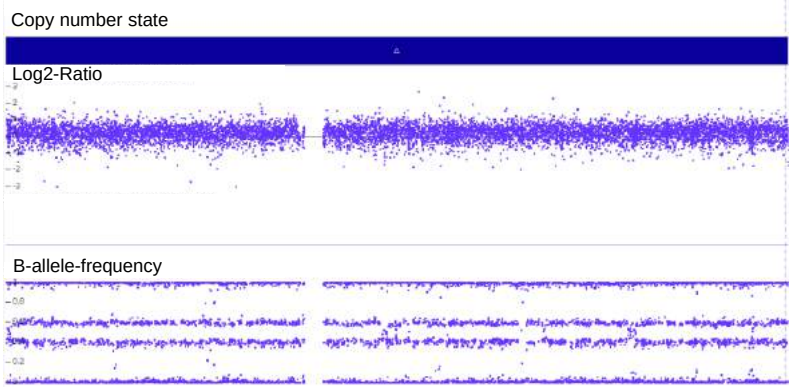

Supplementary Table 1a: Histopathology antibodies for lymphoma diagnosis

ANTIBODY	CLONE
CD5	anti-CD5 (SP19) Rabbit Monoclonal Primary Antibody
CD10	VENTANA anti-CD10 (SP67) Rabbit Monoclonal Primary Antibody
CD20	anti-CD20 (L26) Mouse Primary Antibody
BCL6	bcl-6 (GI191E/A8) Mouse Primary Antibody
BCL2	anti-bcl-2 (SP66) Rabbit Monoclonal Primary Antibody
CD38	Anti CD38(SP149) Rabbit Monoclonal Primary Antibody
MYC	anti-c-MYC (Y69) Rabbit Monoclonal Primary Antibody
Ki-67	Anti Ki-67 (30-9) Rabbit Monoclonal Primary Antibody
CYCLIN D1	anti-Cyclin D1 (SP4-R) Rabbit Monoclonal Primary Antibody
MUM1	MUM1 (EP190) Rabbit Monoclonal Primary Antibody
CD30	anti-CD30 (Ber-H2) Mouse Monoclonal Primary Antibody
TdT	TdT (polyclonal)Rabbit

Supplementary Table 1b: Histopathology antibodies for Papillary Renal Cell Carcinoma diagnosis

ANTIBODY	CLONE
CD10	anti-CD10 (SP67) Rabbit Monoclonal Primary Antibody
CDAE1-AE3	Pan-Keratin (AE1-AE3-PCK26) Primary antibody
HMB45	Anti- melanosome (HMB45) Mouse monoclonal Primary Antibody
CK7	Anti CK7 (SP52) Rabbit Monoclonal Primary Antibody
AMACR	Anti AMACR (SP116) Rabbit Monoclonal Primary Antibody
MELAN-A	Anti MART Mouse Monoclonal Primary Antibody
PAX8	Anti PAX8 (EP-331) Rabbit Monoclonal Primary Antibody
TFE-3	Anti TFE-3 (MRQ/37) Rabbit Monoclonal Primary Antibody

Supplementary Table 2: OncoScan Copy number alterations

Blood			
Type	**Size [kbp]**	**Ensembl Gene Count**	**ISCN 2016 Nomenclature**
LOH	5077	75	arr[GRCh37] 20p12.1p11.23(14929280_20006368) hmz
Lymphoma			
Type	**Size [kbp]**	**Ensembl Gene Count**	**ISCN 2016 Nomenclature**
Gain	1023	31	arr[GRCh37] 5q31.2(136895063_137917826)x3
Gain	2833	96	arr[GRCh37] 6p21.1(41299898_44133019)x4
Gain	1021	22	arr[GRCh37] 6p21.2(36667266_37688151)x6
Gain	3595	47	arr[GRCh37] 6p21.2p21.1(37700946_41296417)x3
Loss	5933	260	arr[GRCh37] 6p21.33p21.2(30726777_36659932)x1
Gain	1003	12	arr[GRCh37] 6p22.3(16744615_17747572)x3
Loss	3850	32	arr[GRCh37] 6p22.3(17773789_21623715)x1
Gain	2763	96	arr[GRCh37] 6p22.3p22.1(24291202_27054497)x3
Gain	1550	10	arr[GRCh37] 6q13(74230396_75780564)x3
Loss	94372	917	arr[GRCh37] 6q14.1q27(76540987_170913051)x1
Gain	46020	575	arr[GRCh37] 8q22.2q24.3(100272246_146292734)x3
Gain	3597	46	arr[GRCh37] 10q26.11q26.13(119589469_123186634)x3
Gain	1299	13	arr[GRCh37] 11q23.3q24.1(120099367_121398578)x7
Gain	2559	96	arr[GRCh37] 11q23.3(117532542_120091272)x8
Loss	13532	225	arr[GRCh37] 11q24.1q25(121406707_134938847)x1
Gain	34639	620	arr[GRCh37] 12p13.33p11.1(189399_34828211)x3
Gain	94572	1722	arr[GRCh37] 12q12q24.33(39245719_133818115)x3
Gain	1224	7	arr[GRCh37] 13q31.3(91257551_92481236)x3
LOH	16823	533	arr[GRCh37] 17p13.3p11.2(400958_17223851) hmz
LOH	47291	1434	arr[GRCh37] 17q12q25.3(32972019_80263427) hmz
LOH	5077	75	arr[GRCh37] 20p12.1p11.23(14929280_20006368) hmz
Loss	841	55	arr[GRCh37] 22q11.22(22371637_23212806)x1
Renal cell carcinoma			
Type	**Size [kbp]**	**Ensembl Gene Count**	**ISCN 2016 Nomenclature**
LOH	120597	2099	arr[GRCh37] 1p36.33p11.2(754191_121350934) hmz
LOH	100168	1769	arr[GRCh37] 1q21.2q44(149044447_249212878) hmz
Gain	243031	2979	arr[GRCh37] 2p25.3q37.3(21493_243052331)x2-3
Gain	197789	2273	arr[GRCh37] 3p26.3q29(63410_197852564)x2-3
Gain	190846	1813	arr[GRCh37] 4p16.3q35.2(69403_190915650)x2-3
LOH	58566	1078	arr[GRCh37] 6p25.3p11.1(204908_58770502) hmz
LOH	109027	1020	arr[GRCh37] 6q11.1q27(61886392_170913051) hmz
Gain	151899	1890	arr[GRCh37] 7p22.3q36.1(41420_151940165)x3
Gain	6926	81	arr[GRCh37] 7q36.1q36.3(152192120_159118443)x3
Gain	146120	1775	arr[GRCh37] 8p23.3q24.3(172416_146292734)x2-3
LOH	38979	432	arr[GRCh37] 9p24.3p13.1(204737_39184065) hmz

Supplementary Table 3: Affected Genes on 20p11.23p12.2

Genes located in long stretch of homozygosity of over 5Mb in 20p11.23p12.2
Gene
MACROD2
RNU6-1159P
RP5-841K13.1
KIF16B
Mir_584
SNRPB2
OTOR
PCSK2
BFSP1
DSTN
RN7SKP69
RRBP1
BANF2
TRNA_Gln
SNX5
SNORD17
MGME1
JB175279
OVOL2
PET117
KAT14
ZNF133
RP4-568F9.6
LINC00851
DZANK1
POLR3F
MIR3192
RBBP9
SEC23B
SMIM26
DTD1
LINC00652
LINC00653
SCP2D1-AS1
SCP2D1
SLC24A3
SLC24A3-AS1
Mir_548

Precursor T-Lymphoblastic Transformation of Mantle cell lymphoma

Mantle cell lymphoma (MCL) is a mature B-cell non-Hodgkin's lymphoma (NHL) and accounts for about 6% of all NHL cases (1). The primary genetic event of MCL is translocation t (11;14) (q13;q32), which results in cyclin D1 overexpression. In addition to this constitutive dysregulation of the cell cycle, other mechanisms such as DNA damage response alterations and activation of cell survival pathways are integrated to drive MCL pathogenesis (2-3). More aggressive histologic variants have been described, as well as rare cases of transformation to other large cell lymphomas (4). Here, we describe a novel case of 79-year-old man presenting with progressive fatigue and dyspnea. Full blood counts documented macrocytic anemia (Hb 9.0, MCV 98) with normal folates and cobalamine levels. White blood cell and platelet counts were $8.11x10^{9/}L$ and $198x10^{9/}L$, respectively. Differentials showed 5% undifferentiated, small-sized peripheral blasts. Contrast-enhanced CT scan of the chest demonstrated multiple confluent lymphadenopathies mainly localized in the anterior mediastinum. PET-CT scan confirmed multiple district FDG-avid lymphadenopathies and enhanced FDG uptake in the spleen and bone marrow. Bone marrow biopsy showed a lymphoid infiltrate composed of small to medium sizes cells with irregular nuclear contours and different immunophenotypes: the major component (60%) was: CD3+, CD5+ CD10+, Tdt+ PAX5-, CD20-, Cyclin d1-, SOX11-, CD34- with 80% of ki67; the minor population (30%) was: CD5+, CD19+, CD20+, CYCLIN-D1+, BCL2+, PAX5+, SOX-11+, CD34-, CD3-, and 30% of ki-67. These data suggested us two hypotheses: they could represent concurrent distinct entities at the same site or it is an example of Progression/transformation of mantle cell lymphoma in lymphoma /leukemia with a T-cell phenotype. According to immunophenotypic results, we performed cytogenetic analysis for t (11;14), using Dual Fusion IGH/CCND1 FISH probe, revealing the t (11;14) in both lymphoid population cells. The combination of immunolabeling for CD3 and Interphase FISH with IGH/CCND1Dual Fusion probe, allowed us to identify t (11;14) in both lymphoid populations: mantle B cell lymphoma phenotype and lymphoblastic T cell phenotype. ImmunoFISH is a method combining immunolabelling, using FISH to simultaneously detect the cytoplasmatic distribution of CD3+ and specific DNA sequences (IGH-CCND1) within interphase nuclei. The application of ImmunoFISH was not easy to perform, because fixation and preparation techniques must be optimised to best preserve nuclear morphology and protein epitopes without the need for any antigen retrieval. Following in situ hybridization, the sections were blocked in blocking buffer. From this step on, sections were kept in a humid chamber to protect the tissue sections from drying out. The blocking buffer was removed, primary antibody diluted in blocking buffer was incubated overnight at 4°C in a humid chamber. Sections were rinsed with 1X PBS and incubated with corresponding secondary antibody. Slides were subsequently rinsed

with 1X PBS, at last nuclear staining with DAPI was performed. At this point, all FISH and immunofluorescence staining steps were complete. After technical standardization, we observe that also CD3+ cells showed t (11;14), characterized by one signal of fusion and two distinct orange and green signals, as reported in table of figure. This case may represent a T-lymphoblastic transformation of Mantle Cell lymphoma, probably due to methylation of PAX-5, a key regulator in the development and differentiation of B-cell (5-6).

FIGURES

1: FISH for t (11;14) in B cell area

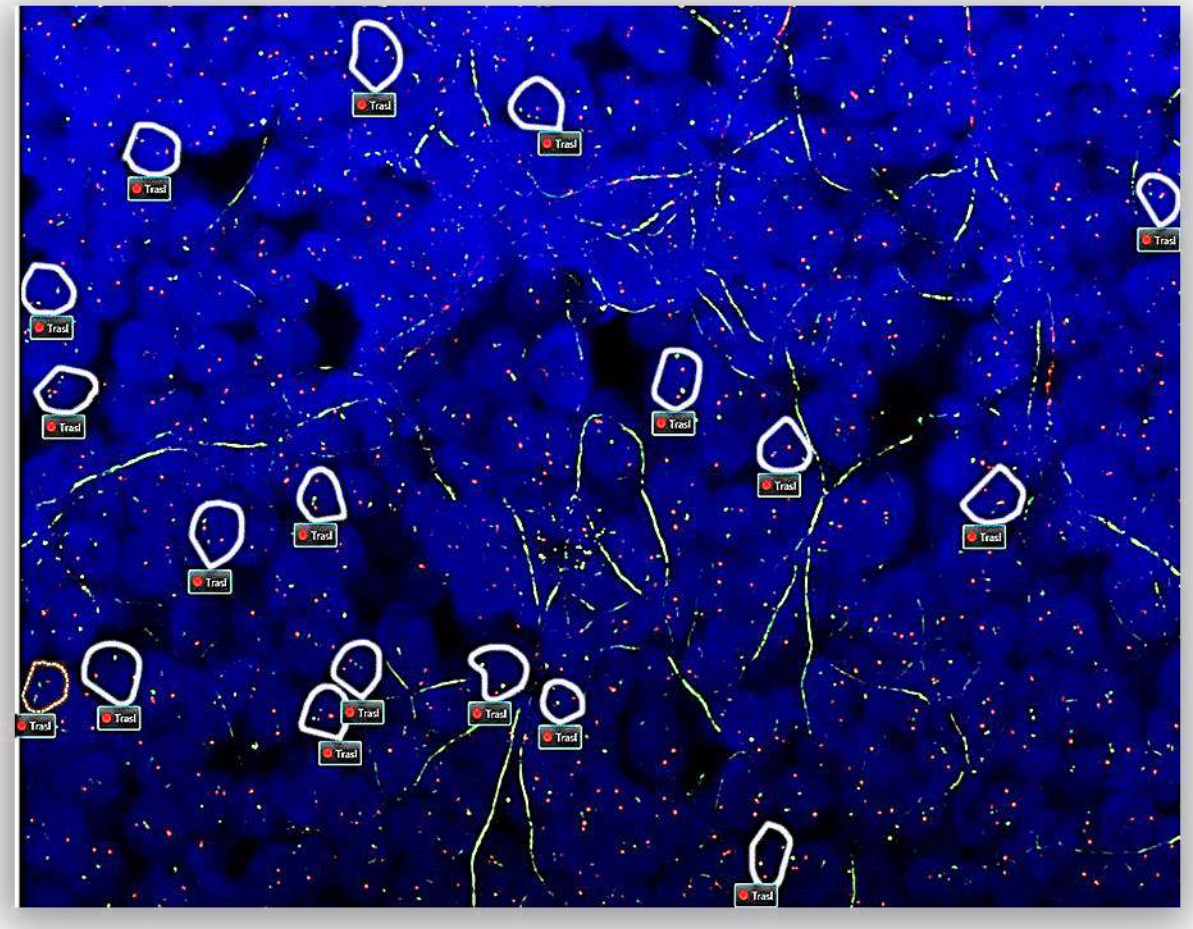

B-cell area (63X magnification). Interphase FISH for IGH/CCND1. We observe a signal of fusion, due to translocation and two single signals of CCND1 (green) and IGH (orange).

Fig.2: FISH for t (11;14) in T-area

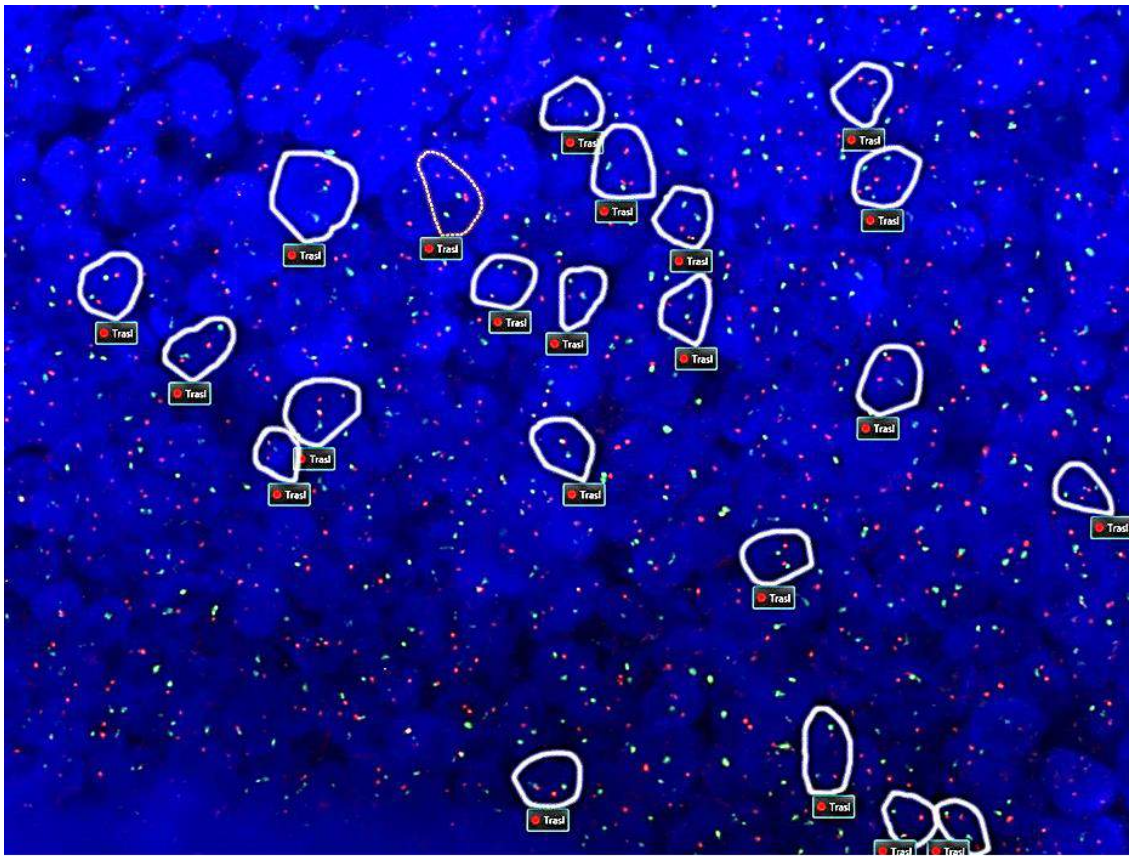

T-cell area (63X magnification). Interphase FISH for IGH/CCND1. We observe a signal of fusion, due to translocation and two single signals of CCND1 (green) and IGH (orange).

Fig3: ImmunoFISH for CD3 labeled with red fluorochrome and Dual Fusion IGH/CCND1 Probe

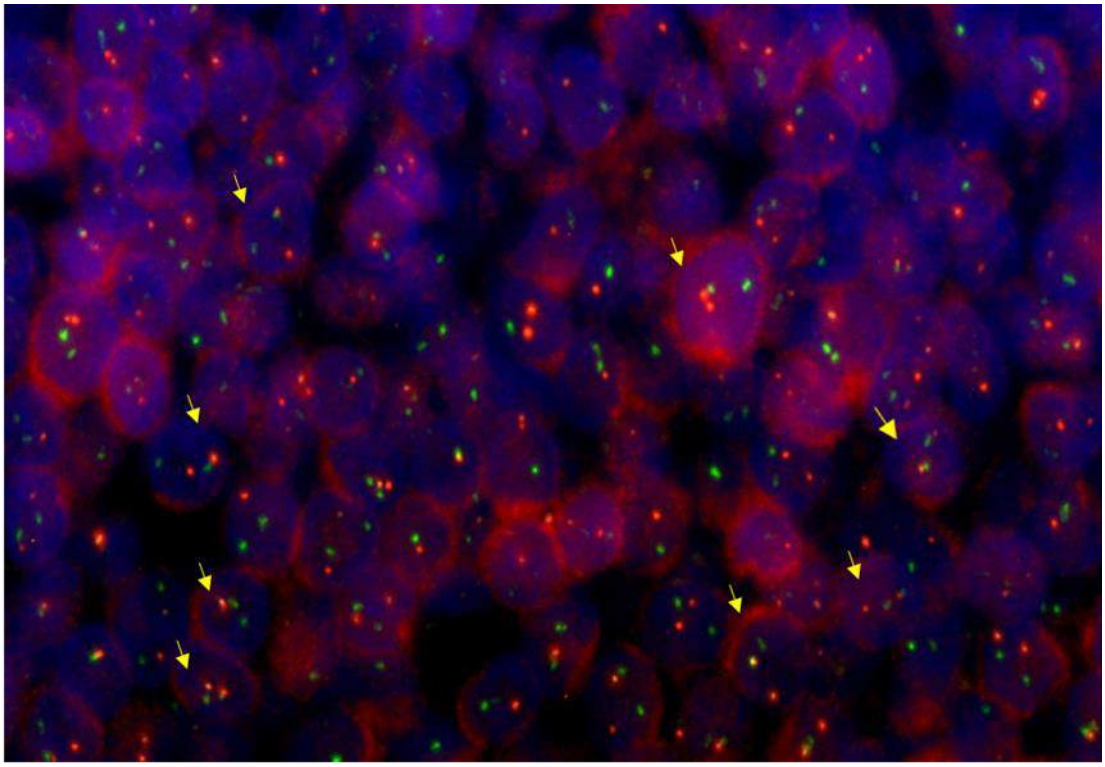

ImmunoFISH for CD3 (red) and IGH/CCND1 (63x magnification)

REFERENCES

1. Skarbnik AP et al; Mantle cell lymphoma: State of the art. Clin. Adv. Hematol. Oncol. 2015.
2. Jares P, et al; Genetic and molecular pathogenesis of mantle cell lymphoma: perspectives for new targeted therapeutics. Nat Rev Cancer;2007.
3. Jares P, et al; Advances in the understanding of mantle cell lymphoma. Br J Haematol. 2008.
4. Michael E.et al; B-lymphoblastic transformation of mantle cell lymphoma/leukemia with "double hit" changes; J Hematopathol. 2015
5. Xianglan Zhang et al; Pax5 expression in Non-Hodgkin's Lymphomas and Acute Leukemias;J Korean Med Sci 2003.
6. Lazzi S. et al; Rare lymphoid neoplasms co-expressing B- and T-cell antigens. The role of PAX-5 gene methylation in their pathogenesis; Human Pathology 2009

CHROMOSOMAL INSTABILITY IN HODGKIN LYMPHOMA

Hodgkin lymphoma (HL), a B-cell originated neoplasia of the immune system, is unique malignancy in that the cancerous cells usually account for a minority of the tumour bulk (as few as one in 100 cells) against an inflammatory background comprising reactive non-clonal lymphocytes, eosinophils, histiocytes and fibroblasts. HL is one of the most frequent lymphomas in the Western world, with an incidence of about 3 new cases per 100,000 individuals per year (1). Based on morphology and immunophenotypical features, HL can be divided into either classical HL (cHL) that represents approximately 90% of all HL, or nodular lymphocyte-predominant HL (NLPHL). Subtypes of classical Hodgkin's lymphoma include: nodular sclerosis, mixed cellularity, lymphocyte-rich and lymphocyte-depleted. The presence of malignant multinucleated giant Reed-Sternberg (RS) cells and the mononuclear Hodgkin (H) cells within the characteristic and reactive microenvironment, is the pathologic hallmark of cHL. Both malignant cell types, referred as HRS cells, represent only 1–2% of the tumour burden, which includes inflammatory cells. RS cells are derived from B lymphocytes of germinal centre origin and arise due to a disturbance in cytokinesis by mononuclear Hodgkin cells (2). Multinucleated RS will not undergo normal replication; their large morphology is considered as one of the consistent characteristic features of senescence (1). One of the major characteristics of RS cells is the occurrence of complex and hyperdiploid chromosomal aberrations that reflect ***chromosomal instability***, a key pathway in the origin of the RS cell. Chromosomal instability is characterized by centrosome amplification that can contribute to aneuploidy by favoring chromosome mis-segregation during mitosis and micronucleus formation (3). Micronucleus formation has been associated with centrosome amplification and spindle assembly defects (2) Centrosome alterations and defects in mitotic spindle formation can be evaluated by Immunofluorescence, using respectively gamma-tubulin and alpha-acetylated tubulin. Gamma-tubulin, a conserved member of the eukaryotic tubulin superfamily specialized for microtubule nucleation is a target of cell cycle. Besides its microtubule nucleation role, gamma-tubulin functions in nuclear and cell cycle related processes. Alteration in gamma-tubulin localization can be correlated to chromosomal instability. Alpha-tubulin is one of the two protein components of a microtubule which plays a critical role in the formation of the cytoskeleton. Also, microtubules participate in several cellular events including cell division, and their morphology is important to establish if there are any aberration during mitotic cycle. Alpha and gamma-tubulin are interconnected because both of them are implicated in the regulation of mitotic division. As well as in other neoplasms, in HL chromothripsis (an oncogenic mechanism whereby small genomic pieces originating from one chromosomal region undergo massive rearrangements in a single step) is a consequence of chromosomal instability (6). A number of alterations including,

del(4q), del(6q), and del(7q), and t (2;5), t (14;18), t (14;19) are observed in HL. Several studies using comparative genomic hybridization (CGH), have revealed specific cytogenetic alterations: dup(2p), dup(9p), dup(17q), dup(19q), dup(20q), chromosome losses, including del(6q), del(13q) and telomere dysfunction. The loss of the protective function of telomeres in HL cell lines induced chromosomal fusions (dicentric chromosome formation) and "breakage-fusion-bridges" (B/F/B) cycles, resulting in a series of chromosomal breaks and duplications, which can lead to chromosome imbalances, gene amplification, non-reciprocal translocation, and altered gene expression (6). The mechanisms underlying genomic instability and the primary transforming events of HL are still obscure. The development of HRS has long been a subject of debate. Recently, has been demonstrated that re-fusion of daughter cells is the main route to giant HRS cell formation and also that RS cells develop neither by endomitosis nor acytokinetic mitosis. (3). HRS cells show deregulated activation of multiple signaling pathways, including: NF-κB, P53, JAK/STAT, ATM and ATR pathways in the transforming events of HRS cells. In some cases the HRS cells display aneuploidy, defined as an ***abnormal chromosome number***. Aneuploidy results from the failure of the mitotic spindle assemble checkpoint (SAC). SAC inactivation can induce resistance to spindle damaging therapeutics. Centrosome amplification may be a direct effect of midbody protein dysfunction or may arise due to the accumulation of centrosomes from failed mitoses. Supernumerary centrosomes cause not correct segregation of chromosomes, in some cases due to multipolar mitoses, leading to cells that have lost or gained chromosomes; the mis- segregated chromosomes may contain tumor suppressor genes or genes that regulate inflammation, favoring the inflammatory functional profile of the RS cell. Interestingly, tumor cells with only one centrosome were mononucleated, whereas the few HRS cells displaying multiple centrosomes were all multinucleated. The acquisition of multiple centrosomes might be associated with defects in the final step of cell division, that is cytokinesis. A defect in this mechanism has been reported to result in bi- or multinucleated cells, which is a typical feature for the Reed–Sternberg cells in cH. In HL, chromosomal instability and microsatellite instability (MSI) have been described for genetic instability. MSI is characterized by very high mutation rates within small DNA repeat sequences (1–6 base pairs in length), caused by the abnormal functioning of DNA mismatch repair (MMR) genes.

AIM OF STUDY

In this study, we applied Double Immunofluorescence in HLs to study chromosomal instability in CD30+ cells and morphological alterations of the mitotic spindle, using Acetylated alpha-tubulin and gamma-tubulin antibodies. The first detects alterations of mitotic spindle and the organization of cytoskeleton, while gamma tubulin identifies centrosome localization. The Immunofluorescence for Gamma-tubulin in CD30+ cells showed a granular pattern, probably because of their genetic instability than the surrounding microenvironment, whose expression was point-like. Acetylated alpha-tubulin showed a filamentous distribution limited to HRS. Atypical and not polarized mitotic fuses, characterized by three centrosomes, are not standard in all HLs examined.

PRELIMINARY DATA

In our study we performed indirect Immunofluorescence in HL tissues, for the evaluation of gamma -tubulin and Acetylated alpha tubulin in CD30+ cells and in their microenvironment. Gamma-tubulin localizes at the centrosome and required for microtubule nucleation from the centrosome. Alpha Tubulin is an important component of microtubule and its acetylation can modulate the stability and dynamic activity of microtubules, which regulates microtubule properties, such as cell shape maintenance, cell mitosis, cell meiosis, intracellular trafficking, and so much the cell fate for survival or apoptosis**.** In all cases, gamma-tubulin in CD30+ cells showed a granular pattern, probably because of their genetic instability, respect to the surrounding microenvironment, whose expression was point-like. (fig.1). Acetylated alpha tubulin showed a filamentous distribution limited to HRS in all cases analyzed (fig.2). Some LHs show typical (fig.3) mitotic spindle, while other display atypical mitotic figures with not polarized microtubules and three centrosomes (fig.4).

PRELIMINARY DATA

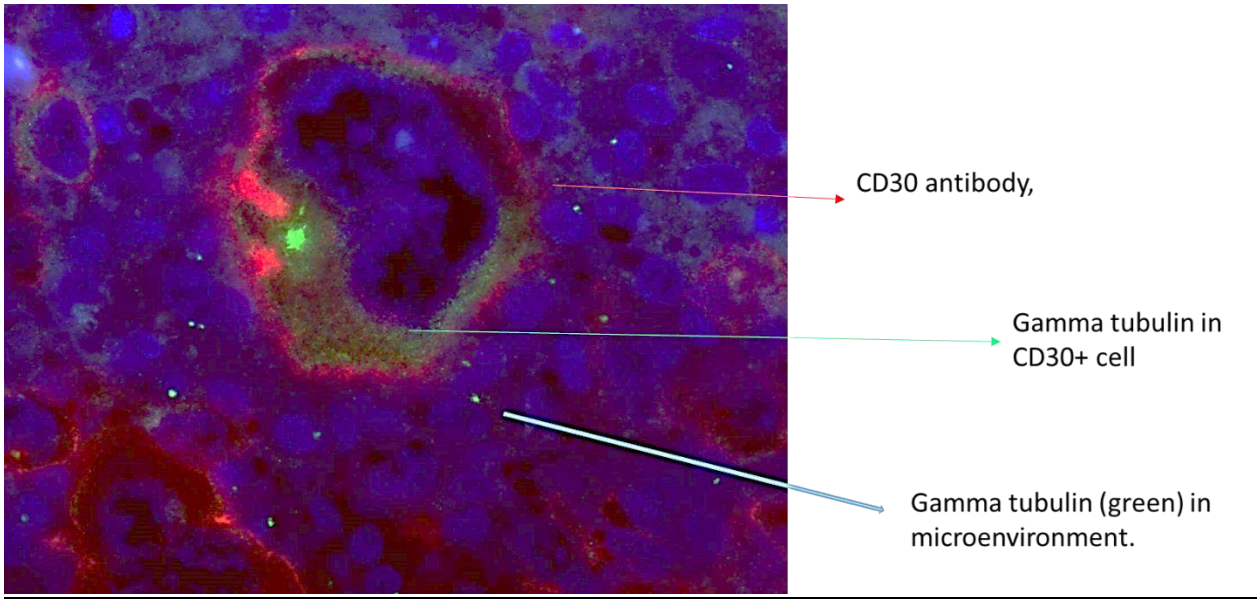

Fig.1 Immunofluorescence for CD30 and gamma-tubulin, labelled respectively with red and green fluorochromes. We observe a different morphology of gamma-tubulin: granular in neoplastic cells, and round-shape in microenvironment, probably because of their immunological response.

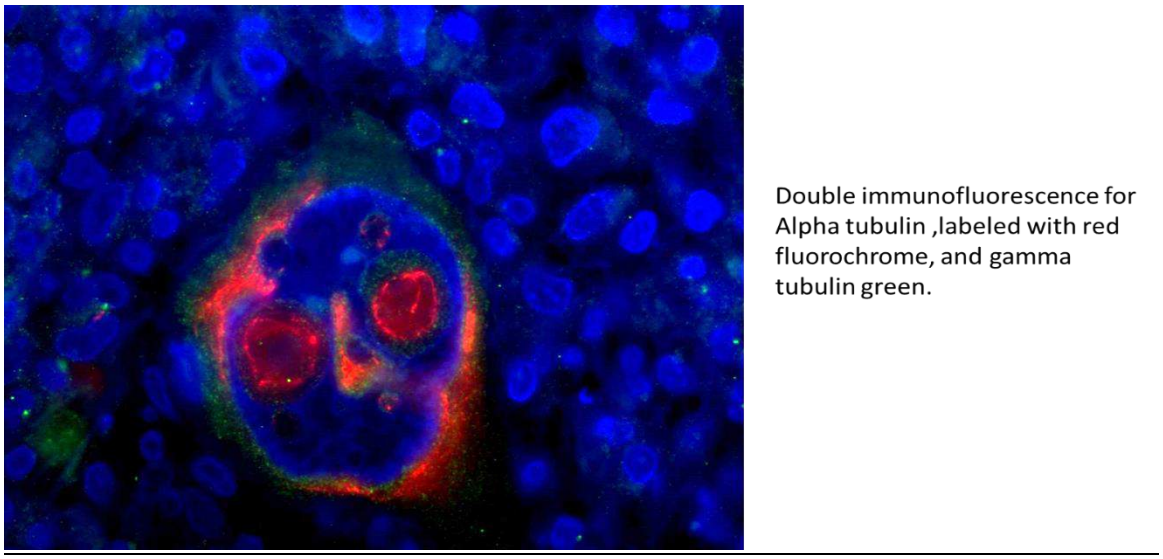

Fig.2 Immunofluorescence for alpha and gamma-tubulin, respectively red and green. We observe the granular pattern of gamma-tubulin and the filamentous pattern of alpha-tubulin.

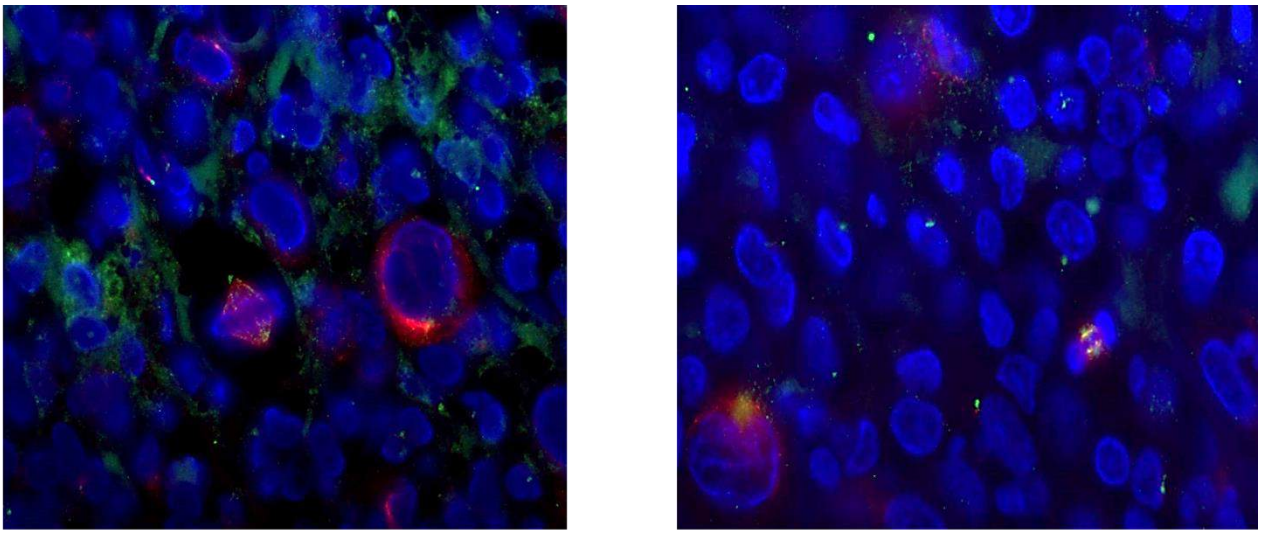

Immunofluorescence for alpha tubulin (red) and gamma tubulin (green).
We observe normal mitotic figures with polarised microtubules and 2 centrosomes.

Fig.3 typical mitotic figures

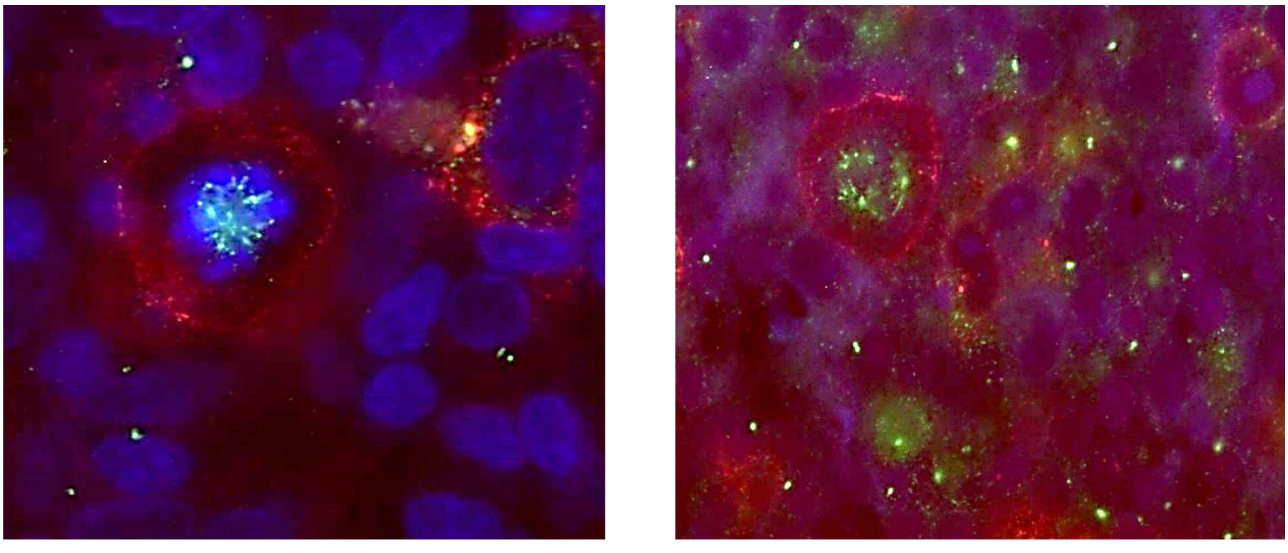

Immunofluorescence for CD30 and gamma tubulin.
We observe atypical mitotic figures , characterized of aberrant and multiple centrosomes

Fig.4: atypical mitosis

REFERENCES

1. Gopas J,et al, Reed-Sternberg cells in Hodgkin's lymphoma present features of cellular senescence; Cell Death Dis. 2016.
2. Krem Maxwell M. et al; Mitotic errors, aneuploidy and micronuclei in Hodgkin lymphoma pathogenesis; Communicative & Integrative Biology; 2013.
3. Cuceu Corina et al; Chromosomal Instability in Hodgkin Lymphoma: An In-Depth Review and Perspectives; Cancers 2018;
4. Carotenuto Piero et al; Therapeutic Approaches Targeting Nucleolus in Cancer; Cells 2019;
5. Cuceu Corina et al; Independent Mechanisms Lead to Genomic Instability in Hodgkin Lymphoma: Microsatellite or Chromosomal Instability; Cancers 2018.
6. Nagel Stefan et al; Chromothripsis in Hodgkin lymphoma.; Genes Chromosomes Cancer 2013.